JAEA-Research
2006-052

JAEA-Research

Evaluation of the (α, xn) Reaction Data for JENDL/AN-2005

Toru MURATA*, Hiroyuki MATSUNOBU*
and Keiichi SHIBATA

Nuclear Data Center
Nuclear Science and Engineering Directorate

July 2006

Japan Atomic Energy Agency

日本原子力研究開発機構

本レポートは日本原子力研究開発機構が不定期に発行する成果報告書です。
本レポートの入手並びに著作権利用に関するお問い合わせは、下記あてにお問い合わせ下さい。
なお、本レポートの全文は日本原子力研究開発機構ホームページ（http://www.jaea.go.jp/index.shtml）より発信されています。このほか財団法人原子力弘済会資料センター*では実費による複写頒布を行っております。

〒319-1195　茨城県那珂郡東海村白方白根 2 番地 4
日本原子力研究開発機構　研究技術情報部　研究技術情報課
電話 029-282-6387, Fax 029-282-5920

*〒319-1195　茨城県那珂郡東海村白方白根 2 番地 4　日本原子力研究開発機構内

This report is issued irregularly by Japan Atomic Energy Agency
Inquiries about availability and/or copyright of this report should be addressed to
Intellectual Resources Section, Intellectual Resources Department,
Japan Atomic Energy Agency
2-4 Shirakata Shirane, Tokai-mura, Naka-gun, Ibaraki-ken 319-1195 Japan
Tel +81-29-282-6387,　Fax +81-29-282-5901

JAEA-Research 2006-052

Evaluation of the (α,xn) Reaction Data for JENDL/AN-2005

Toru MURATA* , Hiroyuki MATSUNOBU** and Keiichi SHIBATA

Division of Nuclear Data and Reactor Engineering
Nuclear Science and Engineering Directorate
Japan Atomic Energy Agency
Tokai-mura, Naka-gun, Ibaraki-ken

(Received June 9, 2006)

Neutron emission data of the (α,xn) reactions were evaluated in the incident α-particle energy region below 15 MeV for nuclides important mainly in nuclear fuel-cycle applications, namely, ^{6,7}Li, ^{9}Be, ^{10,11}B, ^{12,13}C, ^{14,15}N, ^{17,18}O, ^{19}F, ^{23}Na, ^{27}Al and ^{28,29,30}Si. The evaluation was performed on the basis of available experimental data and nuclear model calculations. The evaluated nuclear data were compiled in the ENDF-6 format, and released in June 2005 as JENDL (α,n) Reaction Data File 2005 (JENDL/AN-2005) which is one of JENDL special-purpose files. This report describes evaluation methods and the results on evaluated cross sections and angular- and energy-distributions of emitted neutrons.

Keywords: Nuclear Data, Evaluation, JENDL/AN-2005, (α,xn), Cross Section, Neutron Angular Distribution, Neutron Spectrum, Special-purpose File

---

This report provides the results obtained by the Charged Particle Nuclear Data Working Group established under Japanese Nuclear Data Committee at the former Japan Atomic Energy Research Institute.

* AITEL Corporation
** Previous affiliation ; Sumitomo Atomic Energy Industries, Ltd.

JENDL/AN-2005 のための(α,xn)反応核データの評価

日本原子力研究開発機構
原子力基礎工学研究部門　核工学・炉工学ユニット
村田　徹*、松延　廣幸**、柴田　恵一

(2006 年 6 月 9 日受理)

核燃料サイクル等での利用のために ^{6,7}Li、^{9}Be、^{10,11}B、^{12,13}C、^{14,15}N、^{17,18}O、^{19}F、^{23}Na、^{27}Al 及び ^{28,29,30}Si の(α,xn)反応による中性子放出反応データを入射α粒子エネルギー15 MeV 以下の領域で評価した。評価は実験データ及び原子核反応モデル計算により行った。評価済データは ENDF-6 フォーマットで編集され、2005 年 6 月に JENDL 特殊目的ファイルの 1 つである JENDL (α,n)反応データファイル 2005（JENDL/AN-2005）として公開された。本報告は評価方法及び評価された断面積及び放出中性子の角度・エネルギー分布の結果についてまとめたものである。

本報告書は、旧日本原子力研究所シグマ研究委員会荷電粒子核データワーキンググループの成果を纏めたものである。
原子力科学研究所（駐在）：〒319-1195　茨城県那珂郡東海村白方白根 2-4
*　アイテル技術サービス（株）
**　元住友原子力工業（株）

Contents

1. Introduction 1
2. Evaluation Methods 1
2.1 Resonance Analysis 1
2.2 Multistep Statistical Model 2
2.3 Inverse-reaction Cross Section 3
2.4 Thick-target Neutron Yield 4
3. Lithium 4
3.1 ^{6}Li(α,xn) Reaction 4
3.2 ^{7}Li(α,xn) Reaction 8
3.3 Discussion 12
4. Beryllium 12
4.1 ^{9}Be(α,xn) Reaction 12
4.2 Discussion 17
5. Boron 17
5.1 ^{10}B(α,xn) Reaction 17
5.2 ^{11}B(α,xn) Reaction 21
5.3 Discussion 25
6. Carbon 25
6.1 ^{12}C(α,xn) Reaction 25
6.2 ^{13}C(α,xn) Reaction 27
6.3 Discussion 30
7. Nitrogen 30
7.1 ^{14}N(α,xn) Reaction 30
7.2 ^{15}N(α,xn) Reaction 34
7.3 Discussion 36
8. Oxygen 37
8.1 ^{17}O(α,xn) Reaction 37
8.2 ^{18}O(α,xn) Reaction 39
8.3 Discussion 42
9. Fluorine 42
9.1 ^{19}F(α,xn) Reaction 42
9.2 Discussion 46
10. Sodium 46
10.1 ^{23}Na(α,xn) Reaction 46
10.2 Discussion 50
11. Aluminum 50
11.1 ^{27}Al(α,xn) Reaction 50
11.2 Discussion 53

12. Silicon 53
12.1 ^{28}Si(α,xn) Reaction 53
12.2 ^{29}Si(α,xn) Reaction 55
12.3 ^{30}Si(α,xn) Reaction 57
12.4 Discussion 60
13. Conclusions 60
Acknowledgment 61
References 62

目　次

1.　序論 1
2.　評価方法 1
2.1　共鳴解析 1
2.2　多段階統計模型 2
2.3　逆反応断面積 3
2.4　厚いターゲットによる中性子収量 4
3.　リチウム 4
3.1　^{6}Li(α,xn)反応 4
3.2　^{7}Li(α,xn)反応 8
3.3　考察 12
4.　ベリリウム 12
4.1　^{9}Be(α,xn)反応 12
4.2　考察 17
5.　ホウ素 17
5.1　^{10}B(α,xn)反応 17
5.2　^{11}B(α,xn)反応 21
5.3　考察 25
6.　炭素 25
6.1　^{12}C(α,xn)反応 25
6.2　^{13}C(α,xn)反応 27
6.3　考察 30
7.　窒素 30
7.1　^{14}N(α,xn)反応 30
7.2　^{15}N(α,xn)反応 34
7.3　考察 36
8.　酸素 37
8.1　^{17}O(α,xn)反応 37
8.2　^{18}O(α,xn)反応 39
8.3　考察 42
9.　フッ素 42
9.1　^{19}F(α,xn)反応 42
9.2　考察 46
10.　ナトリウム 46
10.1　^{23}Na(α,xn)反応 46
10.2　考察 50
11.　アルミニウム 50
11.1　^{27}Al(α,xn)反応 50
11.2　考察 53

12. シリコン 53
12.1 ^{28}Si(α,xn)反応 53
12.2 ^{29}Si(α,xn)反応 55
12.3 ^{30}Si(α,xn)反応 57
12.4 考察 60
13. 結論 60
謝辞 61
参考文献 62

List of Figures and Tables

FIGURES

Fig. 1 Thick-target neutron yield of ^{6}Li bombarded by α-particles

Fig. 2 Neutron-production cross sections of ^{6}Li bombarded by α-particles

Fig. 3 Comparison of evaluated cross sections for the (α,n_0), (α,n_1) and (α,n_2) reactions with the experimental values measured by Bochkarev et al.[14)]

Fig. 4 Calculated relative angular distribution compared with the experimental data measured by Mehta et al.[13)]

Fig. 5 Calculated energy spectra of neutrons emitted by α-particle bombardment of ^{6}Li

Fig. 6 Calculated thick-target neutron yield of ^{7}Li bombarded by α-particles together with the experimental values measured by Bair and Gomez del Campo[9)]

Fig. 7 Neutron-production cross section of ^{7}Li bombarded by α-particles

Fig. 8 Comparison of evaluated cross sections for the (α,n_0) and (α,n_1) reactions with the experimental values measured by Van der Zwan and Geiger[16)]

Fig. 9 Calculated energy spectra of neutrons emitted by α-particle bombardment of ^{7}Li

Fig. 10 Evaluated neutron-production cross section of ^{9}Be bombarded by α-particles together with experimental values

Fig. 11 Thick-target neutron yield of ^{9}Be bombarded by α-particles

Fig. 12 Evaluated partial cross sections for the (α,n) reactions together with experimental values

Fig. 13 Calculated energy spectra of emitted neutrons by the ^{9}Be(α,α'n) reaction

Fig. 14 Evaluated neutron-production cross section of ^{10}B bombarded by α-particles together with experimental values

Fig. 15 Calculated thick-target neutron yield together with the experimental yields measured by Bair and Gomez del Campo[9)]

Fig. 16 Calculated thick-target ^{13}N activity yield of ^{10}B bombarded by α-particles together with the experimental yields measured by Roughton et al.[28)]

Fig. 17 Calculated energy spectra of neutrons emitted by α-particle bombardment of ^{10}B

Fig. 18 Evaluated neutron-production cross section of ^{11}B bombarded by α-particles

Fig. 19 Calculated thick-target neutron yield of ^{11}B bombarded by α-particles together with the experimental yields measured by Bair and Gomez del Campo[9)]

Fig. 20 Evaluated cross sections for the (α,n_0), (α,n_1) and (α,n_2) reactions together with experimental values

Fig. 21 Calculated energy spectra of neutrons emitted by α-particle bombardment of ^{11}B

Fig. 22 Evaluated cross section for the $^{12}C(\alpha,n_0)$ reaction together with the experimental values measured by Black et al.[34)]

Fig. 23 Calculated angular distributions of neutrons emitted by the $^{12}C(\alpha,n_0)$ reaction

Fig. 24 Evaluated neutron-production cross section for the $^{13}C(\alpha,xn)$ reactions together with experimental values

Fig. 25 Calculated thick-target neutron yield of natural carbon bombarded by α-particles together with experimental values

Fig. 26 Cross section for the $^{13}C(\alpha,n_0)$ reaction evaluated on the basis of the cross section[38)] for the inverse reaction $^{16}O(n,\alpha_0)$

Fig. 27 Calculated energy spectra of neutrons emitted by α-particle bombardment of ^{13}C

Fig. 28 Calculated ^{17}F activity production cross section of ^{14}N bombarded by α-particles together with experimental values

Fig. 29 Evaluated neutron-production cross section of ^{14}N bombarded by α-particles (solid line) and breakdown of the cross section (dashed and dot-dashed lines)

Fig. 30 Calculated thick-target ^{17}F yield of ^{14}N bombarded by α-particles together with the experimental values measured by Roughton et al.[28)]

Fig. 31 Calculated energy spectra of neutrons emitted by α-particle bombardment of ^{14}N

Fig. 32 Evaluated neutron-production cross section of ^{15}N bombarded by α-particles

Fig. 33 Calculated thick-target ^{18}F activity yield of ^{15}N bombarded by α-particles together with the experimental values measured by Roughton et al.[28)]

Fig. 34 Calculated energy spectra of neutrons emitted by α-particle bombardment of ^{15}N

Fig. 35 Neutron-production cross section of ^{17}O bombarded by α-particles together with experimental values

Fig. 36 Calculated energy spectra of neutrons emitted by α-particle bombardment of ^{17}O

Fig. 37 Evaluated neutron-production cross section of ^{18}O bombarded by α-particles together with experimental values

Fig. 38 Calculated thick-target neutron yield of UO_2 bombarded by α-particles together with experimental yields

Fig. 39 Calculated energy spectra of neutrons emitted by α-particle bombardment of ^{18}O

Fig. 40 Evaluated neutron-production cross section of ^{19}F bombarded by α-particles compared with experimental values.

Fig. 41 Calculated thick-target neutron yield compared with the experimental yields measured by Bair and Gomez del Campo[9)]
Fig. 42 Evaluated $^{19}F(\alpha,n_0)$ cross section compared with the experimental cross section measured by Van der Zwan and Geiger[45)]
Fig. 43 Calculated energy spectrum of neutrons emitted by α-particle bombardment of ^{19}F
Fig. 44 Evaluated neutron-production cross section of ^{23}Na bombarded by α-particles compared with experimental values
Fig. 45 Calculated thick-target neutron yield compared with the experimental cross sections measured by Norman et al.[46)] which were estimated from Eq. (10)
Fig. 46 Comparison of the evaluated (α,n_0) cross section and the ground-state production cross section deduced by Norman et al.[46)]
Fig. 47 Calculated energy spectrum of neutrons emitted by α-particle bombardment of ^{23}Na
Fig. 48 Evaluated neutron-production cross section of ^{27}Al bombarded by α-particles together with experimental cross sections
Fig. 49 Calculated thick-target neutron yield of ^{27}Al bombarded by α-particles together with experimental yields
Fig. 50 Calculated energy spectra of neutrons emitted by α-particle bombardment of ^{27}Al
Fig. 51 Evaluated neutron-production cross section of ^{28}Si bombarded by α-particles together with experimental cross sections
Fig. 52 Calculated energy spectra of neutrons emitted by α-particle bombardment of ^{28}Si
Fig. 53 Evaluated neutron-production cross section of ^{29}Si bombarded by α-particles together with experimental cross sections
Fig. 54 Calculated energy spectra of neutrons emitted by α-particle bombardment of ^{29}Si
Fig. 55 Evaluated neutron-production cross section of ^{30}Si bombarded by α-particles together with experimental cross sections
Fig. 56 Calculated energy spectra of neutrons emitted by α-particle bombardment of ^{30}Si
Fig. 57 Calculated thick-target neutron yields of natural Si (^{28}Si=92.23%, ^{29}Si=4.67%, ^{30}Si=3.10%) bombarded by α-particles together with experimental yields

TABLES

Table 1 Q-values and threshold energies of the ^{6}Li(α,xn) reactions
Table 2 Level scheme of ^{9}B
Table 3 Q-values and threshold energies of the ^{7}Li(α,xn) reactions
Table 4 Level scheme of ^{10}B
Table 5 Q-values and threshold energies of the ^{9}Be(α,xn) reactions
Table 6 Level scheme of ^{12}C
Table 7 Q-values and threshold energies of the ^{10}B(α,xn) reactions
Table 8 Level scheme of ^{13}N
Table 9 Q-values and threshold energies of the ^{11}B(α,xn) reactions
Table 10 Level scheme of ^{14}N
Table 11 Q-value and threshold energy of the ^{12}C(α,xn) reaction
Table 12 Level scheme of ^{15}O
Table 13 Q-values and threshold energies of the ^{13}C(α,xn) reactions
Table 14 Level scheme of ^{16}O
Table 15 Q-values and threshold energies of the ^{14}N(α,xn) reactions
Table 16 Level scheme of ^{17}F
Table 17 Q-values and threshold energies of the ^{15}N(α,xn) reactions
Table 18 Level scheme of ^{18}F
Table 19 Q-values and threshold energies of the ^{17}O(α,xn) reactions
Table 20 Level scheme of ^{20}Ne
Table 21 Q-values and threshold energies of the ^{18}O(α,xn) reactions
Table 22 Level scheme of ^{21}Ne
Table 23 Q-values and threshold energies of the ^{19}F(α,xn) reactions
Table 24 Level scheme of ^{22}Na
Table 25 Q-values and threshold energies of the ^{23}Na(α,xn) reactions
Table 26 Level scheme of ^{26}Al
Table 27 Q-values and threshold energies of the ^{27}Al(α,xn) reactions
Table 28 Level scheme of ^{30}P
Table 29 Q-value and threshold energy of the ^{28}Si(α,xn) reaction
Table 30 Level scheme of ^{31}S
Table 31 Q-values and threshold energies of the ^{29}Si(α,xn) reactions
Table 32 Level scheme of ^{32}S
Table 33 Q-values and threshold energies of the ^{30}Si(α,xn) reactions
Table 34 Level scheme of ^{33}S

1. Introduction

Nuclear data on neutron-production reactions induced by α-particles are required in the fields of design and operation of nuclear fuel-cycle facilities. Strong α-particles are emitted from trans-uranium nuclides accumulated in irradiated nuclear fuel, and neutrons are produced by the (α,xn) reactions on the light elements which are around the fuel. Intensity of emitted neutrons should be estimated for the safe transportation, storage and reprocessing of spent fuel. Therefore, the (α,xn) reaction data play a significant role from the viewpoints of radiation shielding and criticality safety. The present work was undertaken to provide reliable data on (α,xn) reactions in the ENDF-6 format[1] for the development of nuclear fuel-cycle systems.

In the present report, evaluations of nuclear data, such as neutron production cross sections and emitted neutron energy spectra by α-particle irradiation, are described for 17 nuclides: ^{6,7}Li, ^{9}Be, ^{10,11}B, ^{12,13}C, ^{14,15}N, ^{17,18}O, ^{19}F, ^{23}Na, ^{27}Al and ^{28,29,30}Si in the α-particle energy region below 15 MeV.

2. Evaluation Methods

2.1 Resonance Analysis

Experimental neutron production cross sections for the (α,xn) reaction show resonance structures in the incident α-particle energy region below several MeV and are analyzed with a resonance formula. In the present evaluation work, resonance analysis was made for two purposes. The first purpose is to smooth out the fluctuation of experimental cross sections and to obtain smooth evaluated cross section. For this purpose, the single-level Breit-Wigner formula with energy dependent α-particle and neutron widths is employed. Energy dependence of the width is calculated with the centrifugal barrier penetration factors. The single-level formula cannot yield resonance interference and needs corrections by tracing experimental cross sections in some interference region. The second purpose is to obtain resonance parameters and calculate angular distributions of emitted neutrons. A general many-channel multi-level R-matrix formula is applied to do this, although experimental data are required for every open channel. However, in many of the present cases, only neutron-production cross sections are available and the general R-matrix formula is not applicable. Thus, an approximated R-matrix analysis was employed in the present work.

Under the assumption that the same spin-parity resonance levels have the same ratio of reduced-width amplitudes between reaction channels, the collision matrix is given by[2]

$$U^{J}_{cc'} = \exp[i(\omega_c - \phi_c)]\left[\delta_{cc'} + \frac{\sum_{\lambda} i\Gamma_{\lambda c}^{1/2}\Gamma_{\lambda c'}^{1/2}/(E_\lambda - E)}{1+\sum_{\lambda}(\Delta_\lambda - i\Gamma_\lambda/2)/(E_\lambda - E)}\right]_J \exp[i(\omega_{c'} - \phi_{c'})], \qquad (1)$$

where notations are given in the paper by Lane and Thomas[3]. The general R-matrix theory requires all cross section data of relevant channels, but the above formula can be applied to partial cross section data such as the (α,n_i) reaction leaving a residual nucleus in the *i*-th excited state. The reaction cross section is calculated using the collision matrix, *i.e.*,

$$\sigma_{aa'} = \frac{\pi}{k_a^2}\sum_{Jll'ss'}\frac{2J+1}{(2I_1+1)(2I_2+1)}\left|U^{J}_{cc'}\right|^2 \quad \text{for} \quad a \neq a', \qquad (2)$$

and angular distribution of emitted particles is given by

$$d\sigma_{aa'} = \sum_{s,\tau}\frac{k_a^{-2}}{(2s+1)}\sum_{L} B_L(a's';as)P_L(\cos\theta)d\Omega, \qquad (3)$$

$$B_L(a's';as) = \frac{(-1)^{s'-s}}{4}\sum_{J_1J_2l_1l_2l_1'l_2'} i^{l_1-l_2-L}Z(l_1J_1l_2J_2,sL)\times i^{l_1'-l_2'-L}Z(l_1'J_1l_2'J_2,s'L)$$
$$\times \mathrm{Re}[(U^{J_1}_{a's'l_1'asl_1})^{*}\times U^{J_2}_{a's'l_2'asl_2}] \quad \text{for } a \neq a'. \qquad (4)$$

The ARESCAL code was developed to analyze resonance cross sections in this approximation.

2.2. Multistep Statistical Model

Total neutron-production cross section is divided into reaction-wise cross sections using the statistical multistep-reaction code mEXIFON[4], which is a modified version of the EXIFON code[5]. Modification was made to include deuteron, triton and ^{3}He emissions. The code is capable of calculating cross sections and continuous double-differential spectra of emitted particles with the Kalbach systematics[6]. Since the continuous level density is assumed in the code, discrete levels of a nucleus cannot be dealt with. Partial (α,n_i) cross sections are calculated using the branching ratios described below. For other neutron-emission reactions, such as (α,pn) and (α,α'n) reactions, no partial cross section to a discrete level was calculated, because these reactions proceed predominantly through three-body break up or cascade reaction for light nuclei. In a three-body break up reaction, energy spectra of emitted neutrons are continuous. In a cascade reaction, the residual nucleus after neutron emission is highly excited with a broad level-width in light nuclei and emitted neutrons exhibit continuous energy-spectra.

The other multistep statistical code used in the present work for F, Na, Al and Si is

the EGNASH-2 code[7], which is equipped with level scheme data and level density parameters and can calculate cross sections for discrete levels.

Evaluation of each reaction cross section was made by multiplying the evaluated neutron-production cross section $\sigma_{n,prod}$ minus other cross sections σ_{ex} evaluated based on experimental data by the cross-section ratio R_i calculated with the mEXIFON or EGNASH-2 code:

$$\sigma_{\alpha,x_i n} = (\sigma_{n,prod} - \sigma_{ex}) \times R_i \,, \tag{5}$$

where R_i is defined as a ratio of the calculated (α,x_in) cross section to the calculated neutron-production cross sections minus σ_{ex}. When partial cross sections $\sigma_{\alpha,ni}$ for the (α,n_i) reactions of which experimental data are not available, the cross sections are evaluated by multiplying the evaluated cross section σ_R of the (α,n) reaction by a branching ratio B_j. The quantity σ_R is given by

$$\sigma_R = \sigma_{\alpha,n} - \sum_i \sigma_{\alpha,n_i} \,, \tag{6}$$

where σ_{α,n_i} is the evaluated cross section based on experimental data or other methods such as detailed balance of the inverse reaction. The branching ratio B_j for the (α,n_j) reaction is given by

$$B_j(E_n) = \Gamma_j / \sum_k \Gamma_k \,, \tag{7}$$

where Γ_k stands for a partial width for the (α,n_k) reaction. Assuming constant reduced width, the ratio can be written by

$$B_j(E_n) = \frac{P_{l(j)}(E_n)}{\sum_k P_{l(k)}(E_{nk}) + \int P_{l(m)}(E_{nm})\rho_m(E_x)dE_x} \,, \tag{8}$$

where $P_{l(k)}(E_{nk})$ is the centrifugal barrier penetration factor of neutron of which energy is E_{nk} with the k-th level of the residual nucleus and orbital angular momentum $\ell(k)$. The integral term expresses final continuum states and $\rho_m(E_x)$ is the normalized level density[8] of spin-parity designated by m and an excitation energy E_x.

2.3 Inverse-reaction Cross-Section

The detailed balance principle relates the *A(a,b)B* reaction cross section with the *B(b,a)A* reaction cross section:

$$\frac{\sigma_{A(a,b)B}}{\sigma_{B(b,a)A}} = \frac{k_b^2}{k_a^2} \frac{(2I_B+1)}{(2I_A+1)} \frac{(2I_b+1)}{(2I_a+1)} \,, \tag{9}$$

where k_a and k_b are the wave numbers of incident and outgoing particles a and b, and I_a, I_b, I_A, I_B spins of particles a and b and nuclei A and B, respectively. In the present case,

the $A(\alpha,n_0)B$ reaction cross section is obtained from the $B(n,\alpha_0)A$ reaction cross section using Eq.(9).

2.4 Thick-target Neutron Yield

Generally speaking, thick-target neutron yields are measured with higher accuracy than neutron production cross sections of thin targets. Therefore, it is possible to adjust neutron production cross section so as to reproduce measured thick-target neutron yields. Thick-target neutron yields were measured by Bair et al.[9,10] and West and Sherwood[11] for many elements.

Using neutron production cross section $\sigma_{n,prod}$, thick-target neutron yields for incident α-particle energy E_α are calculated by

$$Y_n(E_\alpha) = N_T \int_0^{E_\alpha} \sigma_{n.prod}(E) / |dE/dx| dE \quad \text{(neutrons/α-particle)}, \qquad (10)$$

where N_T is the atomic density of a target nucleus, and dE/dx is the stopping power of the target for α-particles and given in Ziegler's table[12].

3. Lithium

3.1 ^{6}Li(α,xn) Reaction

3.1.1 Basic Data

The reaction Q-values and threshold energies are given in Table 1 for the neutron emission reactions on ^{6}Li by α-particle bombardment.

Table 1 Q-values and threshold energies of the ^{6}Li(α,xn) reactions

Reaction	Q-value (MeV)	Threshold Energy (MeV)
^{6}Li(α,n)^{9}B	-3.974	6.618
^{6}Li(α,pn)^{8}Be	-3.789	6.310
^{6}Li(α,α'n)^{5}Li	-5.663	9.431

The level scheme of ^{9}B in the present work is given in Table 2. The levels above 4.8 MeV are assumed to be continuum. Continuous levels are assumed for ^{8}Be and ^{5}Li.

Table 2 Level scheme of ^{9}B

Level	E_x(MeV)	Spin-Parity
GS	0.0	3/2-
1st	1.600	1/2+
2nd	2.361	5/2-
3rd	2.788	5/2+
4th	4.800	3/2+

3.1.2. Experimental Data

Relative excitation function of neutron production was measured by Mehta et al.[13] at a forward angle (0+/-7deg.) in the incident α-particle energy E_α from threshold to 15 MeV. They also measured angular distributions at E_α = 10, 12 and 14 MeV. Bochkarev et al.[14] measured the (α,n_0) differential cross sections for several angles at E_α = 8.6 and 11.2 MeV, and then deduced the (α,n_0) reaction cross section at E_α = 8.6, and the (α,n_0), (α,n_1) and (α,n_2) reaction cross sections at E_α =11.2 MeV.

Thick-target neutron yields were measured by Bair and Gomez del Campo[9] in the energy region E_α = 6.0 ~ 9.0 MeV.

3.1.3 Evaluation

(1) Neutron-production Cross Section (MF=3; MT=201)

Relative excitation function measured by Mehta et al. [13] was converted to neutron production cross section by applying smoothly energy-dependent factors which were determined to reproduce thick-target neutron yield data of Bair and Gomez del Campo.[9] Calculated thick-target neutron yields are shown in Fig. 1 together with experimental data.

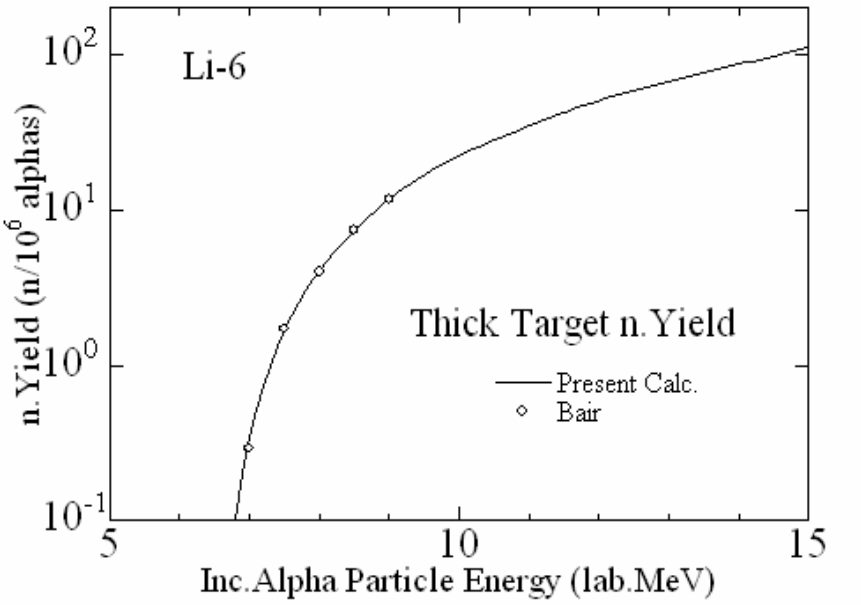

Fig. 1 Thick-target neutron yield of ^{6}Li bombarded by α-particles. Relative forward angle excitation functions measured by Mehta et al.[13] were normalized and adjusted to reproduce the thick-target neutron yields measured by Bair and Gomez del Campo[9].

(2) Cross Sections for the (α,n), (α,pn) and (α,α'n) Reactions (MF=3; MT=4, MT=28 and MT=22)

The cross sections for the (α,n), (α,pn) and (α,α'n) reactions were obtained by

multiplying the neutron-production cross section by individual cross-section ratios calculated with the mEXIFON code.[4] The evaluated cross sections are shown in Fig. 2 compared with the neutron-production cross section deduced from the experimental data by Mehta et al.[13] The (α,α'n) reaction cross section was found to be very small, and it is not shown in the figure.

(3) Partial Cross Sections for the (α,n_i) Reactions (i=0,1,2,3 and continuum) (MF=3; MT=50, MT=51, MT=52, MT=53 and MT=91)

The (α,n) reaction cross section was divided into cross sections for partial reactions which leave residual nuclei in different excited states by applying the branching ratio calculated with Eq. (8). The evaluated cross sections are compared with the experimental values of Bochkarev et al.[14] in Fig. 3.

(4) Energy-angle Distribution of Emitted Neutrons (MF=6; MT=4, MT=22, MT=28)

Relative angular distributions of emitted neutrons measured by Mehta et al.[13] at E_α = 10.0, 12.0 and 14.0 MeV are well reproduced with the Kalbach systematics[6]. The pre-compound fraction which is required in the Kalbach systematics was obtained from the mEXIFON code.[4] As an example, Fig. 4 shows a comparison of calculated and experimental angular distributions at E_α = 10.0 MeV. Figure 5 shows energy spectra of emitted neutrons in the c.m. system. These spectra include contributions of discrete neutrons emitted by the partial (α,n_i) reactions.

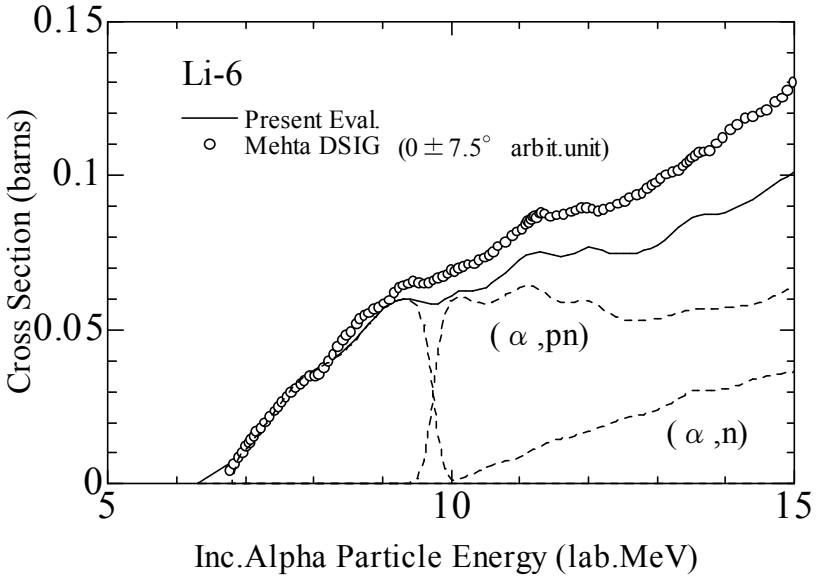

Fig. 2 Neutron-production cross sections of ^{6}Li bombarded by α-particles. Breakdown of the cross section is shown by dashed lines, although the (α,α'n) reaction cross section is not shown since it is very small as compared with other cross sections.

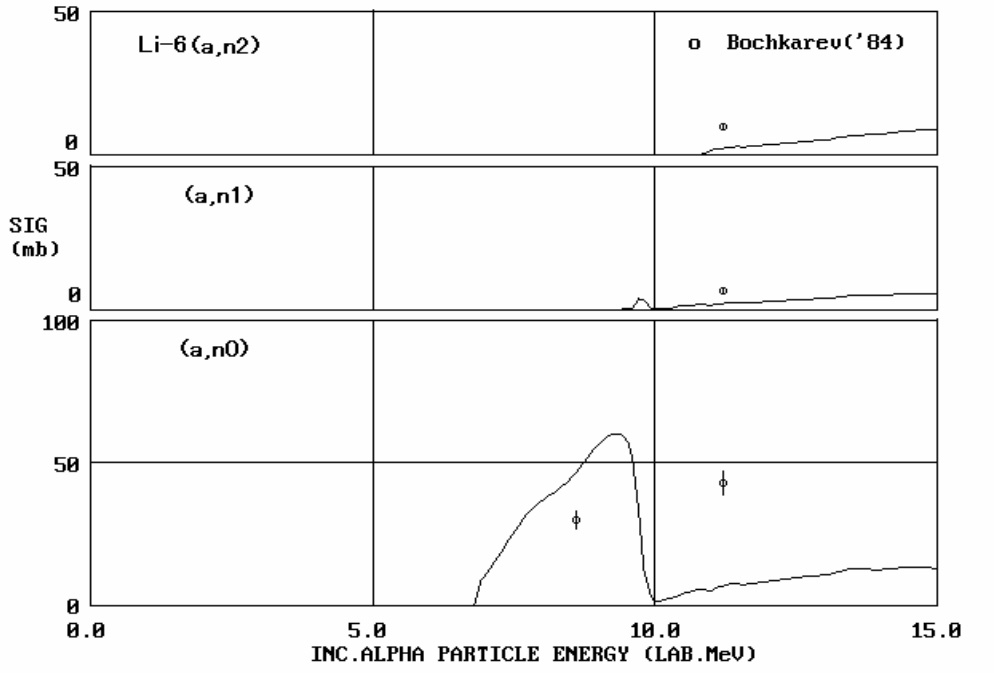

Fig. 3 Comparison of evaluated cross sections for the (α,n_0), (α,n_1) and (α,n_2) reactions with the experimental values measured by Bochkarev et al.[14)]

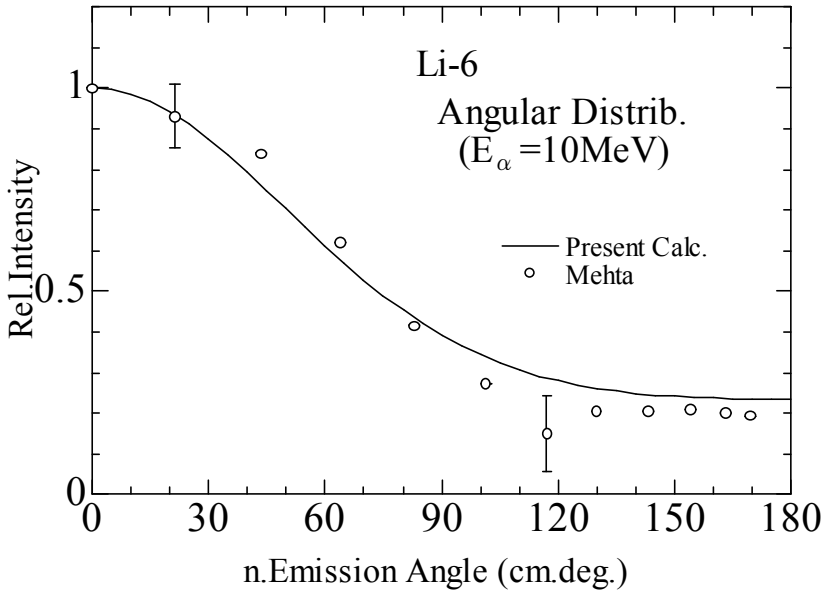

Fig. 4 Calculated relative angular distribution compared with the experimental data measured by Mehta et al.[13)]

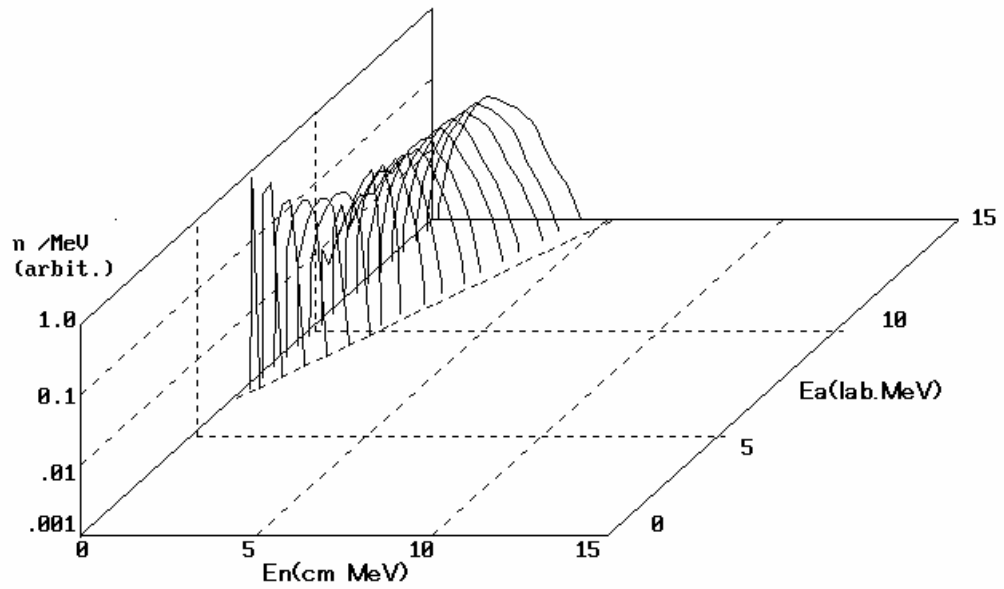

Fig. 5 Calculated energy spectra of neutrons emitted by α-particle bombardment of ^{6}Li. Normalization of spectra was made for each incident α-particle energy E_{α}.

3.2. ^{7}Li(α,xn) Reaction

3.2.1 Basic Data

The reaction Q-values and threshold energies are given in Table 3 for the neutron emission reactions on ^{7}Li by α-particle bombardment.

Table 3 Q-values and threshold energies of the ^{7}Li(α,xn) reactions

Reaction	Q-value (MeV)	Threshold Energy (MeV)
^{7}Li(α,n)^{10}B	-2.790	4.382
^{7}Li(α,pn)^{9}Be	-9.375	14.723
^{7}Li(α,dn)^{8}Be	-8.816	13.846
^{7}Li(α,α'n)^{6}Li	-7.251	11.388

The level scheme of ^{10}B used in the present work is given in Table 4. The levels above 4.774 MeV are assumed to be continuum. Continuous levels are assumed for other residual nuclei.

Table 4 Level scheme of ^{10}B

Level	E_x(MeV)	Spin-Parity
GS	0.0	3+
1st	0.718	1+
2nd	1.740	0+
3rd	2.154	1+
4th	3.587	2+
5th	4.774	3+

3.2.2 Experimental Data

Gibbons and Macklin[15] measured the neutron-production cross section in the incident α-particle energy range E_α < 8.2MeV. Differential cross sections for the (α,n_0), (α,n_1) and (α,n_2) reactions were measured by Van der Zwan and Geiger[16] at E_α = 4.5 ~ 8.0MeV. Mehta et al.[13] measured the differential cross sections for neutron production in the energy range E_α = threshold ~ 15MeV at a forward angle (0+/-15deg.). Sealock et al.[17] measured neutron-production differential cross section at $E_\alpha \leq$ 5.1 MeV, and deduced angle-integrated neutron-production cross section. Olson and Kavanagh[18] measured neutron-production cross section at $E_\alpha \leq$ 5.7 MeV.

Thick-target neutron yields were measured by Bair and Gomez del Campo[9] in the energy region E_α=3.5 ~ 9.0 MeV.

3.2.3 Evaluation

(1) Neutron-production Cross Section (MF=3; MT=201)

In the energy range $E_\alpha \leq$ 5.5 MeV, only the (α,n_0) channel is open, and the most reliable experimental cross section data would be those of Van der Zwan and Geiger[16], who measured the energy spectra of emitted neutrons. In the energy region E_α = 5.5 ~ 8.2 MeV, neutron-production cross sections measured by Gibbons and Macklin[15] are only available. In the energy region E_α = 8 ~ 15 MeV, differential cross sections at a forward angle measured by Mehta et al.[13] were converted to neutron-production cross section by applying smoothly energy-dependent factors which were determined to reproduce thick-target neutron yield data of Bair and Gomez del Campo[9]. The calculated thick-target neutron yields are shown in Fig. 6 compared with experimental data. Figure 7 shows the evaluated neutron-production cross section together with the experimental data by Gibbons and Macklin[15] and by Mehta et al.[13]

(2) Cross Sections for the (α,n), (α,pn), (α,dn) and (α,α'n) Reactions (MF=3; MT=4, MT=28, MT=32 and MT=22)

The cross sections for the (α,n), (α,pn), (α,dn), and (α,α'n) reactions were obtained by multiplying the neutron production cross section by individual cross-section ratios calculated with the mEXIFON code.[4] The calculated cross sections for the

(α,pn) and (α,dn) reactions were found to be fairly small and ignored in the present evaluation. The (α,α'n) reaction cross sections are also small and not shown in Fig. 7.

(3) Partial Cross Sections for the (α,n_i) Reactions (i=0,1,2,3,4 and continuum) (MF=3; MT=50, MT=51, MT=52, MT=53, MT=54 and MT=91)

The (α,n) reaction cross section was divided into partial cross sections by applying the branching ratio calculated with Eq. (8). The evaluated (α,n_0) and (α,n_1) cross sections are compared with the experimental cross sections measured by Van der Zwan and Geiger[16] in Fig. 8.

(4) Energy-angle Distribution of Emitted Neutrons (MF=6; MT=4, MT=22)

Double-differential energy-angle distributions of emitted neutrons were calculated with the mEXIFON code[4] and represented by using the Kalbach systematics[6]. Figure 9 shows energy spectra of emitted neutrons in the c.m. system. These spectra include contributions of discrete neutrons emitted by the partial (α,n_i) reactions.

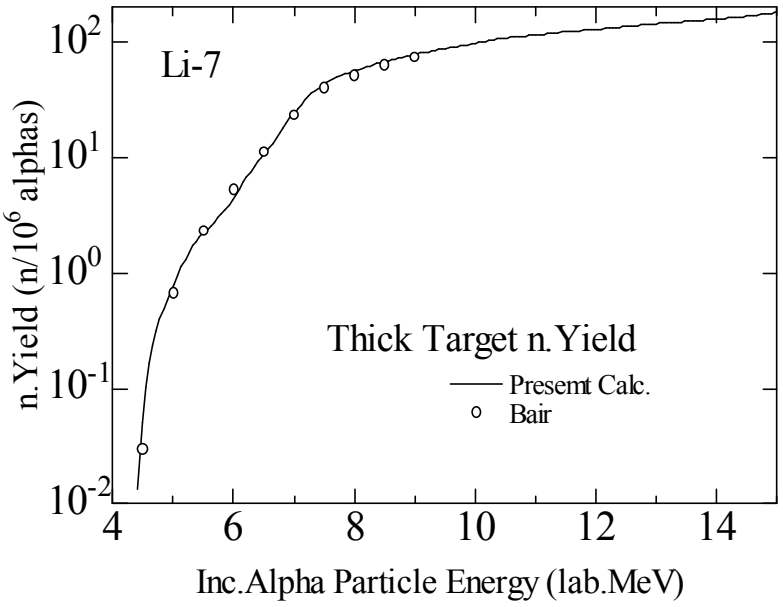

Fig. 6 Calculated thick-target neutron yield of ^{7}Li bombarded by α-particles together with the experimental values measured by Bair and Gomez del Campo[9].

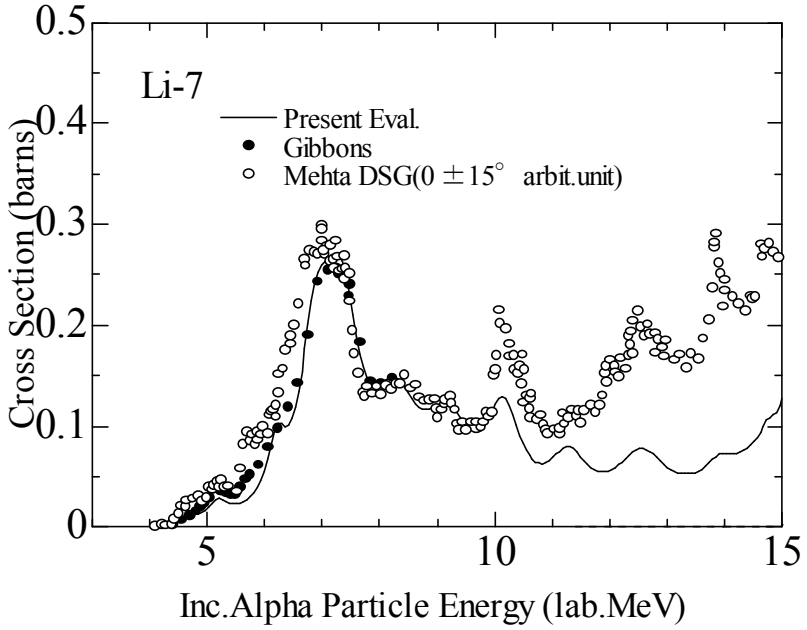

Fig. 7 Neutron-production cross section of ^{7}Li bombarded by α-particles. Experimental values measured by Mehta et al.[13] are relative excitation function at a forward angle.

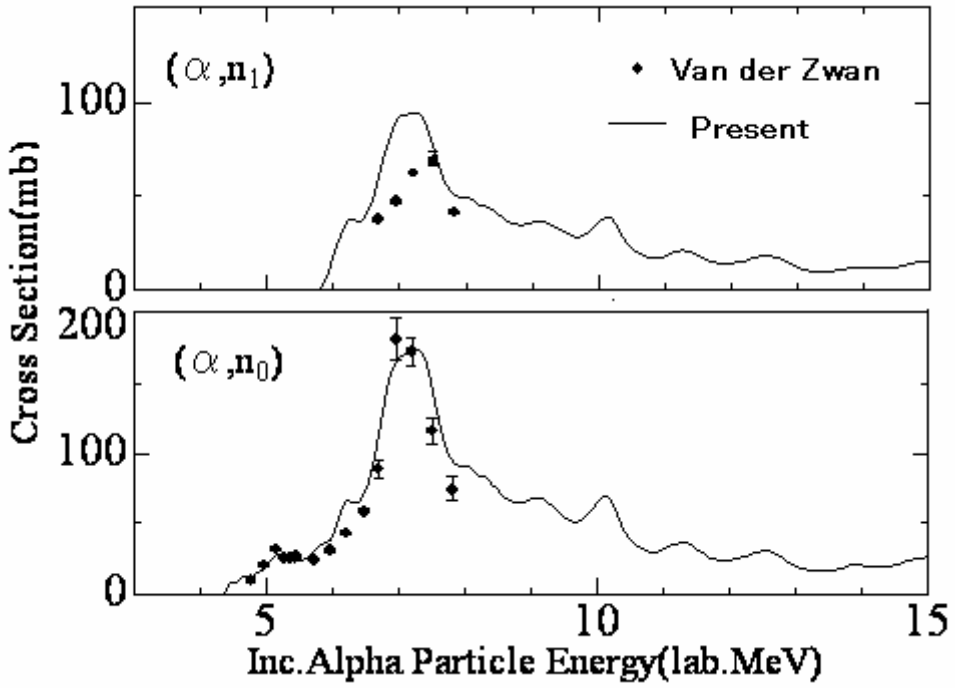

Fig. 8 Comparison of evaluated cross sections for the (α,n_0) and (α,n_1) reactions with the experimental values measured by Van der Zwan and Geiger[16].

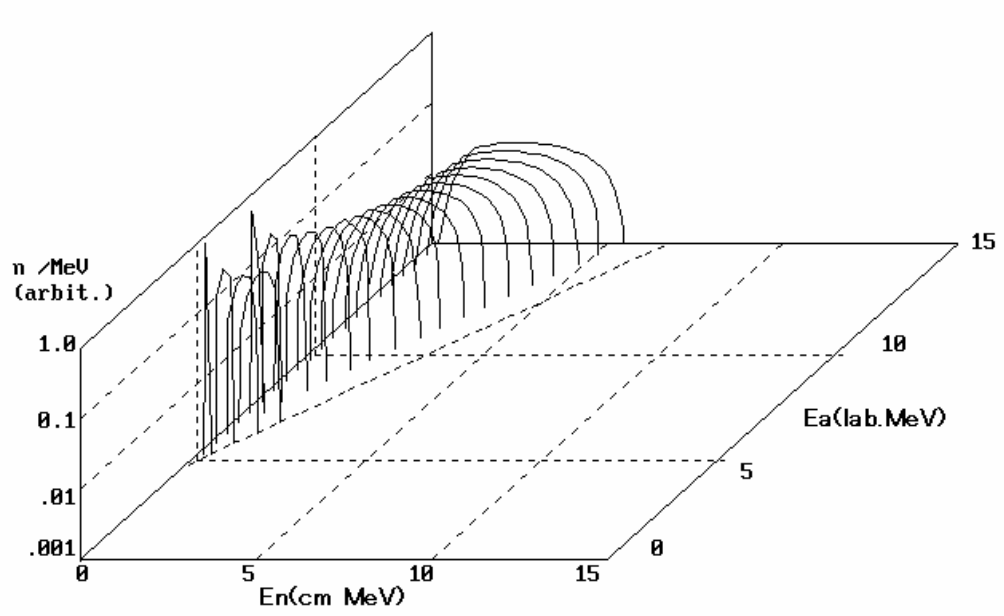

Fig. 9 Calculated energy spectra of neutrons emitted by α-particle bombardment of ^{7}Li. Normalization of spectra was made for each incident α-particle energy E_α.

3.3 Discussion

^{6}Li(α,xn) Reaction

Competing with the (α,pn) reaction, the presently evaluated (α,n) cross section decreases drastically near E_α = 10 MeV and increases slowly for E_α >10 MeV. This tendency seems to be somewhat unnatural. A discrepancy is seen between the calculations and experiments in Fig. 3. Re-evaluation of the breakdown of neutron production cross section seems to be necessary. Experimental angular distributions of emitted neutrons by the ^{6}Li(α,xn) reactions show a strong forward peak in the incident α-particle energy region E_α>10 MeV. In this region, most of neutron emission is caused by the reaction (α,pn) reaction. This may indicate that the reaction occurs through the direct reaction mechanism with the clustering of ^{4}He+D in the ground state of ^{6}Li and the deuteron recoiled by an incident α-particle is dissociated into n+p.

^{7}Li(α,xn) Reaction

Though neutron angular distributions of the (α,n_0) and (α,n_1) reactions were measured by Van der Zwan and Geiger[16], no evaluation was made for these quantities in the present work. Resonance analysis should be made in detail for the evaluation of angular distributions.

4. Beryllium

4.1 ^{9}Be(α,xn) Reaction

4.1.1 Basic Data

The reaction Q-values and threshold energies are given in Table 5 for the neutron

emission reactions on ^{9}Be by α-particle bombardment.

Table 5 Q-values and threshold energies of the ^{9}Be(α,xn) reactions

Reaction	Q-value (MeV)	Threshold Energy (MeV)
^{9}Be(α,n)^{12}C	+5.701	0.0
^{9}Be(α,α'n)^{8}Be	-1.665	2.405

The level scheme of ^{12}C used in the present work is given in Table 6. The levels above 10.3 MeV are assumed to be continuum. Continuous levels are assumed for ^{8}Be.

Table 6 Level scheme of ^{12}C

Level	E_x(MeV)	Spin-Parity
GS	0.0	0+
1st	4.439	2+
2nd	7.654	0+
3rd	9.641	3-
4th	10.3	0+

4.1.2 Experimental Data

Gibbons and Macklin[19] measured neutron-production cross section in the energy range E_α = 1.7 ~ 10.3 MeV. Van der Zwan and Geiger[20] measured differential cross sections for the (α,n_0), (α,n_1) and (α,n_2) reactions and deduced cross sections for these reactions at E_α = 1.5 ~ 7.8 MeV. Obst et al.[21] measured differential cross sections for the (α,n_0), (α,n_1) and (α,n_2) reactions at E_α = 1.7 ~ 6.4 MeV. They also measured the double-differential cross sections for the (α,α'n) reaction and deduced the reaction cross section which corresponds to the emission of neutrons of which energy is greater than 0.5 MeV. In low energy region E_α = 150 keV ~ 1.2 MeV, Wrean et al.[22] measured neutron-production cross sections at fine energy intervals. Cross-section measurements were also made by Kunz et al.[23] for the (α,n_0) and (α,n_1) reactions at E_α = 366 keV ~ 3.552 MeV.

Thick-target neutron yields were measured by Bair and Gomez del Campo[9] in the energy region E_α=3.0 ~ 9.0 MeV. The yields were also measured by West and Sherwood[11] in the energy range E_α=4.0 ~ 10.8 MeV.

4.1.3 Evaluation

(1) Neutron-production Cross Section (MF=3; MT=201)

The neutron-production cross section was evaluated based on the experimental data by Gibbons and Macklin[19] in the energy range E_α = 1.7 ~ 10 MeV, and on the data by Wrean et al.[22] and by Kunz et al.[23] in E_α < 3.5 MeV. In the energy region above

10 MeV, the cross section was calculated with the mEXIFON code[4]. Normalization was made so that the calculations could reproduce experimental data below 10 MeV. Furthermore, the cross section was modified so as to reproduce experimental thick-target neutron yields. Figure 10 shows the evaluated neutron-production cross section and (α,α'n) cross section together with experimental data. The calculated thick-target neutron yields are shown in Fig. 11.

(2) Cross Sections for the (α,n) and (α,α'n) Reactions (MF=3; MT=4 and MT=22)

The (α,α'n) reaction cross section calculated with the mEXIFON code[4] was normalized to the experimental data measured by Obst et al. [21] The (α,n) reaction cross section was obtained by subtracting the (α,α'n) reaction cross section from the neutron production cross section.

(3) Partial Cross Sections for the (α,n_i) Reactions (i=0,1,2,3 and continuum) (MF=3; MT=50, MT=51, MT=52, MT=53 and MT=91)

The (α,n) reaction cross section was divided into partial cross sections by the experimental ratios obtained from the data of Van der Zwan and Geiger[20] at $E_\alpha < 7.8$ MeV. In the energy region $E_\alpha > 7$ MeV, the (α,n_0) cross section was determined from the cross section for the inverse reaction $^{12}C(n,\alpha_0)^9Be$ in JENDL-3.2[24]. Resonance analyses were made for these cross sections and the cross sections were calculated above 7.8 MeV with the same resonance parameters obtained. The cross section to the continuum final state was obtained by subtracting other partial cross sections from the total (α,n) reaction cross section. The evaluated partial (α,n_i) cross sections are shown in Fig. 12 together with experimental data.

(4) Energy-angle Distribution of Emitted Neutrons (MF=6; MT=22, MT=50, 51, 52, 53, 91)

Energy-angle distributions of emitted neutrons by the (α,α'n) reaction were calculated with the mEXIFON code[4] and represented by using the Kalbach systematics[6]. The calculated neutron spectra for the (α,α'n) reaction are illustrated in Fig. 13. Those for the (α, n) reaction to continuum states were also given by the Kalbach systematics.

Angular distributions of neutrons emitted from discrete levels were given in the form of Legendre-polynomial expansion coefficients which were obtained using the experimental angular distributions measured by Obst et al.[21] in the energy region where experimental data are available. In the energy region where the experimental data are not available, Legendre coefficients were calculated using the resonance parameters obtained in the previous subsection.

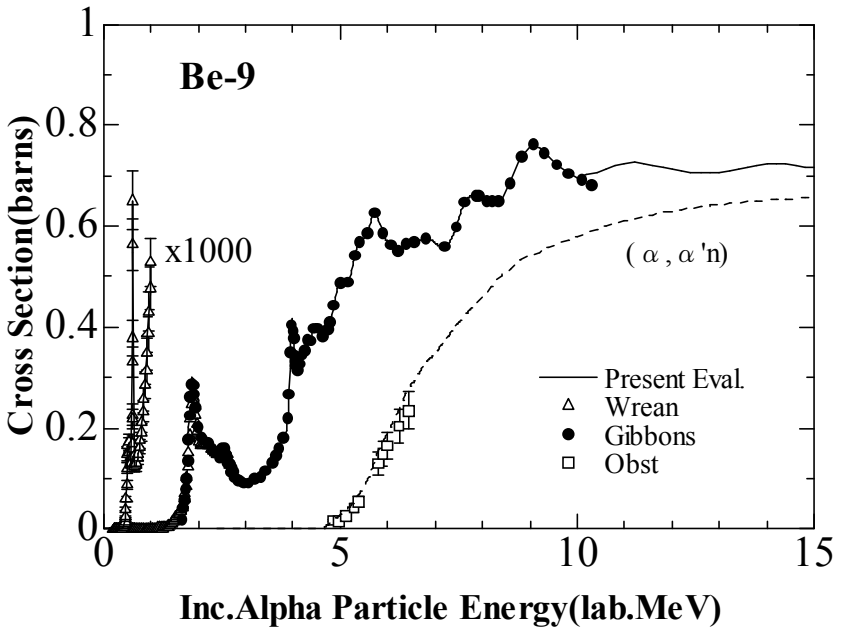

Fig. 10 Evaluated neutron-production cross section of ^{9}Be bombarded by α-particles together with experimental values. The evaluated cross section for (α,α'n) reaction is also compared with the experimental data by Obst et al.[21)]

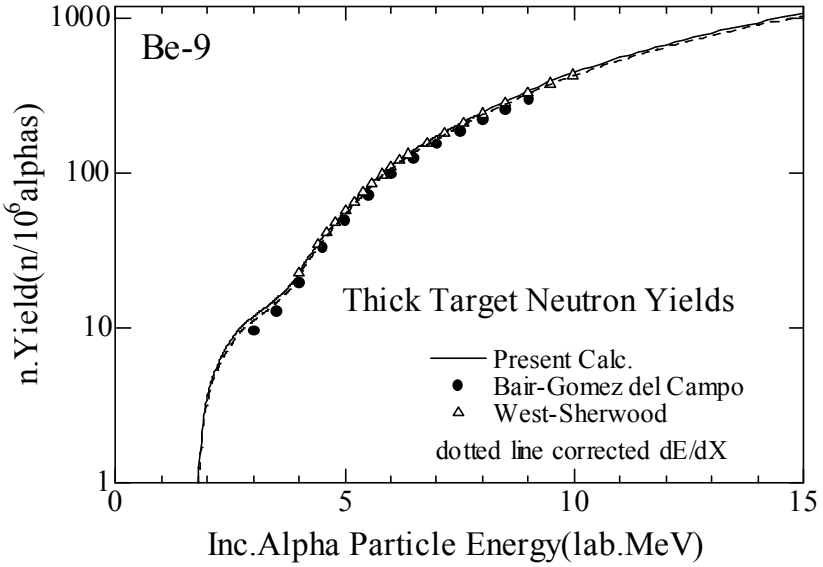

Fig. 11 Thick-target neutron yield of ^{9}Be bombarded by α-particles. The dashed line shows the calculation using the corrected stopping power dE/dX given by Wrean et al.[22)]

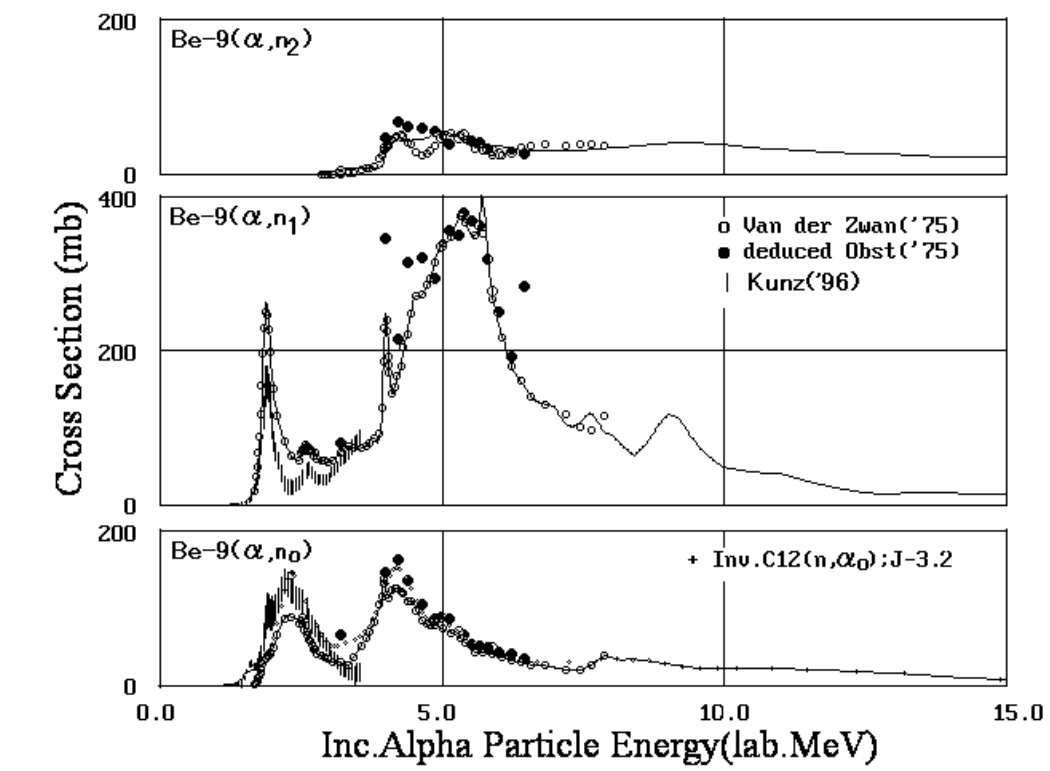

Fig. 12 Evaluated partial cross sections for the (α,n) reactions together with experimental values.

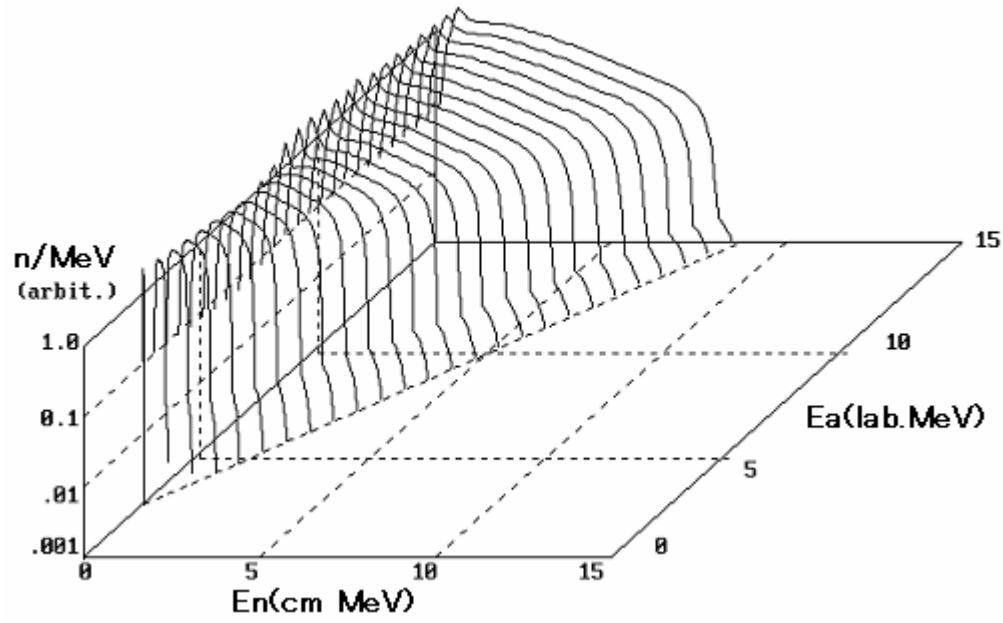

Fig. 13 Calculated energy spectra of emitted neutrons by the ^{9}Be(α,α'n) reaction. Normalization of spectra was made for each incident α-particle energy Ea.

4.2 Discussion

Neutron energy spectra from an ^{241}Am-Be neutron source were measured by Marsh et al.[25] with a high resolution ^{3}He sandwich spectrometer. The spectra reflect individual cross sections for the ^{9}Be(α,xn) reactions and emitted neutron angular distributions, and should be analyzed as an integral test of these quantities below $E_\alpha \approx$ 5.5 MeV. Harano et al.[26] are analyzing the spectra by using a newly developed code and the presently evaluated data. As a result of the analysis, some improvements of the evaluated data might be necessary.

5. Boron

5.1 ^{10}B(α,xn) Reaction

5.1.1 Basic Data

The reaction Q-values and threshold energies are given in Table 7 for the neutron emission reactions on ^{10}B by α-particle bombardment.

The level scheme of ^{13}N used in the present work is given in Table 8. The levels above 6.885 MeV are assumed to be continuum. Continuous levels are assumed for other residual nuclei.

Table 7 Q-values and threshold energies of the ^{10}B(α,xn) reactions

Reaction	Q-value (MeV)	Threshold Energy (MeV)
^{10}B(α,n)^{13}N	+1.059	0.0
^{10}B(α,pn)^{12}C	-0.885	1.238
^{10}B(α,α'n)^{9}B	-8.436	11.809

Table 8 Level scheme of ^{13}N

Level	E_x(MeV)	Spin-Parity
GS	0.0	1/2-
1st	2.365	1/2+
2nd	3.511	3/2-
3rd	3.547	5/2+
4th	6.364	5/2+

5.1.2 Experimental Data

Gibbons and Macklin[15] measured neutron-production cross section in the incident energy range E_α = 2.55 ~ 4.83 MeV. Van der Zwan and Geiger[27] measured the (α,n_0), (α,n_1) and (α,n_2+n_3) differential cross sections at 2 or 3 angles in the energy range E_α = 1.0 ~ 5.0 MeV.

Thick-target neutron yields were measured by Bair and Gomez del Campo[9] in the energy region E_α=3.5 to 7.5 MeV. Roughton et al.[28] measured thick-target ^{13}N activity

yield in the energy range E_α=3.2 ~ 14.2MeV.

5.1.3 Evaluation

(1) Neutron-production Cross Section (MF=3; MT=201)

The evaluated neutron-production cross section was produced based on the experimental data measured by Gibbons and Maclin[15] in the energy region below E_α = 5.0 MeV. Above E_α = 5.0 MeV, no experimental cross section was available, so the cross section was calculated with the mEXIFON code[4] using the normalization constants obtained below E_α = 5.0 MeV where experimental data were available. Then, the cross section was adjusted so as to reproduce experimental thick-target neutron yields. The evaluated neutron-production cross section and calculated thick-target neutron yields are shown in Figs. 14 and 15, respectively.

(2) Cross Sections for the (α,n), (α,pn) and (α,α'n) Reactions (MF=3; MT=4,MT=28 and MT=22)

The cross sections for the (α,n), (α,pn) and (α,α'n) reactions were obtained by applying each cross section ratio calculated with the mEXIFON code[4] to the neutron-production cross section.

(3) Partial Cross Sections for the (α,n_i) Reactions (i=0,1,2,3,4 and continuum) (MF=3; MT=50, MT=51, MT=52, MT=53, MT=54 and MT=91)

The (α,n_i) cross sections were obtained by applying the branching ratios calculated using Eq. (8) to the evaluated (α,n) cross section. The ^{13}N excited states above the 1st excited state mostly decay to ^{12}C by proton emission, so, the ^{13}N activity production cross section is almost equal to the (α,n_0) cross section. The calculated cross section for the (α,n_0) cross section was adjusted to reproduce the thick-target ^{13}N activity yield measured by Roughton et al.[28] The calculated thick-target ^{13}N activity yield is shown in Fig. 16 together with experimental data.

(4) Energy-angle Distribution of Emitted Neutrons (MF=6; MT=4, MT=22 and MT=28)

Double-differential energy-angle distributions of emitted neutrons were calculated with the mEXIFON code[4] and represented by using the Kalbach systematics[6]. Figure 17 shows the calculated energy spectra of emitted neutrons. These spectra include contributions of discrete neutrons emitted by the partial (α,n_i) reactions.

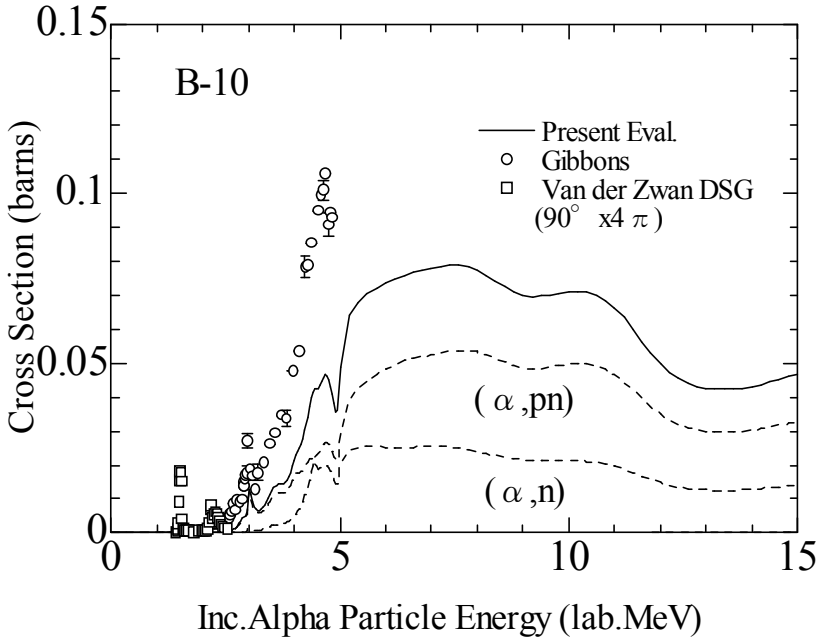

Fig. 14 Evaluated neutron-production cross section of ^{10}B bombarded by α-particles together with experimental values. Breakdown of the cross section is also shown by the dashed lines.

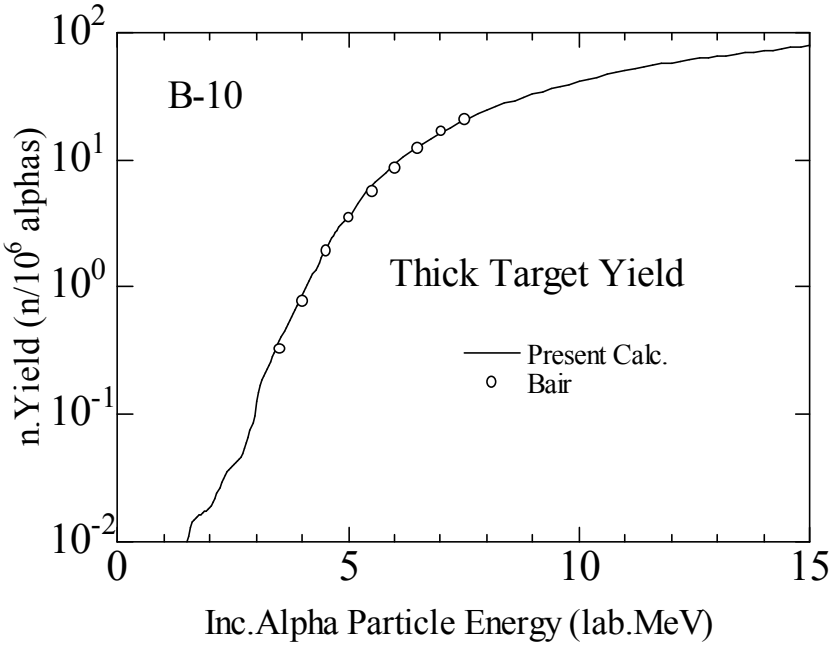

Fig. 15 Calculated thick-target neutron yield together with the experimental yields measured by Bair and Gomez del Campo[9)]

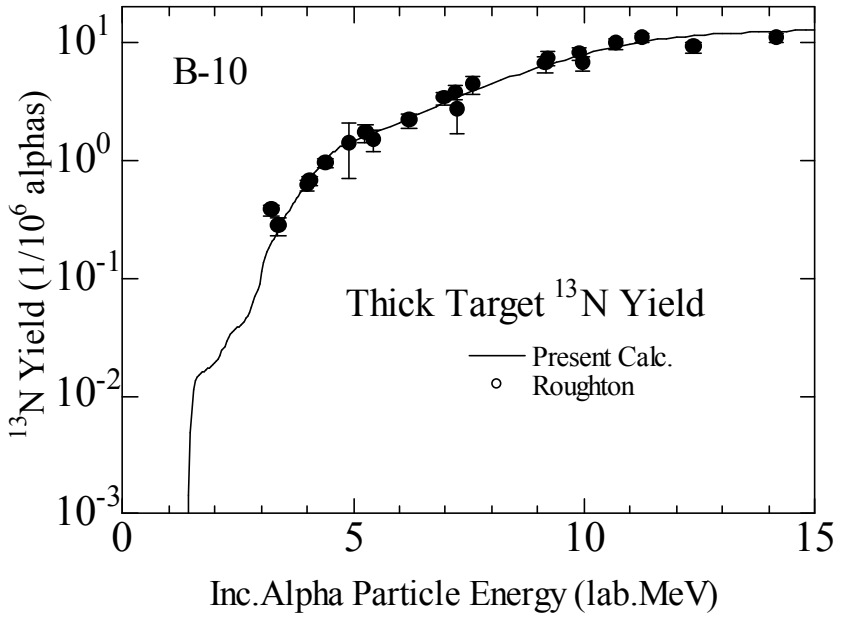

Fig. 16 Calculated thick-target ^{13}N activity yield of ^{10}B bombarded by α-particles together with the experimental yields measured by Roughton et al. [28)]

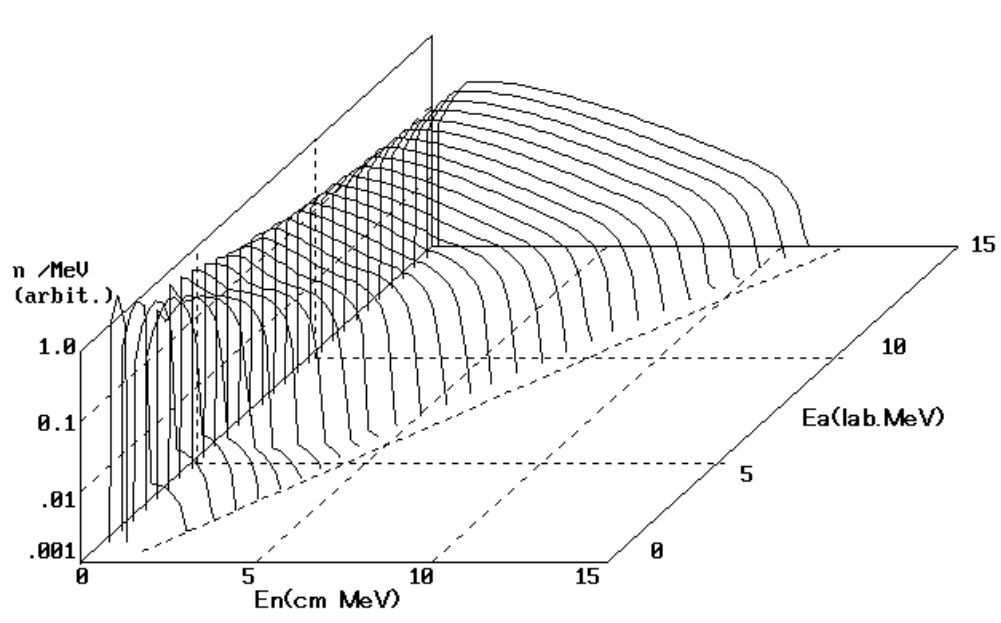

Fig. 17 Calculated energy spectra of neutrons emitted by α-particle bombardment of ^{10}B. Normalization of spectra was made for each incident α-particle energy Ea.

5.2 ^{11}B(α,xn) Reaction

5.2.1 Basic Data

The reaction Q-values and threshold energies are given in Table 9 for the neutron emission reactions on ^{11}B by α-particle bombardment.

The level scheme of ^{14}N used in the present work is given in Table 10. The levels above 5.690 MeV are assumed to be continuum. Continuous levels are assumed for other residual nuclei.

Table 9 Q-values and threshold energies of the ^{11}B(α,xn) reactions

Reaction	Q-value (MeV)	Threshold Energy (MeV)
^{11}B(α,n)^{14}N	+0.158	0.0
^{11}B(α,pn)^{13}C	-7.392	10.080
^{11}B(α,dn)^{13}N	-10.114	13.791
^{11}B(α,2n)^{13}N	-10.395	14.175

Table 10 Level scheme of ^{14}N

Level	E_x(MeV)	Spin-Parity	Isospin
GS	0.0	1+	0
1st	2.313	0+	1
2nd	3.948	1+	0
3rd	4.915	0-	0
4th	5.106	2-	0

5.2.2 Experimental Data

Van der Zwan and Geiger[29] measured differential cross sections for the (α,n_0), (α,n_1) and (α,n_2) reactions in the energy range E_α = 3.7 ~ 7.9 MeV and deduced the cross sections for each reaction. Bonner et al.[30] measured differential cross sections at angle range of 0~20 degrees and 70 ~110 degrees in the incident energy range E_α = 1.95 ~ 5.25 MeV. Niecke et al.[31] measured neutron-production cross section in the energy range E_α = 1.4 ~ 2.2 MeV. Kjellman[32] measured angular distributions of neutrons for the (α,n_0) and (α,n_2) reactions at E_α = 13.5 and 13.9 MeV. Mani and Dutt[33] measured differential cross sections for the (α,n_0) and (α,n_1) reactions at a forward angle in the energy range E_α = 2.4 ~ 4.4 MeV.

Thick-target neutron yields were measured by Bair and Gomez del Campo[9] in the energy region E_α = 3.5 to 7.5 MeV.

5.2.3 Evaluation

(1) Neutron-production Cross Section (MF=3; MT=201)

A sum of the experimental cross sections for the (α,n_0), (α,n_1) and (α,n_2) reactions measured by Van der Zwan and Geiger[29] almost corresponds to the neutron-production

cross section in the energy range E_α = 3.7 ~ 7.9 MeV. Below E_α = 3.7 MeV, the (α,n_1) reaction cross section is quite small because of the isospin selection rule and the neutron-production cross section is dominated by the (α,n_0) reaction cross section, which is calculated with the detailed balance formula from the $^{14}N(n,\alpha_0)^{11}B$ reaction cross section of JENDL-3.2[24]. In the energy range E_α > 8.0 MeV, the neutron-production cross section was calculated with the mEXIFON code[4] using the normalization constants obtained below E_α = 8.0 MeV where experimental data were available. The evaluated neutron-production cross section and calculated thick-target neutron yield are shown in Figs. 18 and 19, respectively.

(2) Cross Sections for the (α,n), (α,2n) and (α,pn) reactions (MF=3; MT=4, MT=16 and MT=28)

The cross sections for the (α,n), (α,2n) and (α,pn) reactions were obtained by applying each cross-section ratio calculated with the mEXIFON code[4] to the neutron-production cross section. The calculated (α,dn) cross section was found to be quite small and ignored.

(3) Partial Cross Sections for the (α,n_i) Reactions (i=0,1,2,3,4 and continuum) (MF=3; MT=50, MT=51, MT=52, MT=53, MT=54 and MT=91)

The (α,n_0) reaction cross section was obtained from the cross section for the inverse reaction $^{14}N(n,\alpha_0)^{11}B$ contained in JENDL-3.2[24]. Other cross sections were obtained by resonance analyses of the experimental cross sections measured by Van der Zwan and Geiger[29] in the energy region below E_α = 8.0 MeV. Above E_α = 8.0 MeV, the (α,n_i) cross sections were obtained by applying the branching ratios calculated with Eq. (8) to the evaluated (α,n) cross section and adjusted to connect smoothly to the cross sections below E_α=8.0 MeV. Figure 20 shows the (α,n_0), (α,n_1) and (α,n_2) reaction cross sections together with experimental values including the ones obtained from the inverse-reaction cross section.

(4) Energy-angle Distribution of Emitted Neutrons (MF=6; MT=4, MT=16 and MT=28)

Double-differential energy-angle distributions of emitted neutrons were calculated with the mEXIFON code[4] and represented by using the Kalbach systematics[6]. Figure 21 shows the calculated energy spectra of emitted neutrons. These spectra include contributions of discrete neutrons emitted by the partial (α,n_i) reactions.

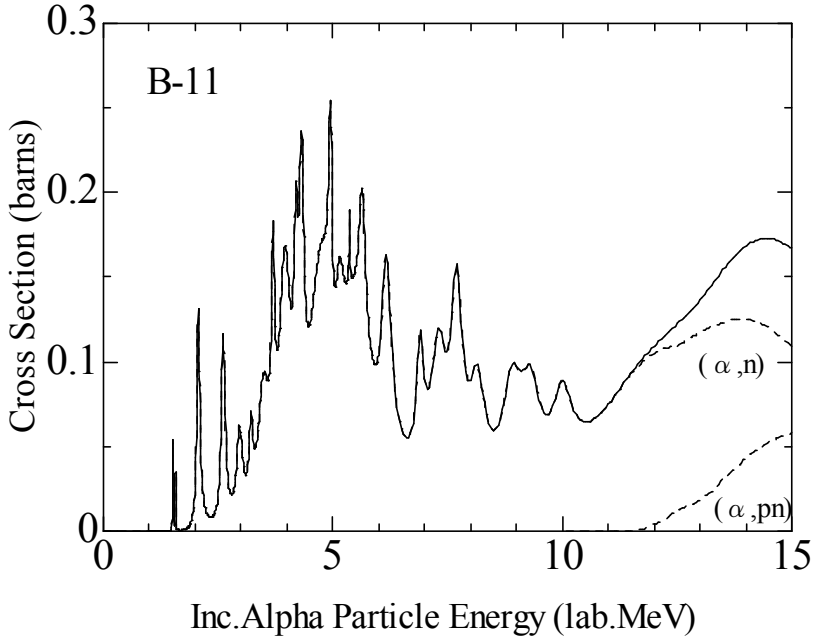

Fig. 18 Evaluated neutron-production cross section of ^{11}B bombarded by α-particles. Breakdown of the cross section is also shown by the dashed lines.

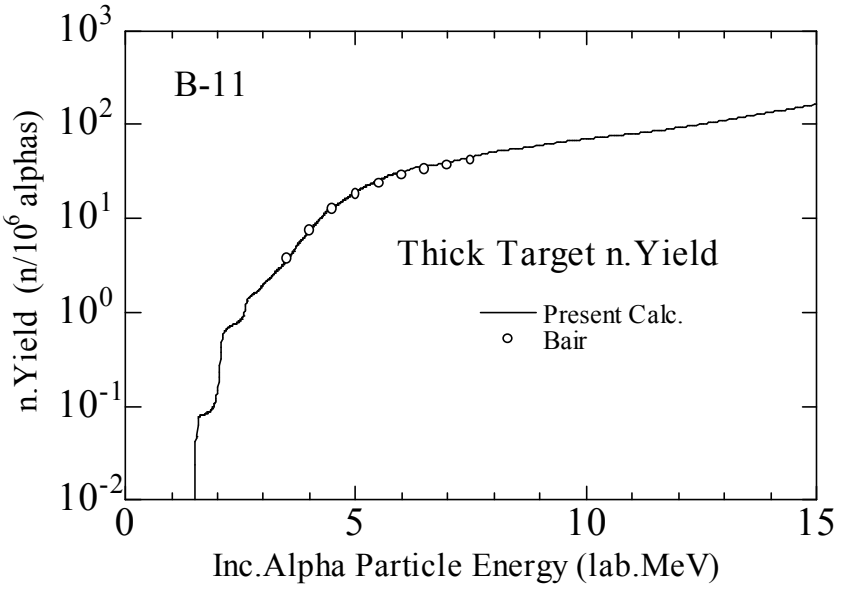

Fig 19 Calculated thick-target neutron yield of ^{11}B bombarded by α-particles together with the experimental yields measured by Bair and Gomez del Campo[9)]

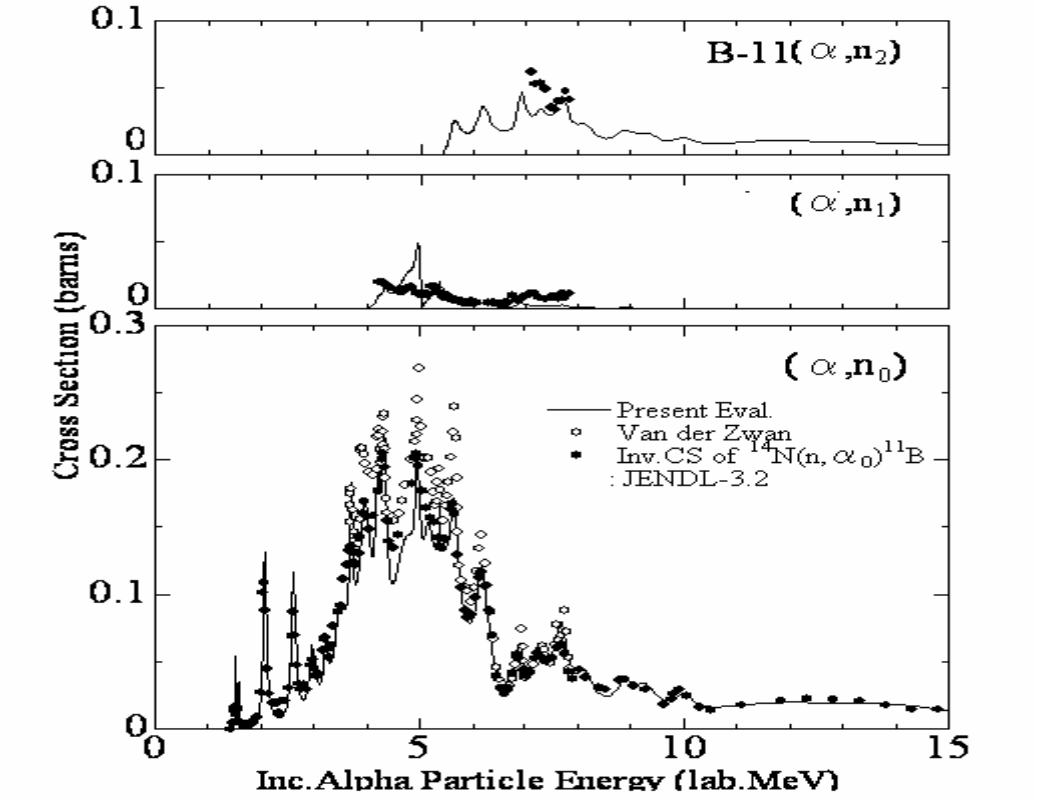

Fig. 20 Evaluated cross sections for the (α,n_0), (α,n_1) and (α,n_2) reactions together with experimental values. For the (α,n_0) reaction, the cross section obtained from the inverse reaction ^{14}N(n,α_0) contained in JENDL-3.2 is also shown.

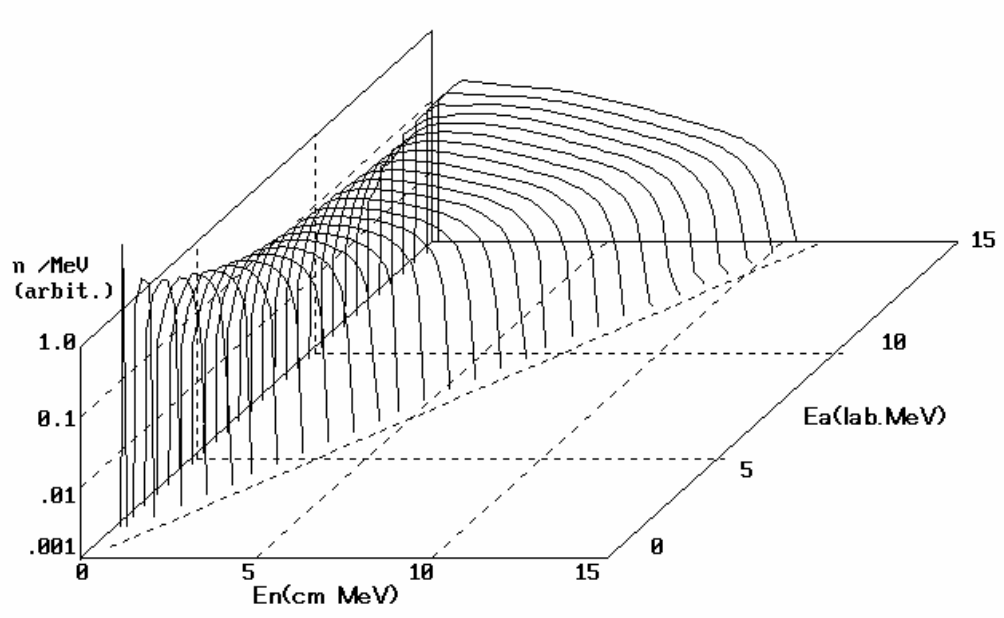

Fig. 21 Calculated energy spectra of neutrons emitted by α-particle bombardment of ^{11}B. Normalization of spectra was made for each incident α-particle energy Ea.

5.3 Discussion

^{10}B(α,xn) Reaction

As is shown in Fig. 14 for neutron-production cross section, the experimental data measured by Gibbons and Macklin[15] are about two times larger than the present evaluated cross section which was determined so as to reproduce thick-target neutron yield data. The reason for this discrepancy is not clear.

6. Carbon

6.1 ^{12}C(α,xn) Reaction

6.1.1 Basic Data

The reaction Q-value and threshold energy are given in Table 11 for the neutron emission reaction on ^{12}C by α-particle bombardment.

Table 11 Q-value and threshold energy of the ^{12}C(α,xn) reaction

Reaction	Q-value (MeV)	Threshold Energy (MeV)
^{12}C(α,n)^{15}O	-8.502	11.338

The level scheme of ^{15}O used in the work is given in Table 12. Only the ground state of ^{15}O is energetically reached by the ^{12}C(α,xn) reaction for incident α-particle energy below 15 MeV.

Table 12 Level scheme of ^{15}O

Level	E_x(MeV)	Spin-Parity
GS	0.0	1/2-

6.1.2 Experimental Data

Black et al.[34] measured ^{15}O production cross section in the incident α-particle energy range E_α = threshold ~ 22.65 MeV. Natural carbon thick-target neutron yields were measured by Bair[10] at E_α = 2.0 ~ 9.0 MeV and by West and Sherwood[11] at E_α = 3.6 ~ 10.0 MeV.

6.1.3 Evaluation

(1) Neutron-production Cross Section (MF=3; MT=201)

Experimental ^{15}O production cross section measured by Black et al.[34] corresponds exactly to the ^{12}C(α,n_0) reaction cross section, which is also equal to neutron-production cross section in the energy range $E_\alpha \leq 15$ MeV. The cross section was analyzed with the ARESCAL code. Figure 22 shows the evaluated cross section for the ^{12}C(α,n_0) reaction together with experimental values.

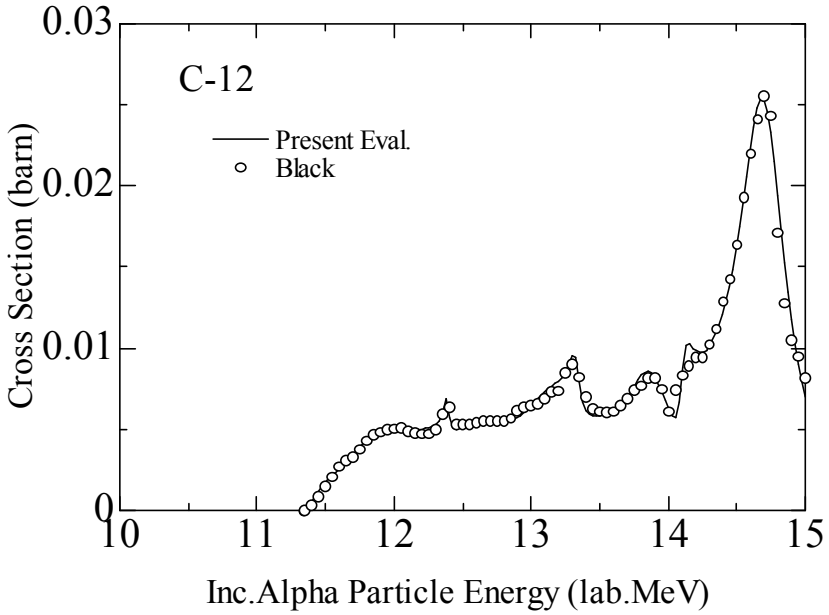

Fig. 22 Evaluated cross section for the $^{12}C(\alpha,n_0)$ reaction together with the experimental values measured by Black et al. [34)]

(2) Partial Cross Sections for the (α,n_i) Reactions (i=0) (MF=3; MT=50)

We adopted the same cross section described above.

(3) Energy-angle Distribution of Emitted Neutrons (MF=6; MT=50)

Angular distributions for the (α,n_0) reaction were calculated with the ARESCAL code using the resonance parameters obtained in the above analysis and are given in the form of Legendre-polynomial expansion coefficients. The evaluated distributions are shown in Fig. 23.

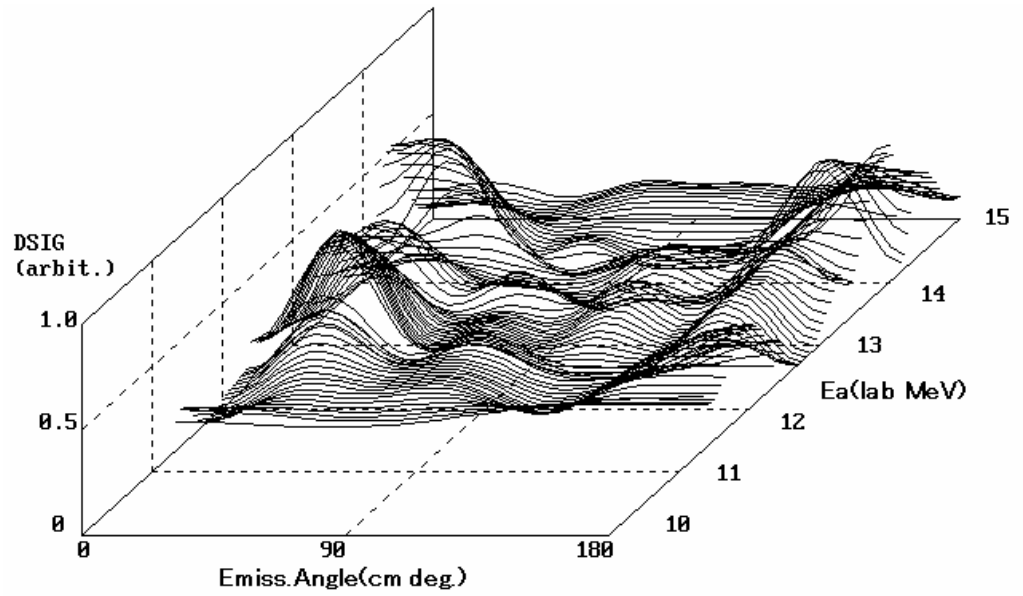

Fig. 23 Calculated angular distributions of neutrons emitted by the $^{12}C(\alpha,n_0)$ reaction. Normalization was made for each distribution at each α-particle energy Ea.

6.2 $^{13}C(\alpha,xn)$ Reaction

6.2.1 Basic Data

The reaction Q-values and threshold energies are given in Table 13 for the neutron emission reactions on ^{13}C by α-particle bombardment.

The level scheme of ^{16}O used in the present work is given in Table 14. The levels above 8.872 MeV are assumed to be continuum. Continuous levels are assumed for other residual nuclei.

Table 13 Q-values and threshold energies of the $^{13}C(\alpha,xn)$ reactions

Reaction	Q-value (MeV)	Threshold Energy (MeV)
$^{13}C(\alpha,n)^{16}O$	+2.216	0
$^{13}C(\alpha,\alpha'n)^{12}C$	-4.946	6.469
$^{13}C(\alpha,pn)^{15}N$	-9.912	12.963

Table 14 Level scheme of ^{16}O

Level	E_x(MeV)	Spin-Parity
GS	0.0	0+
1st	6.049	0+
2nd	6.130	3-
3rd	6.917	2+
4th	7.117	1-

6.2.2 Experimental Data

Sekharan et al.[35] measured neutron-production cross section in the energy range E_α = 1.9~5.6 MeV. Bair and Haas[36] measured the $^{13}C(\alpha,n)$ cross section at E_α=1.0~5.4 MeV. Bonner et al.[30] measured differential neutron-production cross sections at emission angles of 0 ~ 10 deg. and 80 ~ 100 deg. in the incident energy E_α = 2.0 ~ 5.0 MeV. Drotleff et al.[37] measured the neutron-production cross section in the incident energy E_α = 0.28 ~ 1.06 MeV.

Natural carbon thick-target neutron yields were measured by Bair[10] at E_α = 2.0 ~ 9.0 MeV and by West and Sherwood[11] at E_α = 3.6 ~ 10.0 MeV. Though the target is a natural carbon, ^{12}C does not contribute to neutron yields below 10 MeV.

6.2.3 Evaluation

(1) Neutron-production Cross Section (MF=3; MT=201)

Below 5.6 MeV, evaluation of the cross section was made based on experimental data. In the energy region E_α = 5.6 ~ 10 MeV, the cross section was determined on the basis of the experimental data on thick-target neutron yields. Above 10 MeV, the shape of the cross section was determined by the energy dependence of the reaction cross section calculated with the optical model using small imaginary potential.

Normalization was made so that the calculations could reproduce experimental data below 10 MeV. Figure 24 shows the evaluated neutron-production cross section together with experimental data. The thick-target neutron yield of natural carbon including 1.1% ^{13}C was calculated and is shown in Fig. 25.

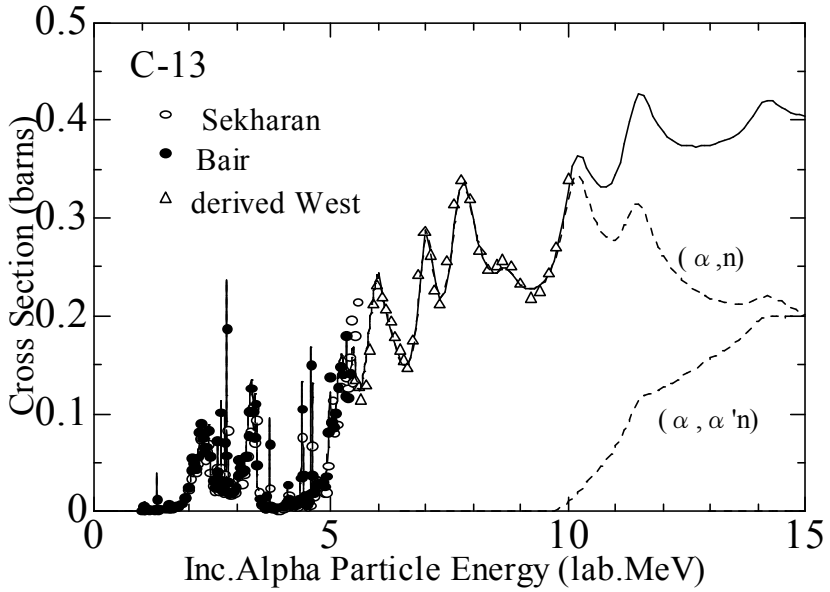

Fig. 24 Evaluated neutron-production cross section for the $^{13}C(\alpha,xn)$ reactions together with experimental values. Breakdown of the cross section is shown by the dashed lines.

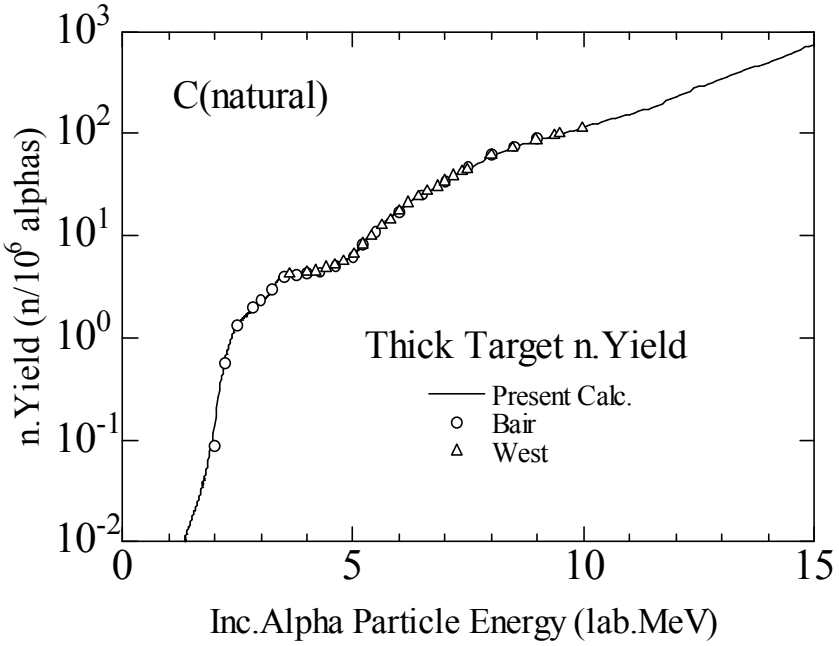

Fig. 25 Calculated thick-target neutron yield of natural carbon bombarded by α-particles together with experimental values.

(2) Cross Sections for the (α,n), (α,α'n) and (α,pn) Reactions (MF=3; MT=4, MT=22 and MT=28)

The cross sections for the (α,n), (α,α'n) and (α,pn) reactions were obtained by applying each cross section ratio calculated with the mEXIFON code[4] to the neutron production cross section.

(3) Partial Cross Sections for the (α,n_i) reactions (i=0,1,2,3,4 and continuum) (MF=3; MT=50, MT=51, MT=52, MT=53, MT=54 and MT=91)

The (α,n_0) reaction cross section was obtained from the cross section for the inverse reaction $^{16}O(n,\alpha_0)^{13}C$ contained in ENDF/B-VI[38] and is shown in Fig. 26. For other (α,n_i) reactions, the cross sections were obtained by applying the branching ratios calculated with Eq. (8) to the evaluated (α,n) cross section.

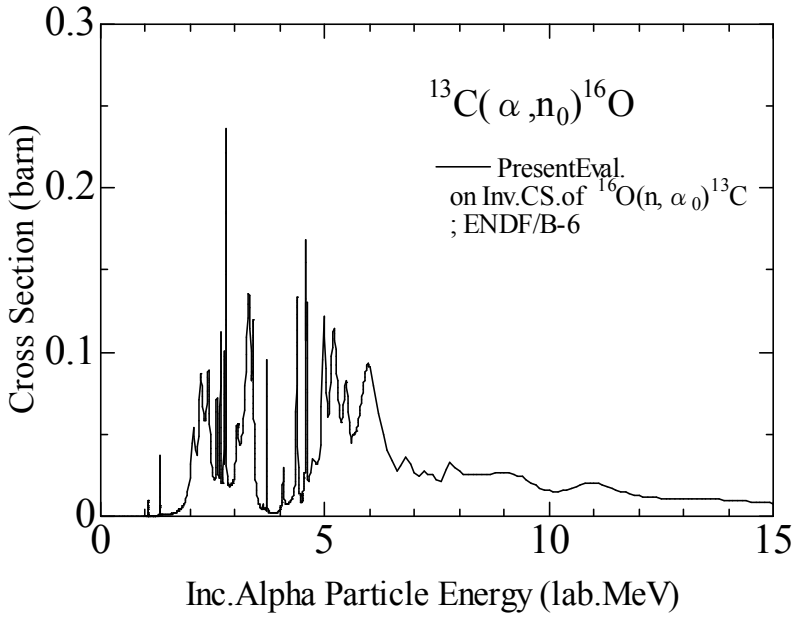

Fig. 26 Cross section for the $^{13}C(\alpha,n_0)$ reaction evaluated on the basis of the cross section[38] for the inverse reaction $^{16}O(n,\alpha_0)$.

(4) Energy-angle Distribution of Emitted Neutrons (MF=6; MT=4, MT=22 and MT=28)

Double-differential energy-angle distributions of emitted neutrons were calculated with the mEXIFON code[4] and represented by using the Kalbach systematics[6]. Figure 27 shows the calculated energy spectra of emitted neutrons. These spectra include contributions of discrete neutrons emitted by the partial (α,n_i) reactions.

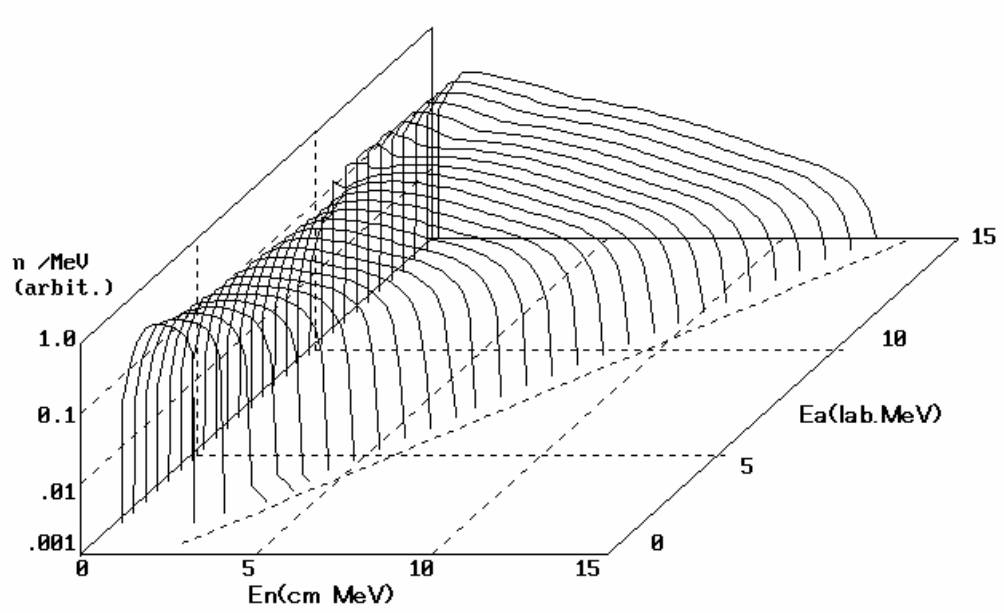

Fig. 27 Calculated energy spectra of neutrons emitted by α-particle bombardment of ^{13}C. Normalization of spectra was made for each incident α-particle energy Ea.

6.3 Discussion

$^{13}C(\alpha,xn)$ Reaction

Though differential cross sections for neutron production were measured at forward and middle angles by Bonner et al.[30], their angular resolution was poor. Therefore, the differential cross-section data were not used in the present work. Further examination should be made to utilize these data.

7. Nitrogen

7.1 $^{14}N(\alpha,xn)$ Reaction

7.1.1 Basic Data

The reaction Q-values and threshold energies are given in Table 15 for the neutron emission reactions on ^{14}N by α-particle bombardment.

Table 15 Q-values and threshold energies of the $^{14}N(\alpha,xn)$ reactions

Reaction	Q-value (MeV)	Threshold Energy (MeV)
$^{14}N(\alpha,n)^{17}F$	-4.734	6.088
$^{14}N(\alpha,pn)^{16}O$	-5.335	6.860
$^{14}N(\alpha,\alpha'n)^{13}N$	-10.553	13.570

The level scheme of ^{13}N used in the present work is given in Table 16. The levels above 5.000 MeV are assumed to be continuum. Continuous levels are

assumed for other residual nuclei.

Table 16 Level scheme of ^{17}F

Level	E_x(MeV)	Spin-Parity
GS	0.0	5/2+
1st	0.495	1/2+
2nd	3.104	1/2-
3rd	3.857	5/2-
4th	4.640	3/2-

7.1.2 Experimental Data

Gruhle et al.[39] measured ^{17}F activity production cross section in the incident α-particle energy range E_α = 5.6 ~ 10 MeV. The excited states of ^{17}F of which excitation energy is greater than 0.6 MeV decay to ^{16}O+p state. So, the ^{17}F activity production cross section is almost equal to a sum of (α,n_0) and (α,n_1) cross sections.

Thick-target ^{17}F activity yields were measured by Roughton et al.[28] in the energy range E_α=6.2~16.8 MeV.

7.1.3 Evaluation

(1) Neutron-production Cross Section (MF=3; MT=201)

The experimental ^{17}F production cross section was analyzed to produce the (α,n_0) and (α,n_1) cross sections with the ARESCAL code. Figure 28 shows the results of the analysis together with the experimental ^{17}F activity production cross section. The total (α,n) cross section was deduced using the branching ratios calculated with Eq. (8), and then the neutron-production cross section was obtained using the ratio of cross sections calculated with the mEXIFON code[4]. The evaluated neutron-production cross section is shown in Fig. 29. Figure 30 shows the calculated thick-target ^{17}F activity yields compared with the experimental data measured by Roughton et al.[28]

(2) Cross Sections for the (α,n), (α,α'n) and (α,pn) Reactions (MF=3; MT=4, MT=22 and MT=28)

The cross sections for the (α,n), (α,α'n) and (α,pn) reactions were obtained in the process of neutron-production cross section evaluation described above.

(3) Partial Cross Sections for the (α,n_i) Reactions (i=0,1,2,3,4 and continuum) (MF=3; MT=50, MT=51, MT=52, MT=53, MT=54 and MT=91)

These cross sections were obtained in the process of neutron-production cross section evaluation described above.

(4)Energy-angle Distribution of Emitted Neutrons (MF=6; MT=4, MT=22 and MT=28)

Double-differential energy-angle distributions of emitted neutrons were calculated with the mEXIFON code[4] and represented by using the Kalbach systematics[6]. Figure 31 shows the calculated energy spectra of emitted neutrons. These spectra include contributions of discrete neutrons emitted by the partial (α,n_i) reactions.

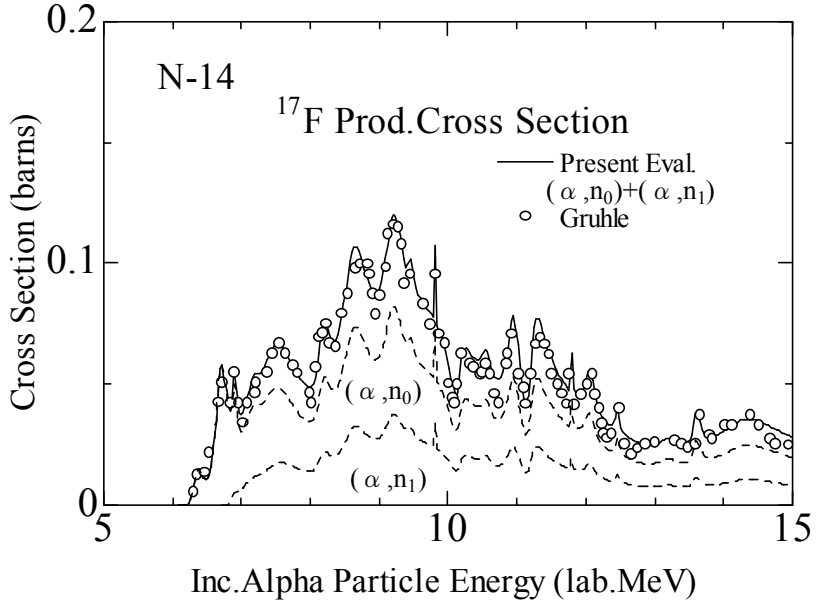

Fig. 28 Calculated ^{17}F activity production cross section of ^{14}N bombarded by α-particles together with experimental values. Breakdown of the cross section is shown in the dashed lines.

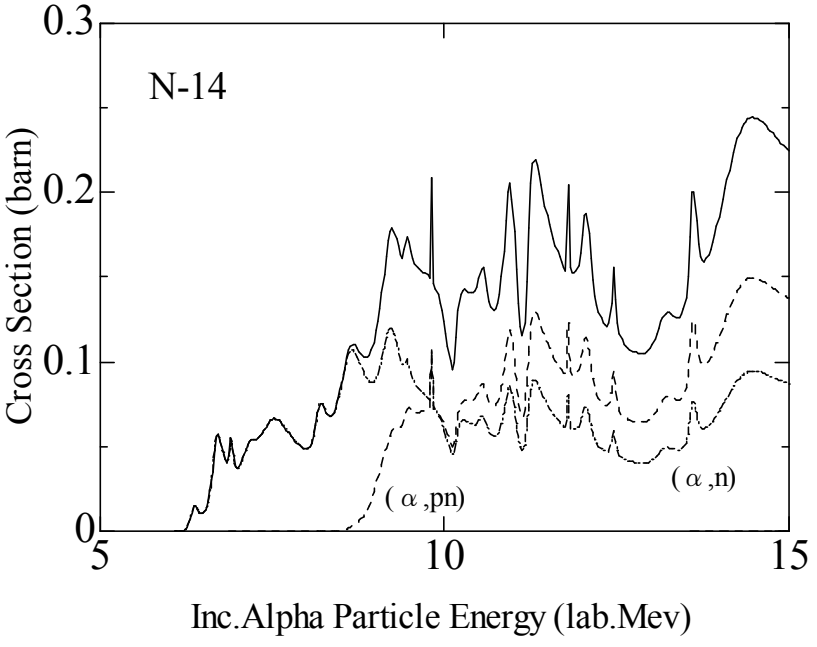

Fig. 29 Evaluated neutron-production cross section of ^{14}N bombarded by α-particles (solid line) and breakdown of the cross section (dashed and dot-dashed lines).

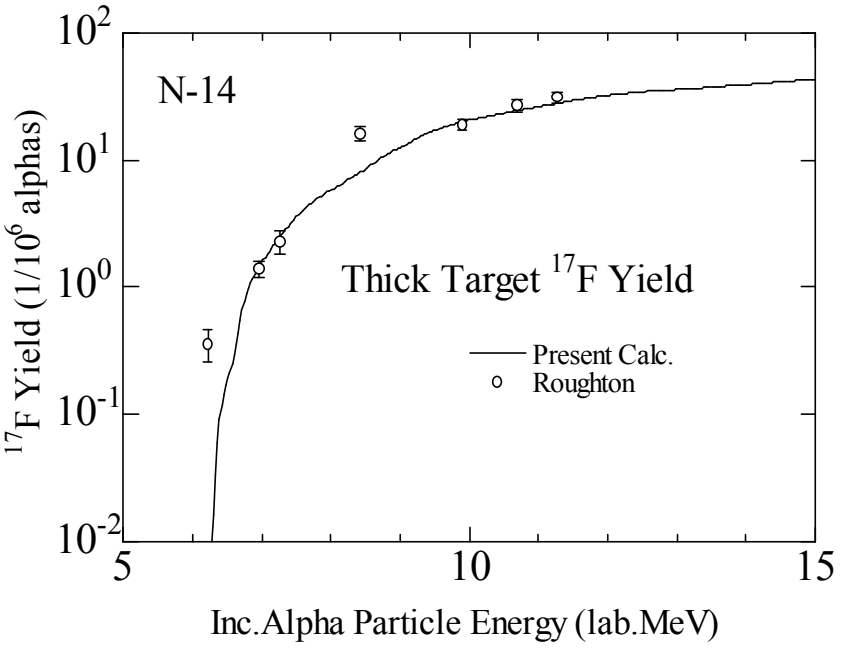

Fig. 30 Calculated thick-target ^{17}F yield of ^{14}N bombarded by α-particles together with the experimental values measured by Roughton et al.[28)]

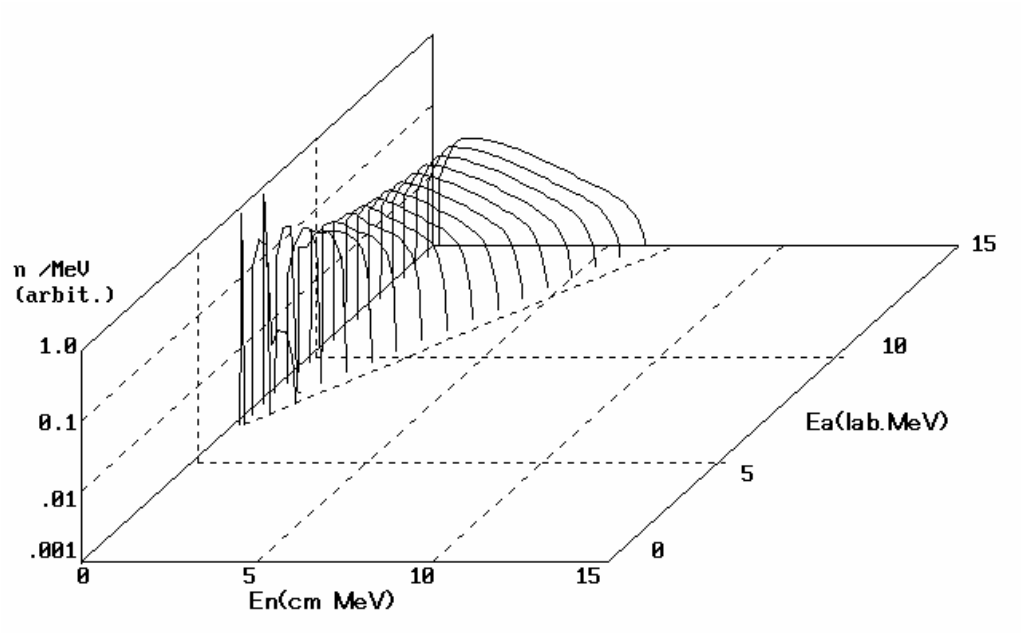

Fig. 31 Calculated energy spectra of neutrons emitted by α-particle bombardment of ^{14}N. Normalization of spectra was made for each incident α-particle energy Ea.

7.2 ^{15}N(α,xn) Reaction

7.2.1 Basic Data

The reaction Q-values and threshold energies are given in Table 17 for the neutron emission reactions on ^{15}N by α-particle bombardment.

Table 17 Q-values and threshold energies of the ^{15}N(α,xn) reactions

Reaction	Q-value (MeV)	Threshold Energy (MeV)
^{15}N(α,n)^{18}F	-6.418	8.131
^{15}N(α,α'n)^{14}N	-10.833	13.572

The level scheme of ^{18}F used in the present work is given in Table 18. The levels above 1.700 MeV are assumed to be continuum. Continuous levels are assumed for ^{14}N.

Table 18 Level scheme of ^{18}F

Level	E_x(MeV)	Spin-Parity
GS	0.0	1+
1st	0.937	3+
2nd	1.042	0-
3rd	1.081	0-
4th	1.121	5+

7.2.2 Experimental Data

No experimental data on neutron-production reactions are available presently. Roughton et al.[28] measured thick-target ^{18}F activity yields in the incident α-particle energy range E_α = 8.4 ~ 16.8 MeV. The activation cross section corresponds approximately to a sum of (α,n_i) cross sections to the ^{18}F excited levels of which excitation energy is less than 4.416 MeV.

7.2.3 Evaluation

(1) Neutron-production Cross Section (MF=3; MT=201)

Resonance levels of the compound nucleus ^{19}F were selected from the level scheme by Tilley et al.[40] to meet the condition of formation by α-particle and neutron emission. Using the resonance parameters (resonance energy, spin-parity, α-particle width, total neutron width) of selected 17 resonances, cross sections for neutron production were calculated with the ARESCAL code and the total neutron width of each level was adjusted so as to obtain a good agreement between calculated and experimental thick target ^{18}F activity yields. With the cross section for the (α,n) reaction thus obtained, and the ratios of cross sections calculated with the mEXIFON code[4], each neutron emission reaction cross section was determined and summed up to

obtain the neutron-production cross section. The evaluated neutron-production cross section is shown in Fig. 32. Figure 33 shows the calculated thick-target ^{18}F activity yield together with the experimental yields measured by Roughton et al.[28)]

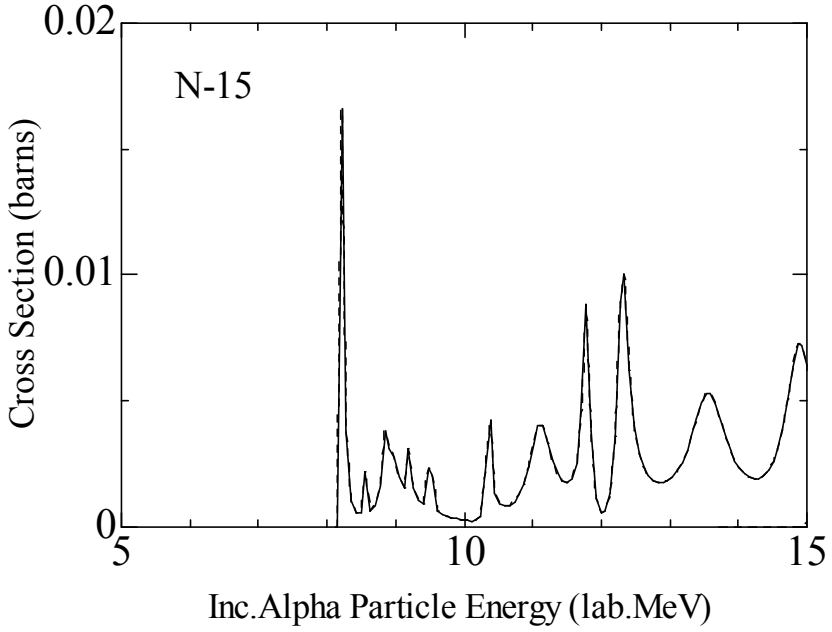

Fig. 32 Evaluated neutron-production cross section of ^{15}N bombarded by α-particles.

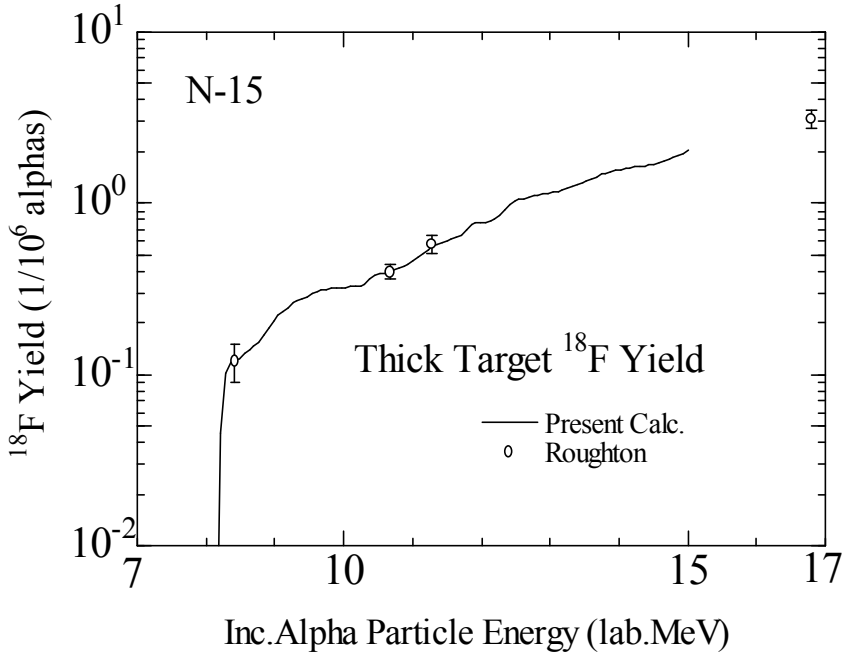

Fig. 33 Calculated thick-target ^{18}F activity yield of ^{15}N bombarded by α-particles together with the experimental values measured by Roughton et al.[28)]

(2) Cross Sections for the (α,n) and (α,α'n) reactions (MF=3; MT=4 and MT=22)

The cross sections for the (α,n) and (α,α'n) reactions were obtained in the process of neutron production cross section evaluation described above.

(3) Partial Cross Sections for the (α,n_i) Reactions (i=0,1,2,3,4 and continuum) (MF=3; MT=50, MT=51, MT=52, MT=53, MT=54 and MT=91)

These cross sections were obtained by applying the branching ratios calculated with Eq. (8) to the evaluated (α,n) cross section.

(4) Energy-angle Distribution of Emitted Neutrons (MF=6; MT=4 and MT=22)

Double-differential energy-angle distributions of emitted neutrons were calculated with the mEXIFON code[4] and represented by using the Kalbach systematics[6]. Figure 34 shows the calculated energy spectra of emitted neutrons. These spectra include contributions of discrete neutrons emitted by the partial (α,n_i) reactions.

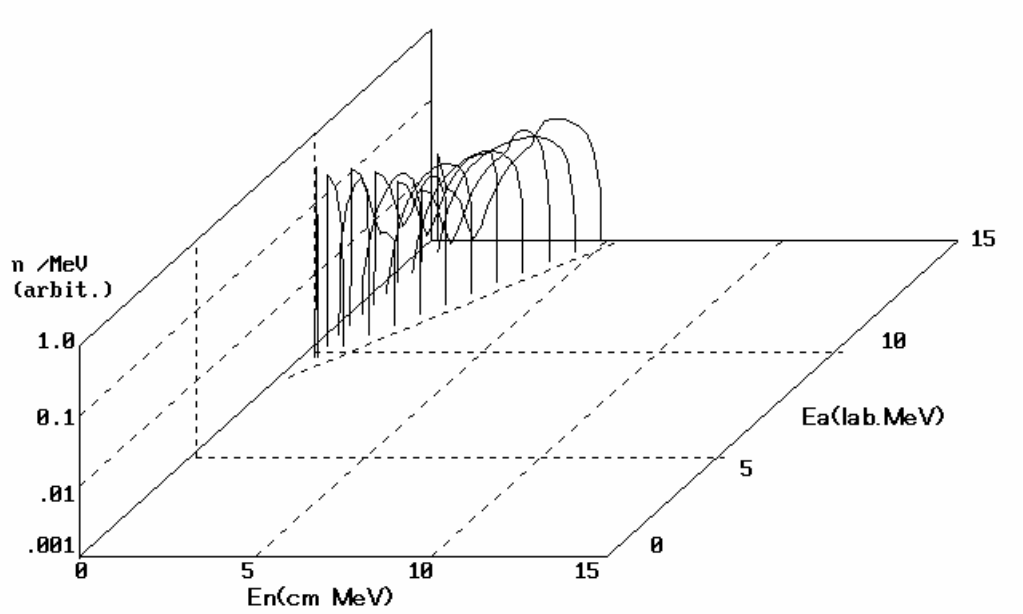

Fig. 34 Calculated energy spectra of neutrons emitted by α-particle bombardment of ^{15}N. Normalization of spectra was made for each incident α-particle energy Ea.

7.3 Discussion

$^{14}N(\alpha,xn)$ Reaction

Thick-target ^{17}F activity yields were calculated using the evaluated (α,n_0) and (α,n_1) cross sections and are shown in Fig. 30 together with the experimental data measured by Roughton et al.[28] It is found from the figure that the calculated values cannot reproduce well 2 energy points. The reason for the discrepancy is not clear.

^{15}N(α,xn) Reaction

The present evaluation was made on the basis of the resonance calculation using the selected resonances for ^{19}F. There are experimental data on α-particle elastic scattering and neutron emission data on the ^{18}O(p,n) reaction. By analyzing these cross sections, more elaborate evaluation might be made.

8. Oxygen

8.1 ^{17}O(α,xn) Reaction

8.1.1 Basic Data

The reaction Q-values and threshold energies are given in Table 19 for the neutron emission reactions on ^{17}O by α-particle bombardment.

The level scheme of ^{20}Ne used in the present work is given in Table 20. The levels above 5.621 MeV are assumed to be continuum. Continuous levels are assumed for ^{16}O.

Table 19 Q-values and threshold energies of the ^{17}O(α,xn) reactions

Reaction	Q-value (MeV)	Threshold Energy (MeV)
^{17}O(α,n)^{20}Ne	+0.587	0
^{17}O(α,α'n)^{16}O	-4.143	5.119

Table 20 Level scheme of ^{20}Ne

Level	E_x(MeV)	Spin-Parity
GS	0.0	0+
1st	1.634	2+
2nd	4.248	4+
3rd	4.968	2-

8.1.2 Experimental Data

Bair and Haas[36] measured the neutron-production cross section in the incident α-particle energy range E_α = 1.0 ~ 5.3 MeV. It was pointed out later[9] that the results should be multiplied by a factor of 1.35. Hansen et al.[41] measured the neutron-production cross section in the energy range E_α = 5 ~ 12.5 MeV with broad incident energy resolution.

Thick UO_2 (natural oxygen) target neutron yields were measured by Bair and Gomez del Campo[9] in the energy region E_α = 3.0 ~ 7.5 MeV and also measured by West and Sherwood[11] in the energy range E_α = 4.2 ~ 10.0 MeV.

8.1.3 Evaluation

(1) Neutron-production Cross Section (MF=3; MT=201)

Evaluation of the neutron-production cross section was made based on the revised experimental data measured by Bair and Haas[36] in the energy range E_α=1.0 ~ 5.3 MeV. In the energy range E_α > 5.3 MeV, we adopted the neutron-production cross section calculated with the mEXIFON code[4]. Normalization was made so that the calculations could reproduce experimental data below E_α = 5.3 MeV. Figure 35 shows the neutron-production cross section of ^{17}O bombarded by α-particles together with experimental values.

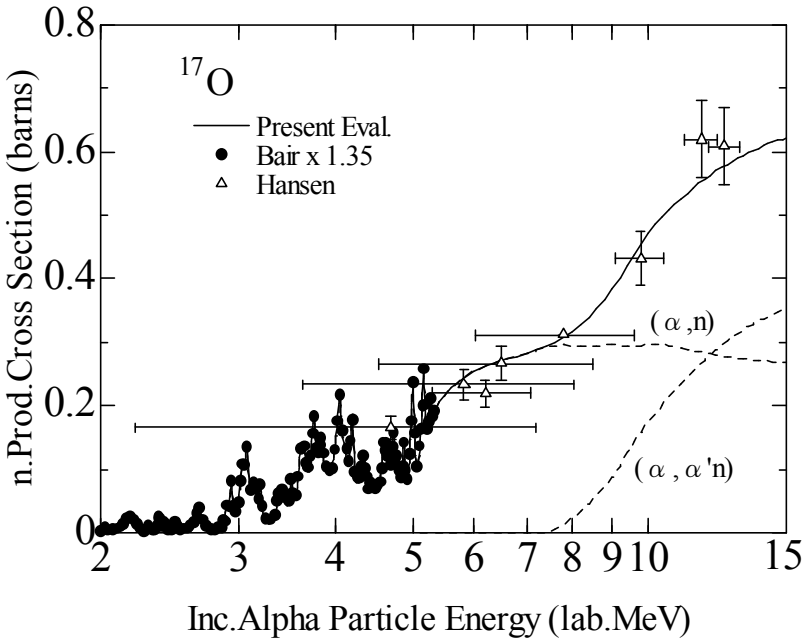

Fig. 35 Neutron-production cross section of ^{17}O bombarded by α-particles together with experimental values. Breakdown of the cross section is shown by the dashed lines.

(2) Cross Sections for the (α,n) and (α, α'n) Reactions (MF=3; MT=4 and MT=22)

The cross sections for the (α,n) and (α,α'n) reactions were obtained by applying the cross-section ratios calculated with the mEXIFON code[4] to the neutron-production cross section.

(3) Partial Cross Sections for the (α,n_i) Reactions (i=0,1,2,3 and continuum) (MF=3; MT=50, MT=51, MT=52, MT=53 and MT=91)

The (α,n_i) cross sections were obtained by applying the branching ratios calculated with Eq. (8) to the evaluated (α,n) cross section.

(4) Energy-angle Distribution of Emitted Neutrons (MF=6; MT=4 and MT=22)

Double-differential energy-angle distributions of emitted neutrons were calculated with the mEXIFON code[4] and represented by using the Kalbach systematics[6]. Figure 36 shows the calculated energy spectrum of emitted neutrons. These spectra include

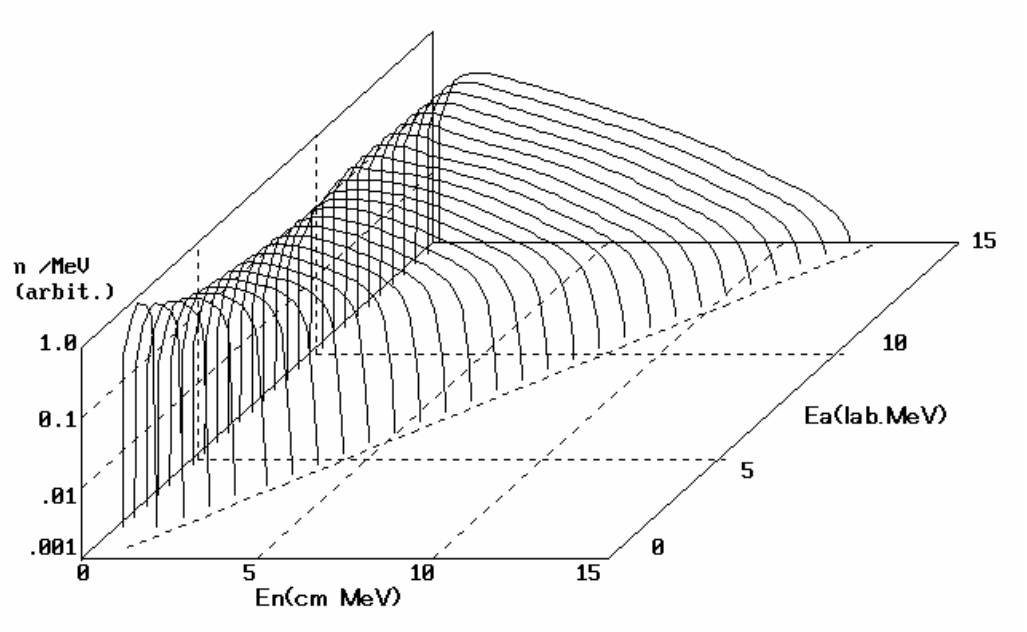

contributions of discrete neutrons emitted by the partial (α,n_i) reactions.

Fig. 36 Calculated energy spectra of neutrons emitted by α-particle bombardment of ^{17}O. Normalization of spectra was made for each incident α-particle energy Ea.

8.2 ^{18}O(α,xn) Reaction

8.2.1 Basic Data

The reaction Q-values and threshold energies are given in Table 21 for the neutron emission reactions of ^{18}O by α-particle bombardment.

Table 21 Q-values and threshold energies of the ^{18}O(α,xn) reactions

Reaction	Q-value (MeV)	Threshold Energy (MeV)
^{18}O(α,n)^{21}Ne	-0.697	0.852
^{18}O(α,2n)^{20}Ne	-7.458	9.116
^{18}O(α,α'n)^{17}O	-8.044	9.833

The level scheme of ^{21}Ne used in the present work is given in Table 22. The levels above 2.867 MeV are assumed to be continuum. Continuous levels are assumed for other nuclei.

Table 22 Level scheme of ^{21}Ne

Level	E_x(MeV)	Spin-Parity
GS	0.0	3/2+
1st	0.351	5/2+
2nd	1.746	7/2+
3rd	2.789	1/2-
4th	2.794	1/2+

8.2.2 Experimental Data

Bair and Willard[42] measured the neutron-production cross section in the incident α-particle energy range E_α = 2.4 ~ 5.1 MeV. It was pointed out later[9] that the results should be multiplied by a factor of 1.35. Bonner et al.[30] measured differential cross sections at emission angles of 0-30 degrees at E_α = 1.9 ~ 5.0 MeV. Hansen et al.[41] measured the neutron-production cross section in the energy range E_α = 5 ~ 12.5 MeV with broad incident energy resolution.

Thick UO_2 (natural oxygen) target neutron yields were measured by Bair and Gomez del Campo[9] in the energy region E_α = 3.0 ~ 7.5 MeV and also measured by West and Sherwood[11] in the energy range E_α = 4.2 ~ 10.0 MeV

8.2.3 Evaluation

(1) Neutron-production Cross Section (MF=3; MT=201)

Evaluation of the neutron-production cross section was made based on the revised experimental data measured by Bair and Willard[42] in the energy range E_α = 2.4 ~ 5.1

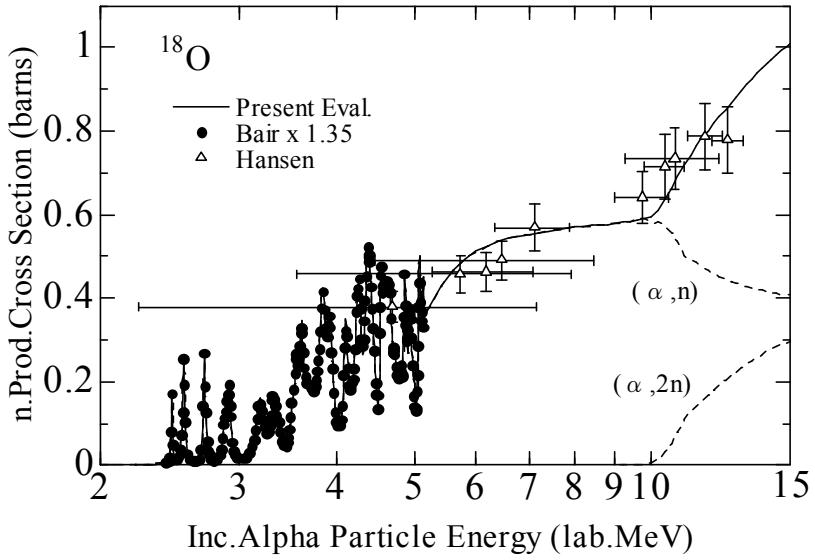

Fig. 37 Evaluated neutron-production cross section of ^{18}O bombarded by α-particles together with experimental values. Dashed lines show the breakdown of the cross section.

MeV. In the energy range $E_\alpha > 5.1$ MeV, we adopted the neutron-production cross section calculated with the mEXIFON code[4]. Normalization was made so that the calculations could reproduce experimental data below $E_\alpha = 5.1$ MeV. The evaluated neutron-production cross section is shown in Fig. 37 together with experimental values. Figure 38 shows the calculated thick-target neutron yield of natural Oxygen (^{16}O=no contribution to neutron production at $E_\alpha < 15$ MeV, ^{17}O=0.037%, ^{18}O=0.204%,) in UO_2 together with the experimental values. It should be noted that the U(α,xn) reaction is practically prohibited because of large negative Q-value and Coulomb barrier.

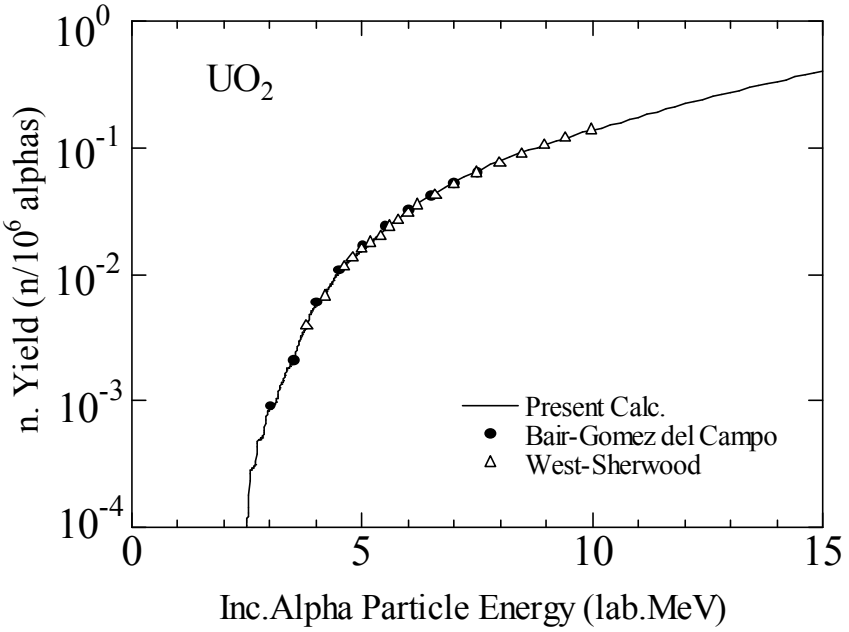

Fig. 38 Calculated thick-target neutron yield of UO_2 bombarded by α-particles together with experimental yields.

(2) Cross Sections for the (α,n), (α,α'n) and (α,2n) Reactions (MF=3; MT=4, MT=22 and MT=16)

The cross sections for the (α,n), (α,α'n) and (α,2n) reactions were obtained by applying each cross-section ratio calculated with the mEXIFON code to the neutron-production cross section.

(3) Partial Cross Sections for the (α,n_i) Reactions (i=0,1,2,3 and continuum) (MF=3; MT=50, MT=51, MT=52, MT=53 and MT=91)

The (α,n_i) cross sections were obtained by applying the branching ratios calculated with Eq. (8) to the evaluated (α,n) cross section.

(4) Energy-angle Distribution of Emitted Neutrons (MF=6; MT=4 and MT=22)

Double-differential energy-angle distributions of emitted neutrons were calculated with the mEXIFON code[4] and represented by using the Kalbach systematics[6]. Figure 39 shows the calculated energy spectra of emitted neutrons. These spectra include contributions of discrete neutrons emitted by the partial (α,n_i) reactions.

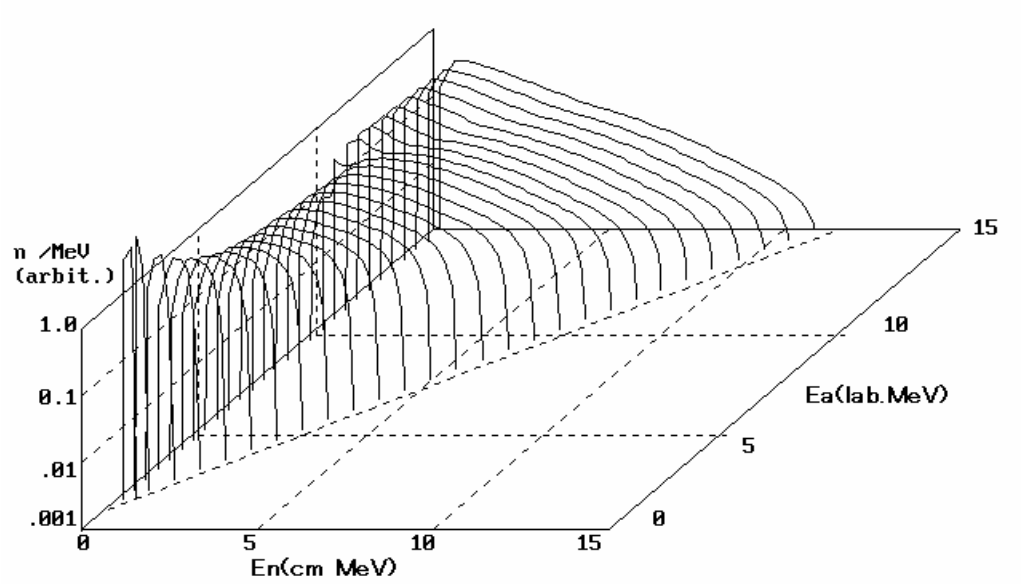

Fig. 39 Calculated energy spectra of neutrons emitted by α-particle bombardment of ^{18}O. Normalization of spectra was made for each incident α-particle energy Ea.

8.3 Discussion

Neutron-emission data on oxygen are one of the most important data for the safety analysis of fuel-cycle facility for oxide nuclear fuels. More cross-section measurements are required, especially in the incident α-particle energy region below 7 MeV. Partial cross sections for the (α,n) reaction and their angular distributions are also required and detailed analyses should be made to estimate the neutron energy spectrum.

9. Fluorine

9.1 ^{19}F(α,xn) Reaction

9.1.1 Basic data

The Q-values and threshold energies are given in Table 23 for the neutron emission reactions on ^{19}F by α-particle bombardment.

The level schemes of the residual nuclides are prepared in the library of EGNASH-2 code[7]. Low-lying levels of ^{22}Na which are observed as some peaks in the spectrum of emitted neutrons are given in Table 24. The levels above 5.317 MeV are assumed to be continuum.

Table 23 Q-values and threshold energies of the $^{19}F(\alpha,xn)$ reactions

Reaction	Q-value (MeV)	Threshold Energy (MeV)
$^{19}F(\alpha,n)^{22}Na$	-1.9517	2.3629
$^{19}F(\alpha,pn)^{21}Ne$	-8.6911	10.522
$^{19}F(\alpha,\alpha'n)^{18}F$	-10.432	12.630

Table 24 Level scheme of ^{22}Na

Level	E_x(MeV)	Spin-Parity
GS	0.0	3+
1st	0.5830	1+
2nd	0.6570	0+
3rd	0.8909	4+
4th	1.5281	5+
5th	1.9369	1+
6th	1.9519	2+
7th	1.9840	3+

9.1.2 Experimental data

Norman et al.[43] gave ^{22}Na production cross section in the incident energy range E_α=3.5 ~ 10 MeV. They measured thick-target neutron yield and deduced ^{22}Na production cross section using the stopping power of target (refer to Eq.(10)). The production cross section of ^{22}Na is equal to the neutron-production cross section in the energy range E_α<10.522 MeV. Above this energy, produced ^{22}Na decays into ^{21}Ne+p mostly and the equality is broken. Wrean and Kavanagh[44] measured neutron-production cross section in the energy region E_α=2.28 ~ 3.1 MeV with a fine energy step. Van der Zwan and Geiger[45] measured the excitation functions of the (α,n_0), $(\alpha,n_{1,2})$, (α,n_3) and (α,n_4) reactions at 0-degree in the incident energy range E_α=2.3 ~ 4.7 MeV. Angular distributions of the (α,n_0) reaction were measured at 9-energy points and cross sections were given for the (α,n_0) reaction.

Thick-target neutron yields were measured by Bair and Gomez del Campo[9] in the energy region E_α=3.5 ~ 8.0 MeV.

9.1.3 Evaluation

(1) Neutron-production Cross Section (MF=3; MT=201)

Experimental ^{22}Na production cross sections given by Norman et al.[43] were reproduced by calculation with the EGNASH-2 code[7] as neutron-production cross section and the extrapolation was made with the calculation up to E_α=15 MeV. The evaluated neutron-production cross section is shown in Fig. 40 compared with experimental data. Figure 41 shows the calculated thick-target neutron yield compared with experimental data.

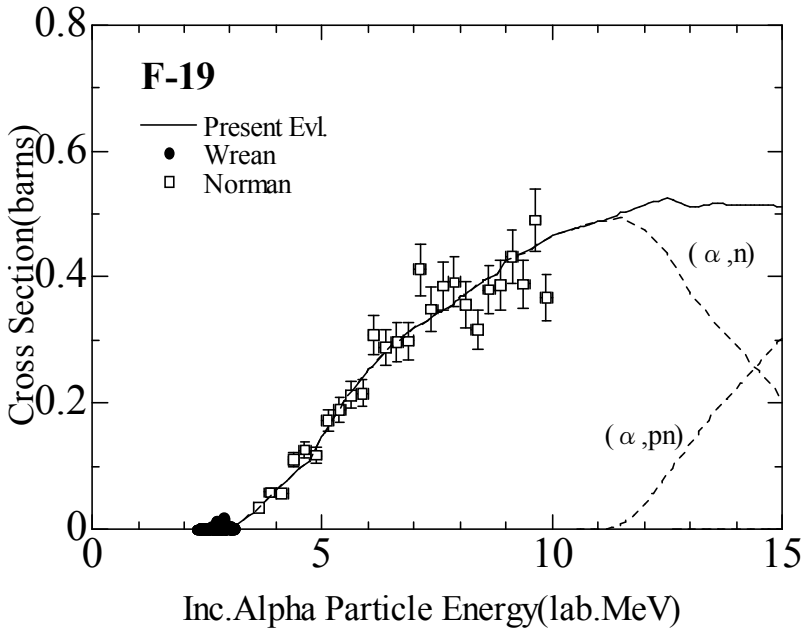

Fig. 40 Evaluated neutron-production cross section of ^{19}F bombarded by α-particles compared with the experimental values. Breakdown of the cross section is also shown by the dashed lines.

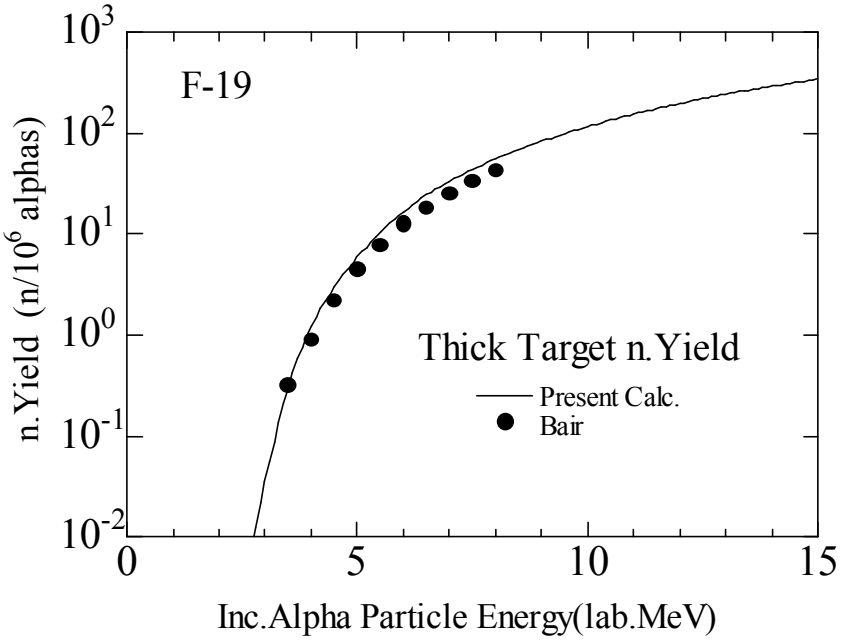

Fig 41 Calculated thick-target neutron yield compared with the experimental yields measured by Bair and Gomez del Campo[9].

(2) Cross Sections for the (α,n), (α,pn) and (α,α'n) Reactions (MF=3; MT=4,MT=28 and MT=22)

The cross sections for the (α,n), (α,pn) and (α,α'n) reactions were obtained by calculation with the EGNASH-2 code[7] and are shown in Fig. 40 by the dashed lines. The (α,α'n) cross section is too small to be seen in the figure.

(3) Partial Cross Sections for the (α,n_i) reactions (i=0,1,2,3,…,27 and continuum) (MF=3; MT=50,…..,77 and MT=91)

The (α,n_i) cross sections were obtained by calculation with the EGNASH-2 code[7]. The evaluated (α,n_0) cross section is compared with the experimental cross section measured by Van der Zwan-and Geiger[45] in Fig. 42.

(4) Energy-angle Distribution of Emitted Neutrons (MF=6; MT=201)

The energy spectra of emitted neutrons were calculated with the EGNASH-2 code[7]. Angular distributions of the emitted neutrons were assumed to be isotropic in the center of mass system. Figure 43 shows the calculated energy spectrum of emitted neutrons.

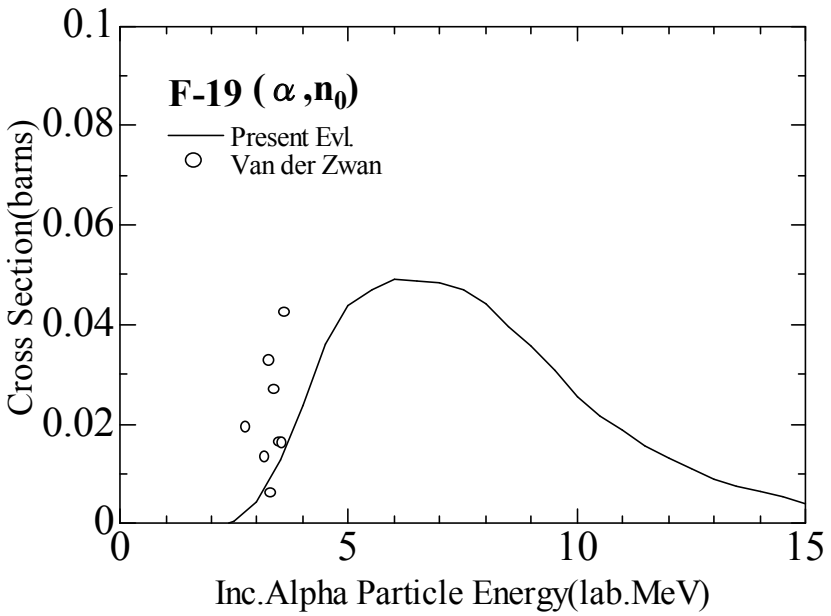

Fig. 42 Evaluated $^{19}F(\alpha,n_0)$ cross section compared with the experimental cross section measured by Van der Zwan and Geiger[45].

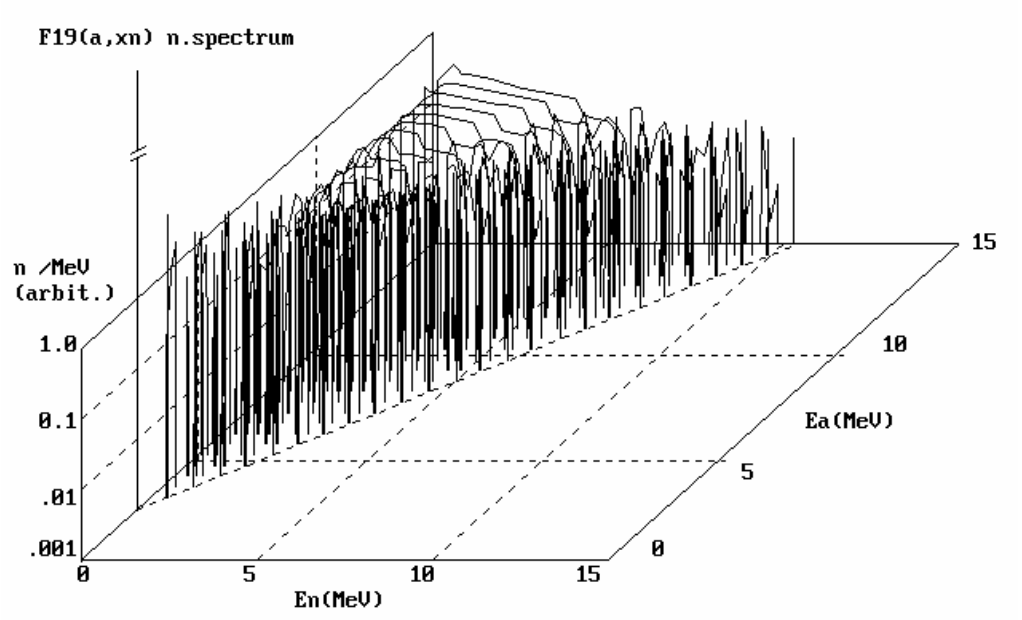

Fig. 43 Calculated energy spectrum of neutrons emitted by α-particle bombardment of ^{19}F. Normalization of spectra was made for each incident α-particle energy Ea.

9.2 Discussion

Experimental cross sections measured by Wrean and Kavanagh[44] show many separated resonance peaks. In the present evaluation, these resonance structures were ignored for simplicity. The structure should be taken into account in the future evaluation.

10. Sodium

10.1 ^{23}Na(α,xn) Reaction

10.1.1 Basic Data

The Q-values and threshold energies are given in Table 25 for the neutron emission reactions on ^{23}Na by α-particle bombardment.

Table 25 Q-values and threshold energies of the ^{23}Na(α,xn) reactions

Reaction	Q-value (MeV)	Threshold Energy (MeV)
^{23}Na (α,n) ^{26}Al	-2.9656	3.4819
^{23}Na (α,pn)^{25}Mg	-9.2721	10.887

The level schemes of the residual nuclides are prepared in the library of EGNASH-2 code[7]. Low-lying levels of ^{26}Al which are observed as some peaks in the

spectrum of emitted neutrons are given in Table 26. The levels above 4.3 MeV are assumed to be continuum.

Table 26 Level scheme of ^{26}Al

Level	E_x(MeV)	Spin-Parity
GS	0.0	5+
1st ($T_{1/2}$=6.3 sec)	0.2282	0+
2nd	0.4169	3+
3rd	1.0578	1+
4th	1.759	2+
5th	1.851	1+
6th	2.0687	4+
7th	2.0695	2+

10.1.2 Experimental Data

Norman et al.[46] measured thick-target neutron yield and deduced neutron-production cross section in the incident energy range E_α=3.615 ~ 10.25 MeV. They also measured ^{26m}Al ($T_{1/2}$=6.3sec.) production cross section in the energy range E_α=4.1 ~ 14.94 MeV and production cross sections of photons (E_γ=417 keV:2nd→GS and E_γ=829 keV:3rd→1st) at 90 degrees in some energy range and deduced the production cross section for the ground state of ^{26}Al in the energy range E_α=4.25 ~ 10.25 MeV. Skelton et al.[47] measured neutron-production cross section in the energy region E_α=3.48 ~ 4.60 MeV with a fine energy step. They also measured ^{26m}Al ($T_{1/2}$=6.3sec.) production cross section and production cross sections of photons (E_γ=417 keV:2nd→GS) and deduced the (α,n_0) cross section in the energy range E_α=3.75 ~ 4.60 MeV.

Though Norman et al.[46] measured thick-target neutron yield, the yield data were not available. No other experimental thick-target yield was published presently.

10.1.3 Evaluation

(1) Neutron-production Cross Section (MF=3; MT=201)

Experimental neutron-production cross sections given by Norman et al.[46] were reproduced by calculation with the EGNASH-2 code[7] as neutron production cross section and the extrapolation was made with the calculation up to E_α=15 MeV. The evaluated neutron-production cross section is shown in Fig. 44 compared with the experimental data. The calculated thick-target neutron yields are illustrated in Fig. 45, where the data of Norman et al.[46] were estimated from Eq. (10).

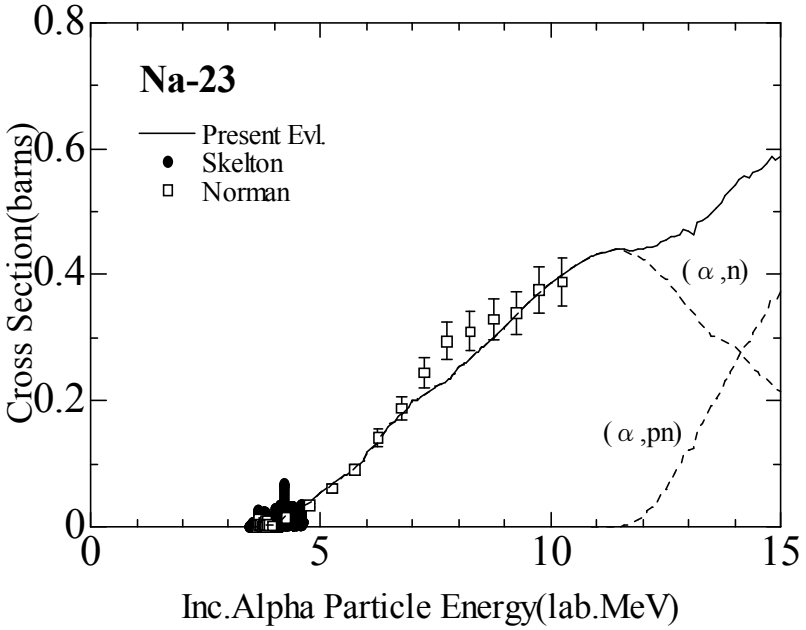

Fig. 44 Evaluated neutron-production cross section of ^{23}Na bombarded by α-particles compared with experimental values. Breakdown of the cross section is also shown by the dashed lines.

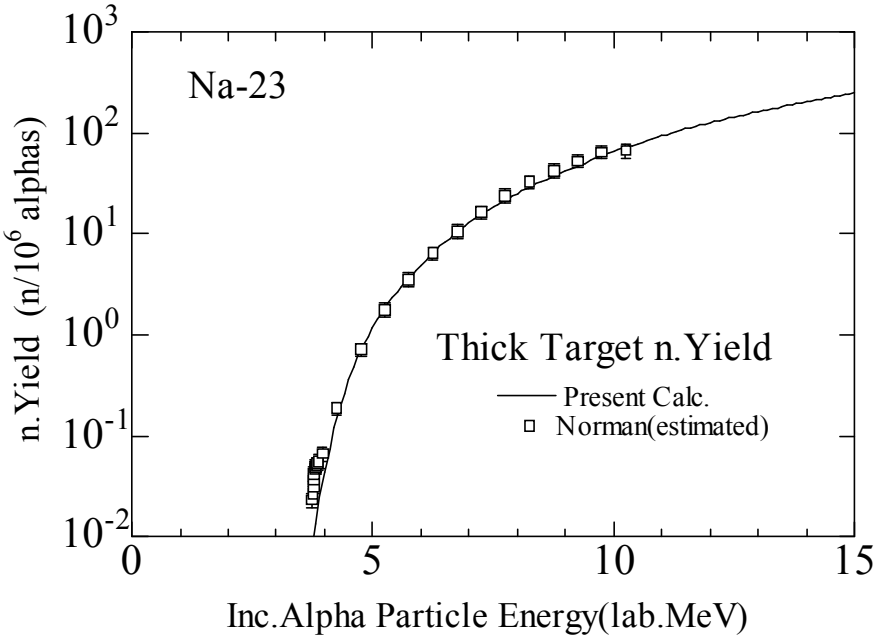

Fig. 45 Calculated thick-target neutron yield compared with the experimental cross sections measured by Norman et al.[46] which were estimated from Eq. (10).

(2) Cross Sections for the (α,n),and (α,pn) reactions (MF=3; MT=4 and ,MT=28)

The cross sections for the (α,n) and (α,pn) reactions were obtained by calculation with the EGNASH-2 code[7] and are shown in Fig. 44 by the dashed lines.

(3) Partial Cross Sections for the (α,n_i) reactions (i=0,1,2,3,…,28 and continuum) (MF=3; MT=50,…..,78 and MT=91)

The (α,n_i) cross sections were obtained by calculation with the EGNASH-2 code[7]. Figure 46 shows a comparison of the evaluated (α,n_0) cross section and the ground-state production cross section deduced by Norman et al.[46]

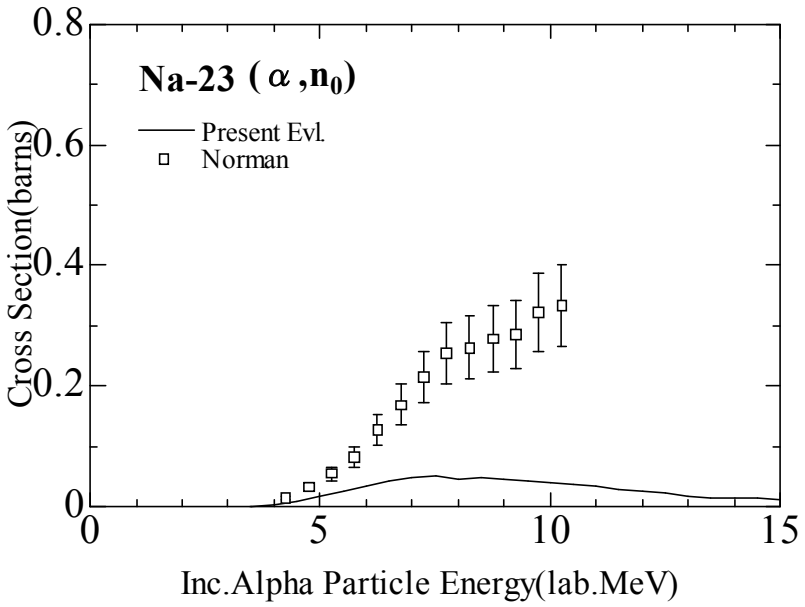

Fig. 46 Comparison of the evaluated (α,n_0) cross section and the ground-state production cross section deduced by Norman et al.[46] See the discussion for this section.

(4) Energy-angle Distribution of Emitted Neutrons (MF=6; MT=201)

The energy spectra of emitted neutrons were calculated with the EGNASH-2 code[7]. Angular distributions of the emitted neutrons were assumed to be isotropic in the center of mass system. Figure 47 shows the calculated energy spectrum of emitted neutrons.

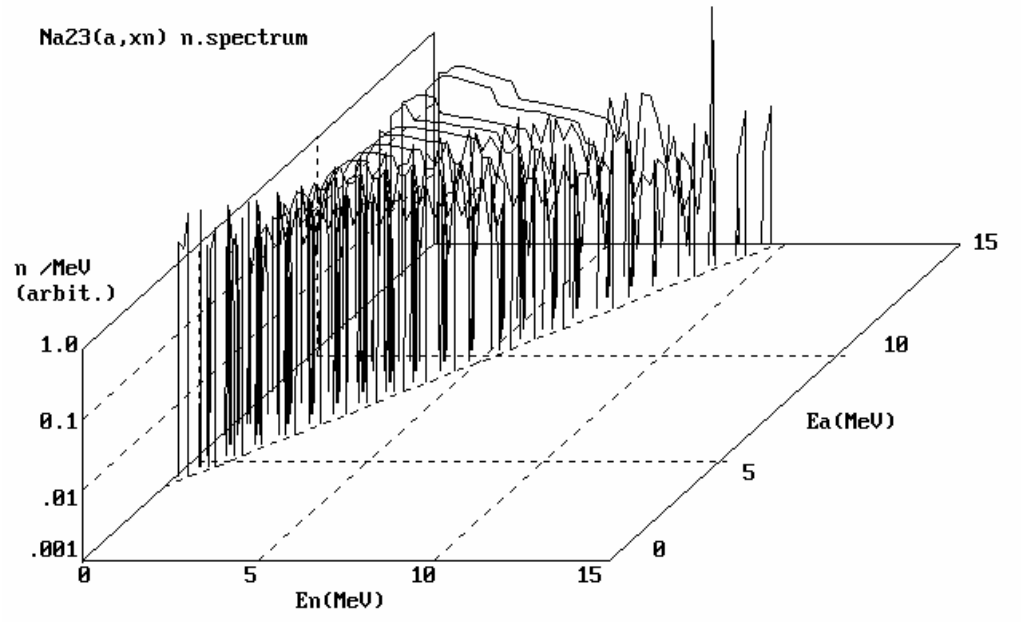

Fig. 47 Calculated energy spectrum of neutrons emitted by α-particle bombardment of ^{23}Na. Normalization of spectra was made for each incident α-particle energy Ea.

10.2 Discussion

Experimental cross section measured by Skelton et al.[47] shows many separated resonance peaks. In the present evaluation, these resonance structures were ignored for simplicity. The structure should be taken into account in the future evaluation.

Though a comparison is shown in Fig. 46 for the evaluated (α,n_0) cross section and the experimental cross section given by Norman et al.[46], the latter cross section was obtained by subtracting the measured ^{26m}Al production cross section from the measured neutron-production cross section. So, the latter should be regarded as the cross section for ^{26}Al ground-state production and differs largely from the (α,n_0) cross section.

11. Aluminum

11.1 ^{27}Al(α,xn) Reaction

11.1.1 Basic Data

The reaction Q-values and threshold energies are given in Table 27 for the neutron emission reactions on ^{27}Al by α-particle bombardment.

The level schemes of the residual nuclei are included in the EGNASH-2 code[7]. As an example, the level scheme of ^{30}P, which is a residual nucleus for the ^{27}Al(α,n) reaction, is given in Table 28. The levels above 0.66 MeV were regarded as continuum in the present calculation.

Table 27 Q-values and threshold energies of the $^{27}Al(\alpha,xn)$ reactions

Reaction	Q-value (MeV)	Threshold Energy (MeV)
$^{27}Al(\alpha,n)^{30}P$	-2.6363	3.0274
$^{27}Al(\alpha,pn)^{29}Si$	-8.2373	9.4593
$^{27}Al(\alpha,2n)^{29}P$	-11.3965	13.0871

Table 28 Level scheme of ^{30}P

Level	E_x(MeV)	Spin-Parity
GS	0.0	1+
1st	0.66	0+
2nd	0.71	1+
3rd	1.45	2+

11.1.2 Experimental Data

Neutron-production cross sections were measured by Holmqvist and Ramstrom[48] in the incident energy range E_α = 3.05 ~ 3.66 MeV, by Flynn et al.[49] at E_α = 3.5 ~ 5.5 MeV, and by Stelson and Mcgowan[50] at E_α = 5.5 ~ 11.0 MeV.

The ^{30}P activity production cross sections were measured by Sahakundu et al.[51] in the incident energy range E_α = 10.5 ~ 37.6 MeV, and by Howard et al.[52] at E_α = 3.05 ~ 3.66 MeV.

Excited states of ^{30}P decay mostly by proton emission when their excitation energy is higher than 5.60 MeV ($E_\alpha \geq 9.46$ MeV). So, in the incident energy range $E_\alpha \geq 9.46$ MeV, ^{30}P activity production cross section does not correspond to the (α,n) reaction cross section.

Thick-target neutron yields were measured by Bair and Gomez del Campo[9] in the energy region E_α=3.5 to 9.0 MeV and also measured by West and Sherwood[11] in the energy range E_α=3.6 to 10.0 MeV

11.1.3 Evaluation

(1) Neutron-production Cross Section (MF=3; MT=201)

Evaluation of the neutron-production cross section was made based on the experimental data measured by Holmqvist and Ramstrom[48] and by Flynn et al.[49] in the energy range E_α=3.0 ~ 5.5 MeV. Above E_α=5.5 MeV, calculation of the cross sections was made with EGNASH-2 code[7] to reproduce the values measured by Stelson and Mcgowan.[50] The evaluated neutron-production cross section is shown in Fig. 48 together with experimental values. Figure 49 shows a comparison of the calculated thick-target neutron yields with experimental data.

(2) Energy-angle Distribution of Emitted Neutrons (MF=6; MT=201)

Double-differential energy-angle distributions of emitted neutrons were calculated

with the EGNASH-2 code[7] and represented by using the Kalbach systematics[6]. Figure 50 shows the calculated energy spectra of emitted neutrons. These spectra include contributions of discrete neutrons emitted by the partial (α,n_i) reactions.

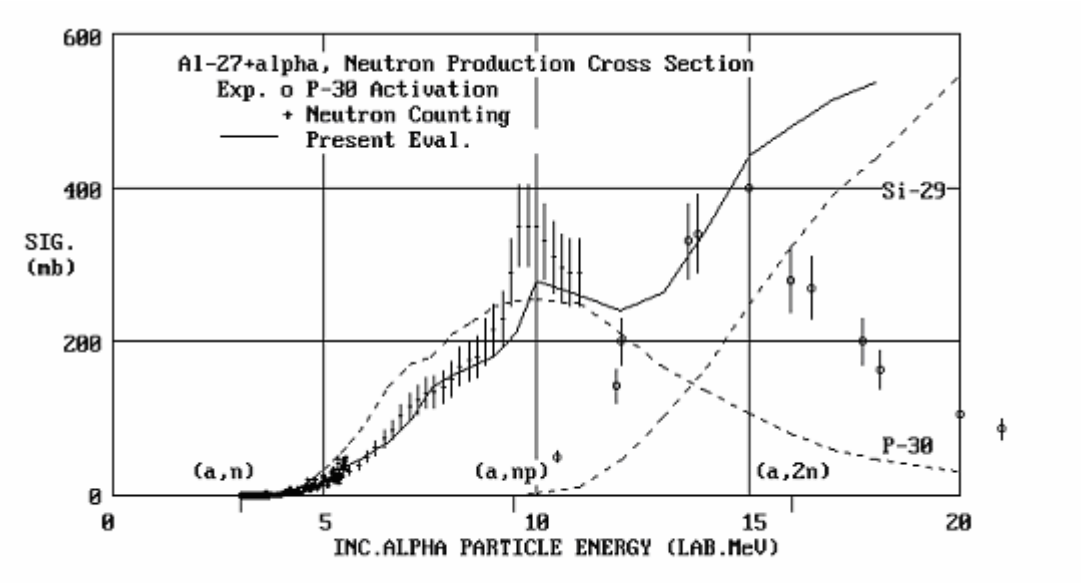

Fig. 48 Evaluated neutron-production cross section of ^{27}Al bombarded by α-particles together with experimental cross sections. For understanding the shape of the cross section, the calculated ^{27}Al(α,n)^{30}P and ^{27}Al(α,np)^{29}Si cross sections are also shown by the dashed lines.

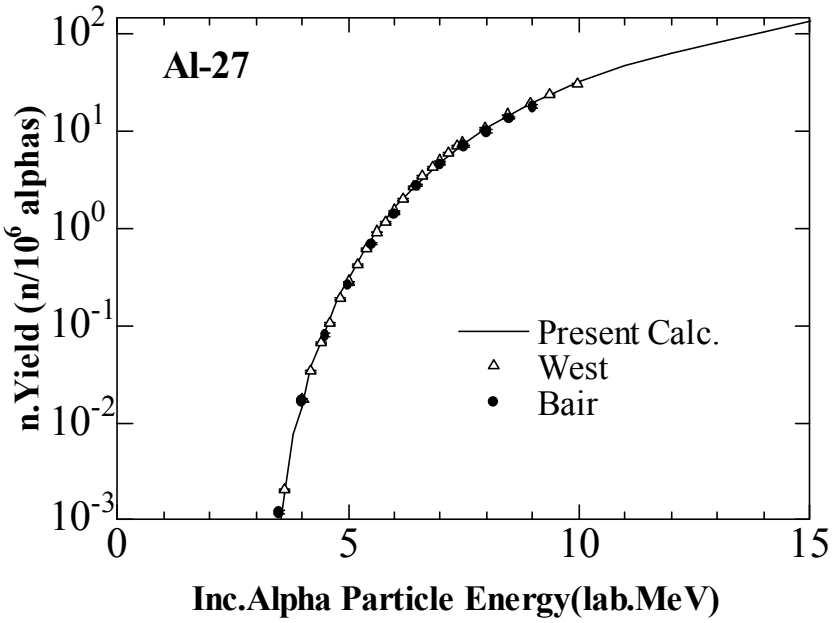

Fig. 49 Calculated thick-target neutron yield of ^{27}Al bombarded by α-particles together with experimental yields.

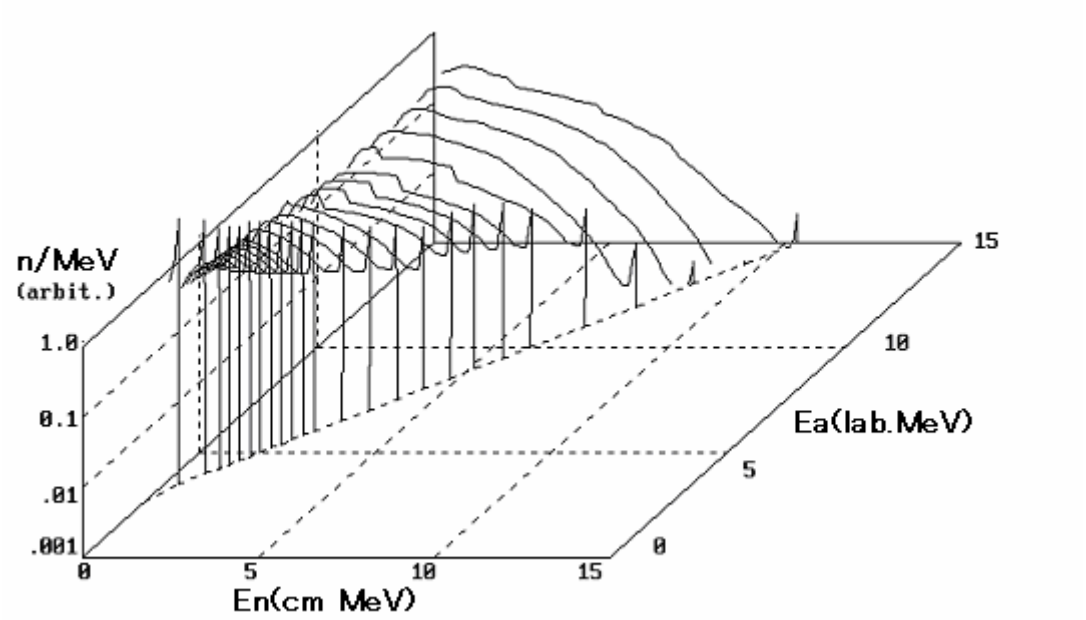

Fig. 50 Calculated energy spectra of neutrons emitted by α-particle bombardment of ^{27}Al. Normalization of spectra was made for each incident α-particle energy Ea.

11.2 Discussion

Experimental cross sections for the (α,n) reaction show resonance structures in the energy region $E_\alpha \leq 5.5$ MeV where the excitation energy of the compound nucleus ^{31}P is higher than 9.6 MeV and the spin-parity of each resonance level is unknown. Thus, nuclear data evaluation based on exact resonance analysis cannot be made presently. Experimental cross section around $E_\alpha = 10$ MeV could not be reproduced well with the EGNASH-2 code[7] by varying some parameters (see Fig. 48). Around the excitation energy of ^{31}P corresponding to this energy, there are photo-neutron giant resonances[53] and somewhat large cross section would be explained by changing the giant resonance parameters in the EGNASH-2 code.

12. Silicon

12.1 ^{28}Si(α,xn) Reaction

12.1.1 Basic Data

The reaction Q-value and threshold energy are given in Table 29 for the neutron emission reactions on ^{28}Si by α-particle bombardment. The (α,n) reaction is solely possible for ^{28}Si below 15 MeV.

Table 29 Q-value and threshold energy of the ^{28}Si(α,xn) reaction

Reaction	Q-value (MeV)	Threshold Energy (MeV)
^{28}Si(α,n)^{31}S	-8.0943	9.2523

Level schemes of the residual nuclei are included in the EGNASH-2 code[7]. The level scheme of ^{31}S, which is a residual nucleus for the ^{28}Si(α,n) reaction, is given in Table 30. The levels above 3.079 MeV are assumed to be continuum.

Table 30 Level scheme of ^{31}S

Level	E_x(MeV)	Spin-Parity
GS	0.0	1/2+
1st	1.2489	3/2+
2nd	2.2356	5/2+
3rd	3.0790	1/2+

12.1.2 Experimental Data

Neutron-production cross sections were measured by Cheng and King[54] in the incident energy range E_α = 8.0 ~ 11.0 MeV.

Natural Si thick-target neutron yields were measured by Bair and Gomez del Campo[9] in the energy region E_α = 4.5 ~ 9.0 MeV and also measured by West and Sherwood[11] in the energy range E_α = 3.6 ~ 10.0 MeV

12.1.3 Evaluation

(1) Neutron-production Cross Section (MF=3; MT=201)

Evaluation of the neutron-production cross section was made based on the experimental data measured by Cheng and King[54] in the energy range E_α = 8.0 ~ 11.0 MeV. Above E_α=11 MeV, we adopted the cross sections calculated with the EGNASH-2 code[7]. Normalization was made so that the calculations could reproduce experimental data below E_α=11 MeV. The evaluated neutron-production cross section is shown in Fig. 51 together with experimental cross sections.

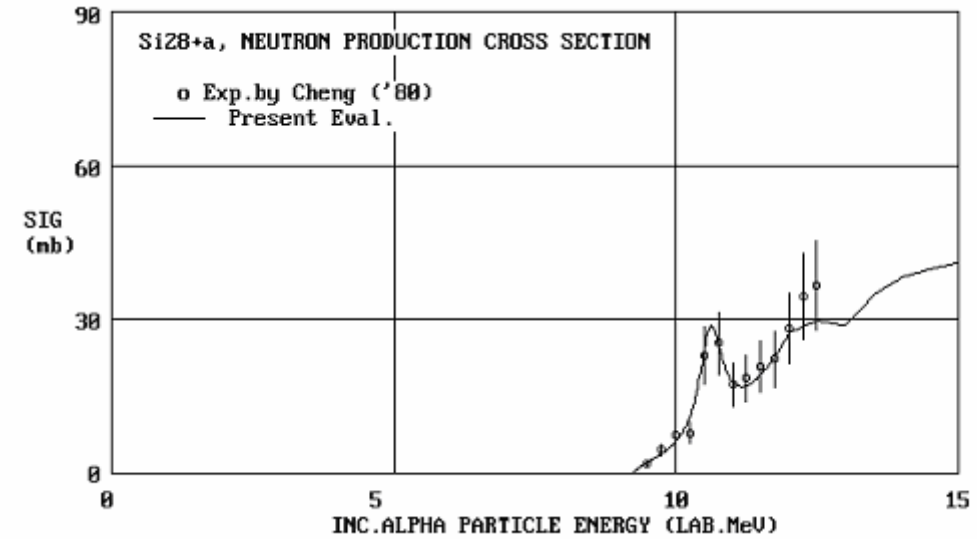

Fig. 51 Evaluated neutron-production cross section of ^{28}Si bombarded by α-particles together with experimental cross sections.

(2) Energy-angle Distribution of Emitted Neutrons (MF=6; MT=201)

Double-differential energy-angle distributions of emitted neutrons were calculated with the EGNASH-2 code[7] and represented by using the Kalbach systematics[6]. Figure 52 shows the calculated energy spectra of emitted neutrons. These spectra include contributions of discrete neutrons emitted by the partial (α,n_i) reactions.

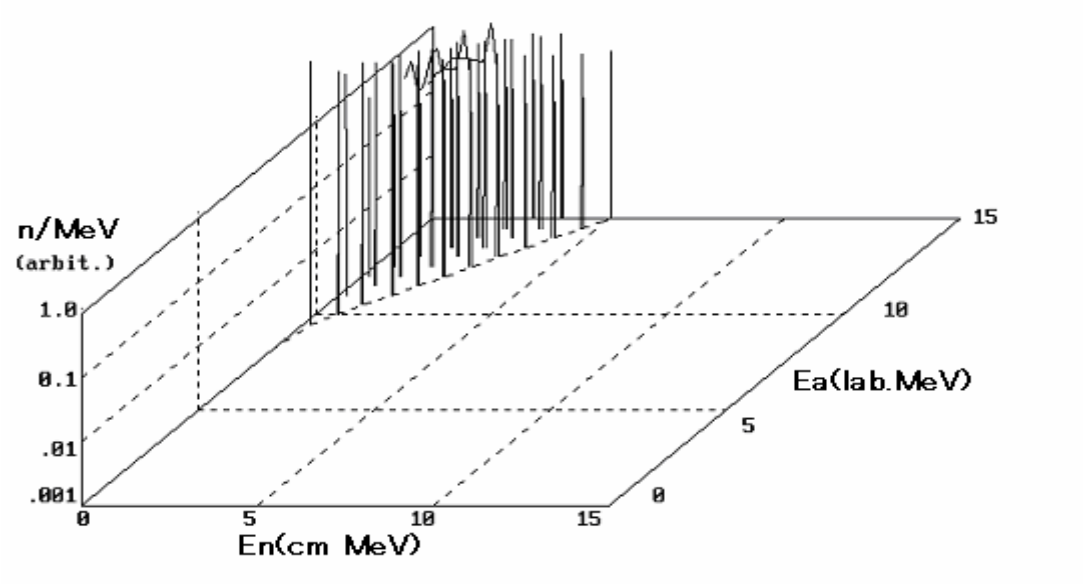

Fig. 52 Calculated energy spectra of neutrons emitted by α-particle bombardment of ^{28}Si. Normalization of spectra was made for each incident α-particle energy Ea.

12.2 ^{29}Si(α,xn) Reaction

12.2.1 Basic Data

The reaction Q-values and threshold energies are given in Table 31 for the neutron emission reactions on ^{29}Si by α-particle bombardment.

Table 31 Q-values and threshold energies of the ^{29}Si(α,xn) reactions

Reaction	Q-value (MeV)	Threshold Energy (MeV)
^{29}Si(α,n)^{32}S	-1.5263	1.7371
^{29}Si(α,pn)^{30}P	-10.391	11.826

Level schemes of the residual nuclei are included in the EGNASH-2 code[7]. As an example, the level scheme of ^{32}S, which is a residual nucleus for the ^{29}Si(α,n) reaction, is given in Table 32. The levels above 6.2243 MeV are assumed to be continuum.

Table 32 Level scheme of ^{32}S

Level	E_x(MeV)	Spin-Parity
GS	0.0	0+
1st	2.2303	2+
2nd	3.7783	0+
3rd	4.2815	2+
4th	4.4589	4+
5th	4.6954	1+
6th	5.0062	3-
7th	5.4130	3+
8th	5.5489	2+
9th	5.7979	1-
10th	6.2243	2-

12.2.2 Experimental Data

Neutron-production cross sections were measured by Flynn et al.[49] in the incident energy range E_α=2.73 ~ 6.77 MeV, and by Gibbons and Macklin[15] at E_α=2.83 ~ 4.28 MeV.

Natural Si thick-target neutron yields were measured by Bair and Gomez del Campo[9] in the energy region E_α = 4.5 to 9.0 MeV and also measured by West and Sherwood[11] in the energy range E_α = 3.6 to 10.0 MeV.

12.2.3 Evaluation

(1) Neutron-production Cross Section (MF=3, MT=201)

Evaluation of the neutron production cross section was made based on the experimental data measured by Flynn et al.[49] and by Gibbons and Macklin[15] in the

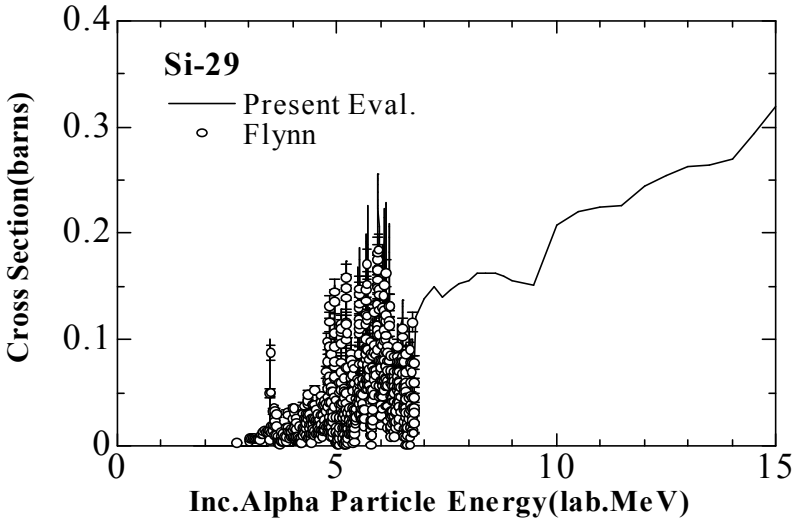

Fig. 53 Evaluated neutron-production cross section of ^{29}Si bombarded by α-particles together with experimental cross sections.

energy range E_α = 2.7 ~ 6.8 MeV. Above E_α = 6.8 MeV, we adopted the cross sections calculated with the EGNASH-2 code[7]. Normalization was made so that the calculations could reproduce experimental data below E_α = 6.8 MeV. The evaluated neutron-production cross section is shown in Fig. 53 together with experimental cross sections.

(2) Energy-angle Distribution of Emitted Neutrons (MF=6; MT=201)

Double-differential energy-angle distributions of emitted neutrons were calculated with the EGNASH-2 code[7] and represented by using the Kalbach systematics[6]. Figure 54 shows the calculated energy spectra of emitted neutrons. These spectra include contributions of discrete neutrons emitted by the partial (α,n_i) reactions.

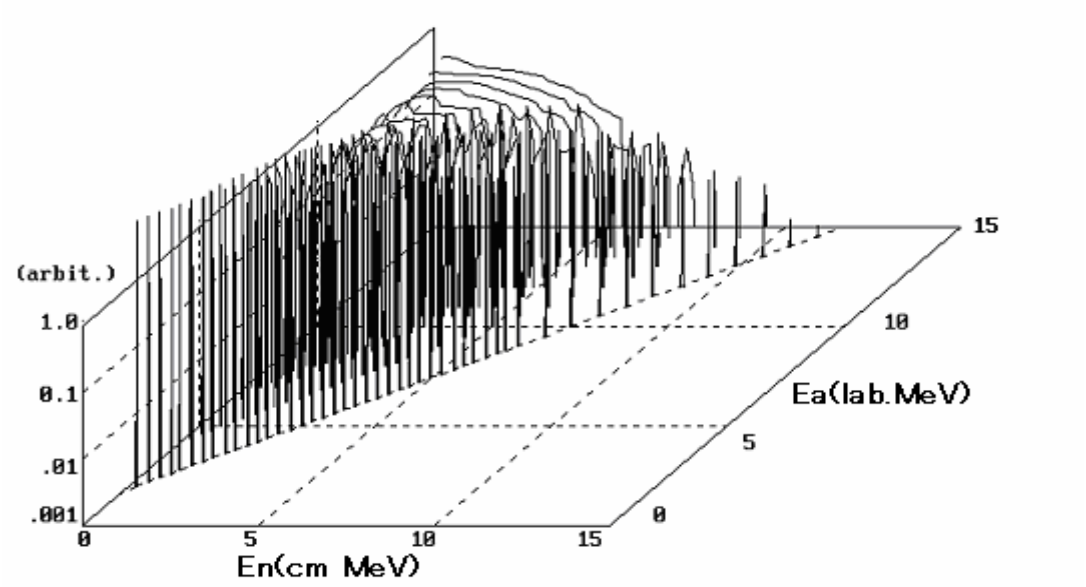

Fig. 54 Calculated energy spectra of neutrons emitted by α-particle bombardment of ^{29}Si. Normalization of spectra was made for each incident α-particle energy Ea.

12.3 ^{30}Si(α,xn) Reaction

12.3.1 Basic Data

The reaction Q-values and threshold energies are given in Table 33 for the neutron emission reactions on ^{30}Si by α-particle bombardment.

Table 33 Q-values and threshold energies of the ^{30}Si(α,xn) reactions

Reaction	Q-value (MeV)	Threshold Energy (MeV)
^{30}Si(α,n)^{33}S	-3.4942	3.9608
^{30}Si(α,2n)^{32}S	-12.136	13.757
^{30}Si(α,pn)^{32}P	-13.064	14.809

Level schemes of the residual nuclei are included in EGNASH-2 code[7]. As an example, the level scheme of ^{33}S, which is a residual nucleus for the $^{30}Si(\alpha,n)$ reaction, is given in Table 34. The levels above 4.4245 MeV are assumed to be continuum.

Table 34 Level scheme of ^{33}S

Level	E_x(MeV)	Spin-Parity
GS	0.0	3/2+
1st	0.8409	1/2+
2nd	1.9663	5/2+
3rd	2.3125	3/2+
4th	2.8664	5/2+
5th	2.9337	7/2-
6th	2.9686	7/2+
7th	3.2199	3/2-
8th	3.8316	5/2+
9th	3.9346	3/2+
10th	4.0476	9/2+
11th	4.0530	1/2+
12th	4.0940	7/2+
13th	4.1437	3/2-
14th	4.2104	3/2-
15th	4.3749	1/2+
16th	4.4245	1/2+

12.3.2 Experimental Data

Neutron-production cross sections were measured by Flynn et al.[49] in the incident energy range E_α = 3.98 ~ 6.28 MeV.

Natural Si thick-target neutron yields were measured by Bair and Gomez del Campo[9] in the energy region E_α = 4.5 ~ 9.0 MeV and also measured by West and Sherwood[11] in the energy range E_α = 3.6 ~ 10.0 MeV

12.3.3 Evaluation

(1) Neutron-production Cross Section (MF=3; MT=201)

Evaluation of the neutron-production cross section was made based on the experimental data measured by Flynn et al.[49] in the energy range E_α=3.9 ~ 6.3 MeV. Above E_α = 6.3 MeV, we adopted the cross sections calculated with the EGNASH-2 code[7]. Normalization was made so that the calculations could reproduce experimental data below E_α = 6.3 MeV. The evaluated neutron-production cross section is shown in Fig. 55 together with experimental cross sections.

(2) Energy-angle Distribution of Emitted Neutrons (MF=6; MT=201)

Double-differential energy-angle distributions of emitted neutrons were calculated with the EGNASH-2 code[7] and represented by using the Kalbach systematics[6]. Figure 56 shows the calculated energy spectra of emitted neutrons. These spectra include contributions of discrete neutrons emitted by the partial (α,n_i) reactions.

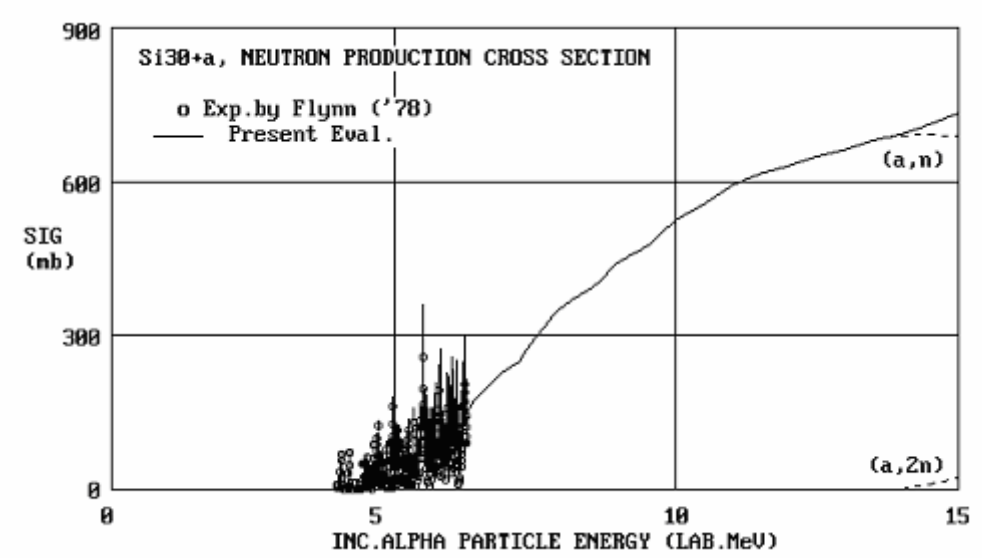

Fig. 55 Evaluated neutron-production cross section of ^{30}Si bombarded by α-particles together with experimental cross sections. Breakdown of the cross section is shown by the dashed lines.

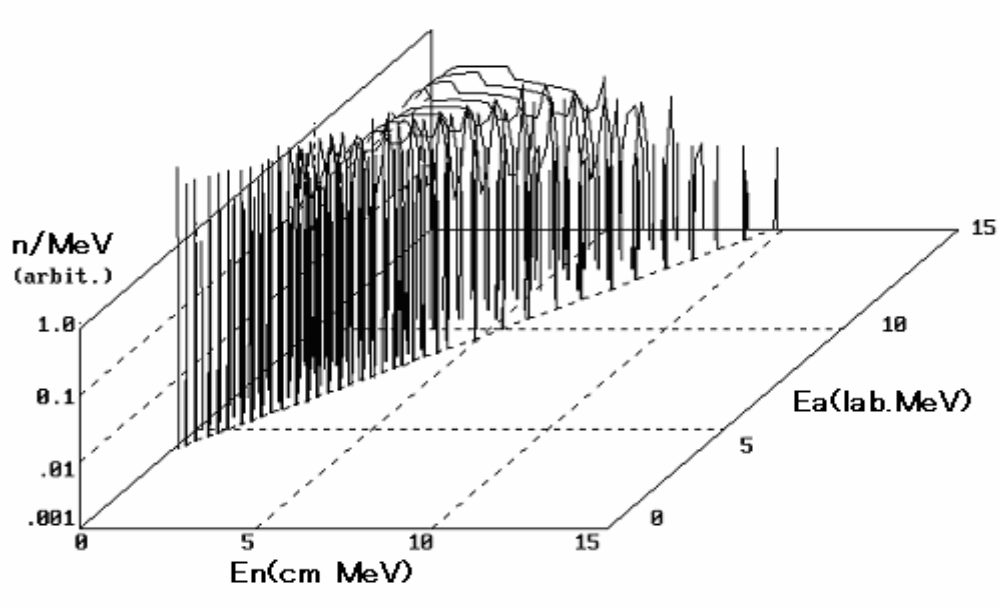

Fig. 56 Calculated energy spectra of neutrons emitted by α-particle bombardment of ^{30}Si. Normalization of spectra was made for each incident α-particle energy Ea.

12.4 Discussion

Thick-target neutron yields from the (α,xn) reactions on natural Si were calculated with the presently evaluated data and are shown in Fig. 57. It is found from the figure that the calculations reproduce experimental data very well. For ^{29}Si and ^{30}Si, experimental cross sections for the (α,n) reaction show resonance structures in the energy region $E_\alpha \leq 6$ MeV where the excitation energy of the compound nucleus ^{33}S or ^{34}S is higher than 7.0 MeV and the spin-parity of each resonance level is unknown. Thus, nuclear data evaluation based on exact resonance analysis cannot be made presently.

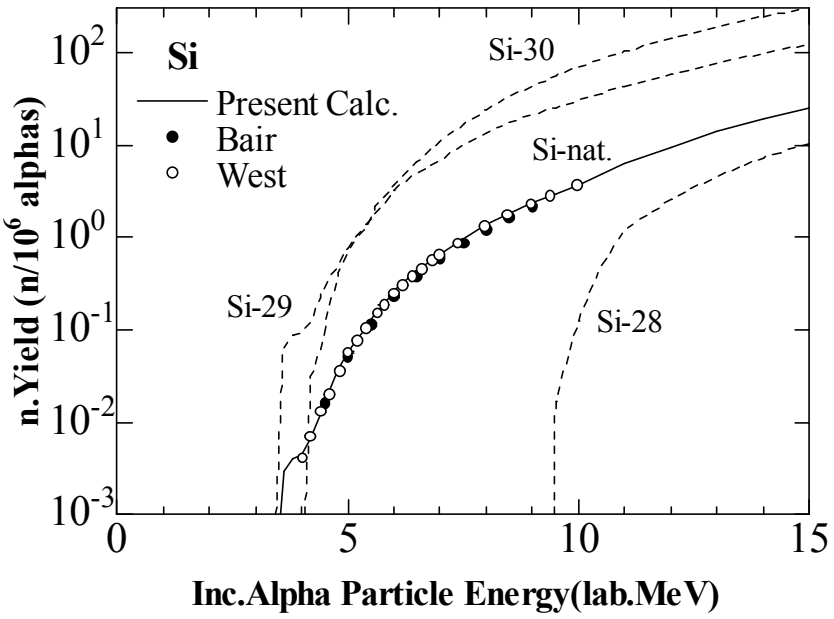

Fig 57 Calculated thick-target neutron yields of natural Si (^{28}Si=92.23%, ^{29}Si =4.67%, ^{30}Si=3.10%) bombarded by α-particles together with experimental yields. The dashed lines show the neutron yields for individual Si isotopes.

13. Conclusions

Neutron-production data of 17 nuclides by α-particle bombardment were evaluated to deduce cross sections, angular distributions and emitted neutron energy spectra. The evaluations were performed on the basis of available experimental data and calculations with the R-matrix and the statistical model. In some cases, the total neutron-production cross section was adjusted so as to reproduce measured thick-target neutron yields. The evaluated data were compiled in the ENDF-6 format[1)], and they were released in June 2005 as JENDL (α,n) Reaction Data File (JENDL/AN-2005). The database provides reliable (α,n) reaction data mainly for nuclear fuel-cycle applications.

Although detailed discussion and future problems were described in each section, the following problems still remain as a whole. Neutron-production cross sections were normalized to experimental thick-target neutron yield using the simple calculation method given by Eq. (10). This formula postulates continuous and straggling-free energy loss of incident α-particles in a thick target. More elaborate method to calculate thick-target neutron yield should be adopted, such as Monte Carlo method, in the future. In the present evaluation, angular distributions of emitted neutrons are given by the Kalbach systematics[6] for most nuclei except ^{9}Be and ^{12}C. The continuous spectrum includes neutrons to discrete levels. Exactly, as for ^{9}Be, discrete neutrons should be separated from continuous spectrum and energy and intensity of discrete neutrons should be calculated using kinematics and angular distributions. In resonance calculation, angular distribution depends strongly on spin-parity. However, it is difficult to assign spin-parity correctly by resonance analysis of the (α,n) cross section only. Therefore, we used the statistical model for the calculation of energy-angle distributions, as was described.

Acknowledgment

Thanks are due to all member of Charged Particle Nuclear Data Working Group of Japanese Nuclear Data Committee for useful discussion, suggestion and cooperation.

References

1) M. Herman (ed.): "ENDF-6 Formats Manual," BNL-NCS-44945-05-Rev, (2005).
2) T. Murata: *Proc. Int. Conf. on Nuclear Data for Science and Technology*, Mito 1988, p.557 (1988).
3) A. Lane and R.G. Thomas: *Rev. Mod. Phys.*, **30**, 257 (1958).
4) T. Murata : JAERI-Conf 97-005, p.286 (1997).
5) H. Kalka: *Z. Phys*., **A341**, 289 (1992).
6) C. Kalbach: *Phys. Rev.*, **C37**, 2350 (1988).
7) N. Yamamuro: JAERI-M 90-006 (1990).
8) T. Murata: JAERI-Conf 2001-006, p.289 (2001).
9) J.K. Bair and J. Gomez del Campo: *Nucl. Sci. Eng*., **71**, 18 (1979).
10) J.K. Bair: *Nucl. Sci. Eng*., **51**, 83 (1973).
11) D. West and A.C. Sherwood: *Ann. Nucl. Energy*, **9**, 551 (1982).
12) J.F. Ziegler: "Helium: Stopping Powers and Ranges in All Elements", Pergamon Press,1977.
13) M.K. Mehta, et al.: *Nucl. Phys*., **48**, 90 (1963).
14) O.V. Bochkarev, et al.: Proc. of 6-th All Union Conf. on Neutron Physics, Kiev **3**, 116, (1984).
15) J.H. Gibbons and R.L. Macklin: *Phys. Rev*., **114**, 571 (1959).
16) L. Van der Zwan and K.W. Geiger: *Nucl. Phys*., **A180**, 615 (1972).
17) R.M. Sealock, et al.: *Nucl. Phys*., **A357**, 279 (1981).
18) M.D. Olson and R.W. Kavanagh: *Phys. Rev*., **C30**, 1375 (1984).
19) J.H. Gibbons and R.L. Macklin: *Phys. Rev.*, **137**, B1508 (1965).
20) L. Van der Zwan and K.W. Geiger: *Nucl. Phys.*, **A152**, 481 (1970).
21) A.W. Obst, et al.: *Phys. Rev*., **C5**, 738 (1972).
22) P.R. Wrean, et al.: *Phys. Rev.*, **C49**, 1205 (1994).
23) R. Kunz, et al.: *Phys. Rev.*, **C53**, 2486 (1996).
24) T. Nakagawa, et al.: *J. Nucl. Sci. Technol.*, **32**, 1259 (1995).
25) J.W. Marsh, et al.: *Nucl. Instrum. Methods*, **A366**, 340 (1995).
26) H. Harano, et al.: Private communication (2005).
27) L. Van der Zwan and K.W. Geiger: *Nucl. Phys*., **A216**, 188 (1973).
28) N.A. Roughton, et al.: *Atom. Data Nucl. Data Tables*, **28**, 341 (1983).
29) L. Van der Zwan and K.W. Geiger: *Nucl. Phys*., **A246**, 93 (1975).
30) T.W. Bonner, et al.: *Phys. Rev*., **102**, 1348 (1956).
31) M. Niecke, et al.: *Nucl. Phys.*, **A289**, 408 (1977).
32) J. Kjellman: *Arkiv for Fysik*, **21**, 543 (1962).
33) G.S. Mani and G.C. Dutt: *Nucl. Phys.*, **78**, 613 (1966).
34) J.L. Black et al.: *Nucl. Phys.*, **A115**, 683 (1968).
35) K.K. Sekharan, et al.: *Phys. Rev.*, **156**, 1187 (1967).
36) J.K. Bair and F.X. Haas: *Phys. Rev.*, **C7**, 1356 (1973).

37) H.W. Drotleff, et al.: *Astrophys. J.*, **414**, 735 (1993).
38) G.M. Hale, et al.: *Proc. Int. Conf. Nuclear Data for Science and Technology*, Julich 1991, p.921 (1992).
39) W. Gruhle, et al.: *Nucl. Phys.*, **A186**, 257 (1972).
40) D.R. Tilley, et al: *Nucl. Phys.*, **A595**,1 (1995).
41) L.F. Hansen, et al.: *Nucl. Phys.*, **A98**, 25 (1967).
42) J.K. Bair and H.B. Willard: *Phys. Rev.*, **128**, 299 (1962).
43) E.B.Norman, T.E.Chupp, K.T.Lesko, P.J.Grant, G.L.Woodruff: *Phys. Rev.*, **C30**, 1339 (1984).
44) P.R.Wrean and R.W.Kavanagh: *Phys. Rev.*, **C62**, 055805 (2000).
45) L.Van der Zwan, K.W.Geiger: *Nucl. Phys.*, **A284**, 189 (1977).
46) E.B. Norman, T.E. Chupp, K.T. Lesko, P. Schwalbach, P.J.Grant: *Nucl. Phys.*, **A390**, 561 (1982).
47) R.T. Skelton, R.W. Kavanagh and D.G. Sargood: *Phys. Rev.*,**C35**, 45 (1987).
48) B. Holmqvist and E. Ramstrom: *Physica Scripta*, **33**, 107 (1986).
49) D.S. Flynn, et al.: *Phys. Rev.*, **C18**, 1566 (1978).
50) R.H. Stelson and F.K. Mcgowan: *Phys. Rev.*, **133**, B911 (1964).
51) S.M. Sahakundu, et al.: *Appl. Rad. Isotope*, **30**, 3 (1979).
52) A.J. Howard, et al.: *Astrophys. J.*, **188**, 131 (1974).
53) S.S. Dietrich and B.L. Berman: *Atom. Data. Nucl. Data Tables*, **38**, 199 (1988).
54) C.W. Cheng and J.D. King: *Can. J. Phys.*, **58**, 697 (1980).

This is a blank page.

国際単位系（SI）

表１．SI 基本単位

基本量	SI 基本単位	
	名称	記号
長さ	メートル	m
質量	キログラム	kg
時間	秒	s
電流	アンペア	A
熱力学温度	ケルビン	K
物質量	モル	mol
光度	カンデラ	cd

表２．基本単位を用いて表されるSI組立単位の例

組立量	SI 基本単位	
	名称	記号
面積	平方メートル	m^2
体積	立法メートル	m^3
速さ，速度	メートル毎秒	m/s
加速度	メートル毎秒毎秒	m/s^2
波数	毎メートル	m^{-1}
密度（質量密度）	キログラム毎立法メートル	kg/m^3
質量体積（比体積）	立法メートル毎キログラム	m^3/kg
電流密度	アンペア毎平方メートル	A/m^2
磁界の強さ	アンペア毎メートル	A/m
（物質量の）濃度	モル毎立方メートル	mol/m^3
輝度	カンデラ毎平方メートル	cd/m^2
屈折率	（数の） 1	1

表５．SI 接頭語

乗数	接頭語	記号	乗数	接頭語	記号
10^{24}	ヨタ	Y	10^{-1}	デシ	d
10^{21}	ゼタ	Z	10^{-2}	センチ	c
10^{18}	エクサ	E	10^{-3}	ミリ	m
10^{15}	ペタ	P	10^{-6}	マイクロ	μ
10^{12}	テラ	T	10^{-9}	ナノ	n
10^{9}	ギガ	G	10^{-12}	ピコ	p
10^{6}	メガ	M	10^{-15}	フェムト	f
10^{3}	キロ	k	10^{-18}	アト	a
10^{2}	ヘクト	h	10^{-21}	ゼプト	z
10^{1}	デカ	da	10^{-24}	ヨクト	y

表３．固有の名称とその独自の記号で表されるSI組立単位

組立量	SI 組立単位			
	名称	記号	他のSI単位による表し方	SI基本単位による表し方
平面角	ラジアン(a)	rad		$m \cdot m^{-1}=1$(b)
立体角	ステラジアン(a)	sr(c)		$m^2 \cdot m^{-2}=1$(b)
周波数	ヘルツ	Hz		s^{-1}
力	ニュートン	N		$m \cdot kg \cdot s^{-2}$
圧力，応力	パスカル	Pa	N/m^2	$m^{-1} \cdot kg \cdot s^{-2}$
エネルギー，仕事，熱量	ジュール	J	N・m	$m^2 \cdot kg \cdot s^{-2}$
工率，放射束	ワット	W	J/s	$m^2 \cdot kg \cdot s^{-3}$
電荷，電気量	クーロン	C		s・A
電位差（電圧），起電力	ボルト	V	W/A	$m^2 \cdot kg \cdot s^{-3} \cdot A^{-1}$
静電容量	ファラド	F	C/V	$m^{-2} \cdot kg^{-1} \cdot s^4 \cdot A^2$
電気抵抗	オーム	Ω	V/A	$m^2 \cdot kg \cdot s^{-3} \cdot A^{-2}$
コンダクタンス	ジーメンス	S	A/V	$m^{-2} \cdot kg^{-1} \cdot s^3 \cdot A^2$
磁束	ウエーバ	Wb	V・s	$m^2 \cdot kg \cdot s^{-2} \cdot A^{-1}$
磁束密度	テスラ	T	Wb/m^2	$kg \cdot s^{-2} \cdot A^{-1}$
インダクタンス	ヘンリー	H	Wb/A	$m^2 \cdot kg \cdot s^{-2} \cdot A^{-2}$
セルシウス温度	セルシウス度(d)	℃		K
光束	ルーメン	lm	cd・sr(c)	$m^2 \cdot m^{-2} \cdot cd=cd$
照度	ルクス	lx	lm/m^2	$m^2 \cdot m^{-4} \cdot cd=m^{-2} \cdot cd$
（放射性核種の）放射能	ベクレル	Bq		s^{-1}
吸収線量，質量エネルギー分与，カーマ	グレイ	Gy	J/kg	$m^2 \cdot s^{-2}$
線量当量，周辺線量当量，方向性線量当量，個人線量当量，組織線量当	シーベルト	Sv	J/kg	$m^2 \cdot s^{-2}$

(a)ラジアン及びステラジアンの使用は、同じ次元であっても異なった性質をもった量を区別するときの組立単位の表し方として利点がある。組立単位を形作るときのいくつかの用例は表４に示されている。
(b)実際には、使用する時には記号rad及びsrが用いられるが、習慣として組立単位としての記号“１”は明示されない。
(c)測光学では、ステラジアンの名称と記号srを単位の表し方の中にそのまま維持している。
(d)この単位は、例としてミリセルシウス度m℃のようにSI接頭語を伴って用いても良い。

表４．単位の中に固有の名称とその独自の記号を含むSI組立単位の例

組立量	SI 組立単位		
	名称	記号	SI 基本単位による表し方
粘度	パスカル秒	Pa・s	$m^{-1} \cdot kg \cdot s^{-1}$
力のモーメント	ニュートンメートル	N・m	$m^2 \cdot kg \cdot s^{-2}$
表面張力	ニュートン毎メートル	N/m	$kg \cdot s^{-2}$
角速度	ラジアン毎秒	rad/s	$m \cdot m^{-1} \cdot s^{-1}=s^{-1}$
角加速度	ラジアン毎平方秒	rad/s^2	$m \cdot m^{-1} \cdot s^{-2}=s^{-2}$
熱流密度，放射照度	ワット毎平方メートル	W/m^2	$kg \cdot s^{-3}$
熱容量，エントロピー	ジュール毎ケルビン	J/K	$m^2 \cdot kg \cdot s^{-2} \cdot K^{-1}$
質量熱容量（比熱容量），質量エントロピー	ジュール毎キログラム毎ケルビン	J/(kg・K)	$m^2 \cdot s^{-2} \cdot K^{-1}$
質量エネルギー（比エネルギー）	ジュール毎キログラム	J/kg	$m^2 \cdot s^{-2} \cdot K^{-1}$
熱伝導率	ワット毎メートル毎ケルビン	W/(m・K)	$m \cdot kg \cdot s^{-3} \cdot K^{-1}$
体積エネルギー	ジュール毎立方メートル	J/m^3	$m^{-1} \cdot kg \cdot s^{-2}$
電界の強さ	ボルト毎メートル	V/m	$m \cdot kg \cdot s^{-3} \cdot A^{-1}$
体積電荷	クーロン毎立方メートル	C/m^3	$m^{-3} \cdot s \cdot A$
電気変位	クーロン毎平方メートル	C/m^2	$m^{-2} \cdot s \cdot A$
誘電率	ファラド毎メートル	F/m	$m^{-3} \cdot kg^{-1} \cdot s^4 \cdot A^2$
透磁率	ヘンリー毎メートル	H/m	$m \cdot kg \cdot s^{-2} \cdot A^{-2}$
モルエネルギー	ジュール毎モル	J/mol	$m^2 \cdot kg \cdot s^{-2} \cdot mol^{-1}$
モルエントロピー，モル熱容量	ジュール毎モル毎ケルビン	J/(mol・K)	$m^2 \cdot kg \cdot s^{-2} \cdot K^{-1} \cdot mol^{-1}$
照射線量（X線及びγ線）	クーロン毎キログラム	C/kg	$kg^{-1} \cdot s \cdot A$
吸収線量率	グレイ毎秒	Gy/s	$m^2 \cdot s^{-3}$
放射強度	ワット毎ステラジアン	W/sr	$m^4 \cdot m^{-2} \cdot kg \cdot s^{-3}=m^2 \cdot kg \cdot s^{-3}$
放射輝度	ワット毎平方メートル毎ステラジアン	$W/(m^2 \cdot sr)$	$m^2 \cdot m^{-2} \cdot kg \cdot s^{-3}=kg \cdot s^{-3}$

表６．国際単位系と併用されるが国際単位系に属さない単位

名称	記号	SI 単位による値
分	min	1 min=60s
時	h	1h =60 min=3600 s
日	d	1 d=24 h=86400 s
度	°	1°=(π/180) rad
分	’	1’=(1/60)°=(π/10800) rad
秒	”	1”=(1/60)’=(π/648000) rad
リットル	l、L	1l=1 $dm^3=10^{-3}m^3$
トン	t	1t=10^3 kg
ネーパ	Np	1Np=1
ベル	B	1B=(1/2)ln10(Np)

表７．国際単位系と併用されこれに属さない単位でSI単位で表される数値が実験的に得られるもの

名称	記号	SI 単位であらわされる数値
電子ボルト	eV	1eV=1.60217733(49)×10^{-19}J
統一原子質量単位	u	1u=1.6605402(10)×10^{-27}kg
天文単位	ua	1ua=1.49597870691(30)×10^{11}m

表８．国際単位系に属さないが国際単位系と併用されるその他の単位

名称	記号	SI 単位であらわされる数値
海里		1海里=1852m
ノット		1ノット=1海里毎時=(1852/3600)m/s
アール	a	1 a=1 $dam^2=10^2m^2$
ヘクタール	ha	1 ha=1 $hm^2=10^4m^2$
バール	bar	1 bar=0.1MPa=100kPa=1000hPa=10^5Pa
オングストローム	Å	1 Å=0.1nm=10^{-10}m
バーン	b	1 b=100$fm^2=10^{-28}m^2$

表９．固有の名称を含むCGS組立単位

名称	記号	SI 単位であらわされる数値
エルグ	erg	1 erg=10^{-7} J
ダイン	dyn	1 dyn=10^{-5}N
ポアズ	P	1 P=1 dyn・s/cm^2=0.1Pa・s
ストークス	St	1 St =$1cm^2/s=10^{-4}m^2/s$
ガウス	G	1 G ^10^{-4}T
エルステッド	Oe	1 Oe ^(1000/4π)A/m
マクスウェル	Mx	1 Mx ^10^{-8}Wb
スチルブ	sb	1 sb =$1cd/cm^2=10^4cd/m^2$
ホト	ph	1 ph=10^4lx
ガル	Gal	1 Gal =$1cm/s^2=10^{-2}m/s^2$

表10．国際単位に属さないその他の単位の例

名称	記号	SI 単位であらわされる数値
キュリー	Ci	1 Ci=3.7×10^{10}Bq
レントゲン	R	1 R = 2.58×10^{-4}C/kg
ラド	rad	1 rad=1cGy=10^{-2}Gy
レム	rem	1 rem=1 cSv=10^{-2}Sv
X線単位		1X unit=1.002×10^{-4}nm
ガンマ	γ	1γ=1 nT=10^{-9}T
ジャンスキー	Jy	1 Jy=$10^{-26}W \cdot m^{-2} \cdot Hz^{-1}$
フェルミ		1 fermi=1 fm=10^{-15}m
メートル系カラット		1 metric carat = 200 mg = 2×10^{-4}kg
トル	Torr	1 Torr = (101 325/760) Pa
標準大気圧	atm	1 atm = 101 325 Pa
カロリー	cal	
ミクロン	μ	1 μ =1μm=10^{-6}m

（第７版，1998年改訂）